

Doctoral thesis

Doctoral theses at NTNU, 2021:410

Andreas Strand

# Uncertainty quantification for multiphase flow

**NTNU**  
Norwegian University of Science and Technology  
Thesis for the Degree of  
Philosophiae Doctor  
Faculty of Engineering  
Department of Structural Engineering



Norwegian University of  
Science and Technology



Andreas Strand

# Uncertainty quantification for multiphase flow

Thesis for the Degree of Philosophiae Doctor

Trondheim, December 2021

Norwegian University of Science and Technology  
Faculty of Engineering  
Department of Structural Engineering



Norwegian University of  
Science and Technology

**NTNU**

Norwegian University of Science and Technology

Thesis for the Degree of Philosophiae Doctor

Faculty of Engineering

Department of Structural Engineering

© Andreas Strand

ISBN 978-82-326-6519-8 (printed ver.)

ISBN 978-82-326-6928-8 (electronic ver.)

ISSN 1503-8181 (printed ver.)

ISSN 2703-8084 (online ver.)

Doctoral theses at NTNU, 2021:410

Printed by NTNU Grafisk senter

# Preface

This thesis is submitted to the Norwegian University of Science and Technology (NTNU) for partial fulfillment of the requirements for the degree of philosophiae doctor. This doctoral work has been performed at the Department of Structural Engineering, NTNU, Trondheim from August 2017 through August 2021 under the supervision of Leif Rune Hellevik.

The funding is received from Petromaks 2, a large-scale program from the Research Council of Norway [1]. The program aspires optimal management of the Norwegian petroleum resources and a future-oriented development of petroleum technology. The strategy is continually managed by OG21 – Oil and Gas for the 21<sup>st</sup> century, with mandate from the Norwegian Ministry of Petroleum and Energy [2]. From 2013 to February 2021, the program has awarded NOK 2.4 billion across 432 projects [3].

This work is part of the project SUM – Scaling and Uncertainty in Multiphase flow, supported by the Norwegian Research Council, grant number 267620, and industrial partners from SINTEF, IFE and Multiflow JIP (Schlumberger Information Solutions, Equinor, ESSS, Lundin Norway, LedaFlow Technologies DA, Gassco, Vår Energi and TechnipFMC).

The thesis is a collection of papers published in or submitted to international peer-reviewed journals. The thesis is organized in two parts. Part I is an introductory section that presents the themes and background of the thesis and part II includes the journal papers.



# Abstract

The purview of this thesis is insight into, and development of, methods for uncertainty quantification in multiphase flow. The work is directed towards commercial simulators for transport of gas and liquid in pipelines and the primary quantities of interest are pressure drop and liquid holdup.

In science and engineering, processes are frequently described by mathematical models, which generally include several uncertain components. The specification of model structure may be associated to simplifications or lack of knowledge. Uncertainty also arise when the state of the system is gauged. In practice, the models are implemented on computers, and are also referred to as simulators. The simulator representations of variables and operations are prone to errors as well.

Also multiphase flow simulators include several layers of uncertain quantities and closure laws. Consequently, predictions are not exactly equal to the outcomes of the experiment or operation they represent. Investigations and development of methods to quantify three sources of uncertainty are described in this thesis.

The focus of the first paper was uncertainty in input variables of a steady-state simulator. Uncertainty propagation with a Monte Carlo method was faster and more robust than polynomial chaos expansions. Further, the coverage of prediction intervals was satisfactory for liquid holdup but rather low for pressure drop.

In the second paper, the focus is shifted to uncertainty in model formulation. Closure laws are modeled as stochastic components of the simulator, and two methods to quantify uncertainty were developed. The aim was to tune closure law uncertainty such that simulator prediction intervals were adequate with respect to observations. The two methods yielded similar estimates for closure law uncertainties.

Variability is the topic of the third paper, and refers to uncertainty about the state of the process due to excluded variables or fundamental stochastic phenomena. Repeatability, which is closely related to variability, was quantified based on novel replicated experiments. The relative deviations in pressure drop and volume flow rates were found to be much less than one percent for nearly all replicates, and express a high degree of repeatability.

The collection of papers constitute a comprehensive overview of uncertainty in multiphase pipe flow, in terms of variable uncertainty, model uncertainty and variability. Accessible methods are developed to quantify uncertainty to make improved predictions and more effectively plan and make decisions for multiphase pipe flow operations.





# Acknowledgments

There are many people I would like to thank. First of all I would like to thank my main supervisor, Leif Rune Hellevik. Thanks for the opportunity and your relentless effort for our group. I would also like to give a special thanks to my co-supervisor Ingelin Steinsland for guidance. Being part of SUM was incredible, and each member brought outstanding expertise in multiphase flow. Thank you.

Experimental data was required to demonstrate and validate the statistical methods we have developed. Thanks to everyone working at the SINTEF Multiphase Flow Laboratory and IFE Well Flow Loop along with VOMS JIP, MultiFlow JIP and LYTT Ltd.

The companionship of my colleagues and friends Lucas, Jacob, Fredrik, Nikolai and Friederike is much appreciated. Many thanks to my dear friends in the departments of structural engineering and mathematical sciences. Thanks to Bjørn Helge Skallerud for counsel in planning. Finally, big thanks to Aina for brilliant edits.



# List of papers

## Journal papers

**Paper 1: Uncertainty Propagation through a Point Model for Steady-State Two-Phase Pipe Flow**

*A. Strand, I.E. Smith, T.E. Unander, I. Steinsland, L.R. Hellevik*

*Algorithms*, 2020.

**Paper 2: Closure Law Model Uncertainty Quantification**

*A. Strand, J. Kjølås, T.H. Bergstrøm, I. Steinsland, L.R. Hellevik*

*International Journal for Uncertainty Quantification*, 2021.

**Paper 3: Repeatability in a Multiphase Pipe Flow Case Study**

*A. Strand, C. Brekken, P.R. Leinan, I. Steinsland, L.R. Hellevik*

*International Journal of Multiphase Flow*, 2021.

## Other contributions

**Paper 4: Uncertainty Quantification and Sensitivity Analysis for Computational FFR Estimation in Stable Coronary Artery Disease**

*F.E. Fossan, J. Sturdy, L.O. Müller, A. Strand, A. Bråten, A. Jørgensen, R. Wiseth, L.R. Hellevik*

*Cardiovascular Engineering and Technology*, 2018.







# Contents

<b>Preface</b>	<b>iii</b>
<b>Abstract</b>	<b>v</b>
<b>Acknowledgments</b>	<b>vii</b>
<b>List of papers</b>	<b>ix</b>
Journal papers . . . . .	ix
Other contributions . . . . .	ix
<b>Contents</b>	<b>xiv</b>
<b>I Introductory section</b>	<b>1</b>
<b>1 Introduction</b>	<b>5</b>
<b>2 Multiphase flow</b>	<b>7</b>
2.1 Two-phase flow . . . . .	7
2.2 Steady-state modeling . . . . .	8

2.3	Closure laws . . . . .	12
2.4	Simulators . . . . .	16
2.5	Experiments . . . . .	17
<b>3</b>	<b>Uncertainty quantification</b>	<b>19</b>
3.1	Sources of uncertainty . . . . .	19
3.2	Framework . . . . .	20
3.3	Uncertainty propagation . . . . .	21
<b>4</b>	<b>Summary of appended papers</b>	<b>27</b>
4.1	Statement of authorship . . . . .	29
<b>5</b>	<b>Conclusions and directions for further work</b>	<b>31</b>
5.1	Conclusions . . . . .	31
5.2	Future work . . . . .	32
	<b>Bibliography</b>	<b>33</b>
<b>II</b>	<b>Research Papers</b>	<b>45</b>
<b>6</b>	<b>Uncertainty Propagation through a Point Model</b>	<b>47</b>
<b>7</b>	<b>Closure Law Model Uncertainty Quantification</b>	<b>71</b>
<b>8</b>	<b>Repeatability in a Multiphase Pipe Flow Case Study</b>	<b>91</b>



# **Part I**

## **Introductory section**



# Nomenclature

CL - Closure law

ES - Energy score

FNN - Feedforward neural network

IFE - Institute for energy technology

ISO - International organization for standardization

IQ - Integrated quadratic distance

KL - Karhunen-Loève

MC - Monte Carlo

MCMC - Markov chain Monte Carlo

MFL - Multiphase flow laboratory

NS - Navier-Stokes

PC - Polynomial chaos

SA - Sensitivity analysis

UP - Uncertainty propagation

UQ - Uncertainty quantification

VOMS - Viscous oil multi scale

WFL - Well flow loop



# Chapter 1

## Introduction

This thesis has been pursued at the Department of Structural Engineering at the Norwegian University of Science and Technology. The topic has been multiphase flow with focus on uncertainty in measurements and uncertainty in predictions of simulator models. The Department of Mathematical Sciences has also been involved as well as external laboratories and industry partners.

The advent of multiphase flow modeling is a milestone in the Norwegian petroleum industry. These models were essential for determining if transport of oil and gas in the same pipeline was possible, and if so, how. Multiphase transport bypassed the need of constructing a new oil platform at each new reservoir. In 2012 the Norwegian newspaper Aftenposten named multiphase technology the most important Norwegian innovation since 1980 [4].

Multiphase modeling is still used extensively, to operate and develop new oil fields and to assure safe operations. The information from modeling reduces the risk and lowers the cost. The structural challenges are bigger than ever as the new oil fields are deeper and colder [5]. Simultaneously, models are enhanced to give more accurate representations. In fact, the level of accuracy is not only required to be high, but preferably also known [6].

The thesis is based on simulators and experiments for multiphase flow in pipelines. Broadly speaking, a simulator is a program for computing the pressure drop in a conduit based on flow rates. Geometry and material properties are also required. Additionally, some simulators provide detailed estimates of the flow profile. The usefulness of a simulator is ultimately determined by performance in field operations. Several components of a simulator are empirical models, and relevant data is

essential for tuning them. The most relevant data comes from field, but laboratory experiments are more accessible and precise.

Uncertainty quantification (UQ) is to identify all uncertain components in the simulators and experiments and quantify the impact of uncertainties on predictions. Uncertainty quantification is an essential part of risk assessment and management, and provides a basis for decision making [7, 8]. The available tools for UQ are manifold and the appropriate choice depends on the application [9].

We have aspired to develop accessible UQ methods for multiphase flow, to make it worthwhile for practitioners to run their own analysis with relevant data. The UQ methods in the thesis are directly compatible with commercial simulators such as LedaFlow [10]. Furthermore, we have pursued a comprehensive description of sources of uncertainty, which we categorize by variable uncertainty, simulator uncertainty and variability [11]. The categories are described in detail in Section 3.1 followed by an outline of UQ methods and literature.

The doctoral work is motivated by specific needs for knowledge. Among numerous methods for uncertainty propagation, it was not clear which were more suitable for multiphase pipe flow [6, 12, 13]. Picchi et al. [14] applied a Monte Carlo (MC) method which they proposed as a benchmark for validation of more complex methods such as polynomial chaos (PC) expansions. Performance of PC in comparison to MC is the topic of the first paper of the thesis. However, the uncertainty description seemed incomplete without consideration of closure laws [15]. The second paper is dedicated to closure law UQ through uncertainty propagation, to extend existing work on closure laws where uncertainties were determined by expert elicitation or separate experiments [15–19]. Further, we recognized that repeatability of multiphase flow experiments had not been thoroughly studied. Only few prior experimental campaigns included replicates, and only particular settings therein were replicated [20, 21]. For the third paper of the thesis, eleven settings of a flow loop were each replicated 23 times or more, in order to make inference on repeatability and variability.

The thesis consists of a collection of papers and is divided into two parts. The first part is an introductory section and consists of Chapters 1-5. A brief introduction to multiphase flow which is relevant for this thesis is given in Chapter 2. In Chapter 3, uncertainty categories are presented along with methods to quantify uncertainty. Chapter 4 is a summary of the appended papers, accompanied by the main conclusion drawn from the thesis and directions for further work in Chapter 5. The second part of the thesis includes Chapters 6-8 which consist of the appended papers.

# Chapter 2

## Multiphase flow

This chapter gives a brief introduction to the components of multiphase flow, modeling and experiments.

Multiphase flow consists of materials in two or more thermodynamic phases. A basic example is any interaction between liquid water and steam, which is a single substance in two phases. However, we often encounter processes where multiple substances mix, such as carbonated drinks. A larger scale example is sedimentation of sand in rivers.

The purview of this section is restricted to simultaneous flow of gas and liquid commonly known as two-phase flow. Moreover, only flow in pipes is considered. Two-phase pipe flow occurs in several industries. A major example is power systems, ranging from coal [22] to nuclear [23]. Another example is epidemiology [24]. However, the main application of this work is long distance transport of oil and gas in pipelines.

### 2.1 Two-phase flow

One aim of two-phase modeling is to determine the composition of gas and liquid along a pipe. At a cross-section of area  $A$  where gas occupies an area  $A_g$ , the liquid covers  $A_l = A - A_g$ . Moreover, each fluid moves according to a velocity field. Depending on the level of detail required, it may be sufficient to operate in terms of the average velocity at cross-sections. In that regard, some essential definitions are listed in Table 2.1. Subscript  $p$  refers to phase, either gas (g) or liquid (l). The holdup  $H_p$  is the fraction of phase  $p$  at the cross-section. The average velocities are proportional to the volume flow rates  $Q_p$  and are also called the bulk velocities.

**Table 2.1:** Terms used to describe the composition of gas and liquid in two-phase pipe flow. Notation is given in the second column and third is the definition in terms of a cross-sectional average.

Variable	Symbol	Definition
Holdup	$H_p$	$A_p/A$
Velocity	$\bar{u}_p$	$Q_p/A$
Superficial velocity	$U_p$	$Q_p/A_p$

Sometimes superficial velocities  $U_p = \bar{u}_p/H_p$  are used for convenience.

### 2.1.1 Flow regimes

The simultaneous flow of gas and liquid in the same pipe may either be structured or chaotic. The deformable complex interfaces between the liquid and the gas are key characteristics of two-phase flow. The literature is consistent in the categorization of flow based on interfaces. The categories are called flow regimes, and illustrated in Figure 2.1. On the bottom left we see stratified flow, in which the fluids are separated as layers. Gas is light and flows above the heavier oil layer. Wavy flow is also stratified, but the gas moves forward relative to the liquid and creates waves, as demonstrated at sea. If the waves are large enough, they cover the whole cross-section of the pipe, and this is then called slug flow. Slugs refer to the segments where liquid fills the cross-section, and they move faster than the liquid in the stratified segments. Gas is also dispersed in the slugs as illustrated in Figure 2.1. Bubbly flow is primarily liquid with some gas dispersed therein. The last flow regime discussed here is annular flow where a liquid film covers the pipe wall. Moreover, gas flows in the center of the pipe and suspends droplets of liquid. Figure 2.1 is inspired by the work of Taitel and Dukler [25].

For given fluid properties and geometry, it is to some extent possible to map out flow regimes in terms of superficial velocities such as in Figure 2.1. Each flow regime corresponds to a region in the space of  $U_g$  and  $U_l$ , with boundaries separating the regions. The challenge of modeling flow regime boundaries is ongoing research and has been for decades [26–29]. The prevailing regime for specific conditions may be determined by watching experiments in transparent pipes, direct numerical simulation or other ways of modeling. However, two-phase flow generally evolves with time, even at fixed flow rates. The flow is unstable near the boundaries, and the instabilities grow and cause transitions in regime. Thus, boundaries are sometimes represented as transition bands rather than lines [30].

## 2.2 Steady-state modeling



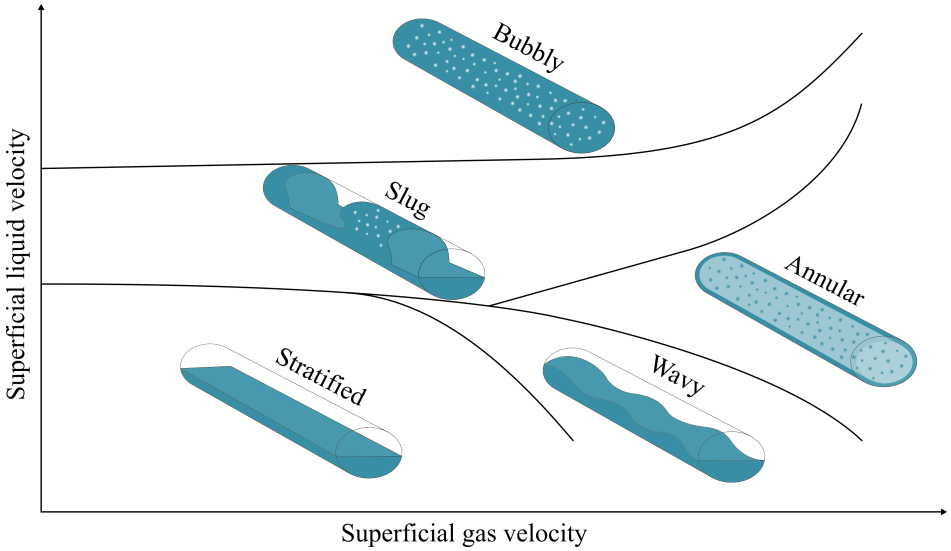


**Figure 2.1:** Flow map of two-phase flow in near-horizontal pipes.

### 2.2.1 Stratified flow

In stratified flow the light gas flows on top of the heavier liquid. Figure 2.2 illustrates flow in an upwards inclined pipe where the gas (transparent) moves faster than the liquid (blue). Pressure decreases in the direction of  $x$ , which corresponds to a driving force. Gravity works with acceleration  $g$ , with a fraction  $\sin \theta$  in the direction of negative  $x$ . Moreover, two types of shear stress apply to each phase. Shear stress  $\tau_{wg}$  acts on the the gas-wall perimeter  $S_g$ , and  $\tau_{wl}$  acts on the the liquid-wall perimeter  $S_l$ . At the interface  $S_i$ , the fluids inflict shear stress  $\tau_i$  on each other, and thus the liquid is pulled by the faster moving gas. In steady state, the derivatives of fluid momentum in time and space are zero. Furthermore, effects from a hydrostatic level gradient, entrainment and deposition are disregarded for this purpose. The simplified momentum equations for gas and liquid are [31]

$$-A_g \frac{\partial p}{\partial x} - S_g \tau_{wg} - S_i \tau_i - A_g \rho_g g \sin \theta = 0, \quad (2.1a)$$

$$-A_l \frac{\partial p}{\partial x} - S_l \tau_{wl} + S_i \tau_i - A_l \rho_l g \sin \theta = 0. \quad (2.1b)$$

Multiplying (2.1b) by  $H_g$  and subtracting (2.1a) multiplied by  $H_l$  eliminates the pressure gradient and yields

$$H_g S_l \tau_{wl} - H_l S_g \tau_{wg} + S_i \tau_i + H_g H_l A (\rho_l - \rho_g) g \sin \theta = 0, \quad (2.2)$$

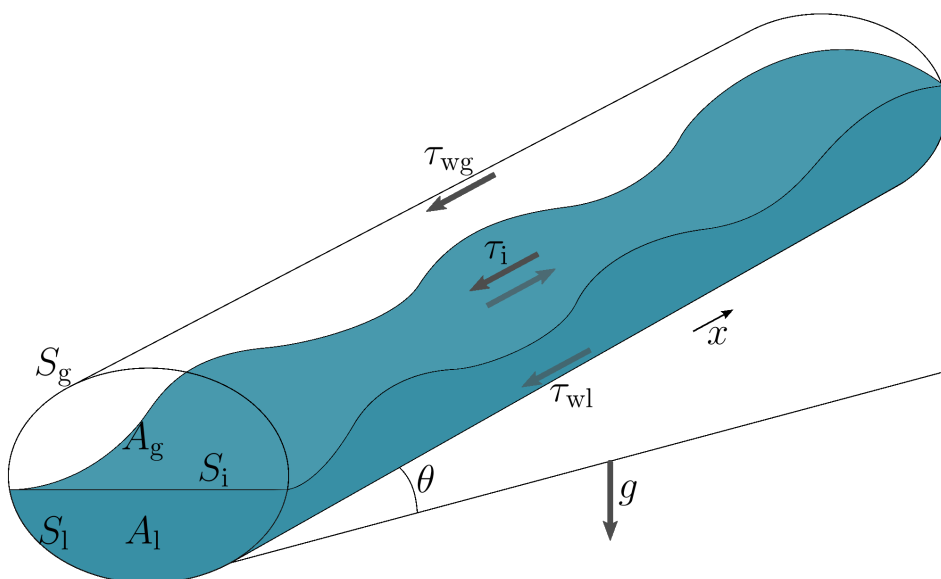


**Figure 2.2:** Liquid (blue) and gas (transparent) in stratified wavy flow in a pipe of upwards inclination  $\theta$ . At the near end cross-section, gas covers an area  $A_g$  located above the liquid area  $A_l$ . There are three phase perimeters, gas-liquid  $S_i$ , gas-wall  $S_g$  and liquid-wall  $S_l$ , with shear stresses  $\tau_i$ ,  $\tau_{wg}$  and  $\tau_{wl}$  respectively. Additionally, gravity applies with acceleration  $g$ .

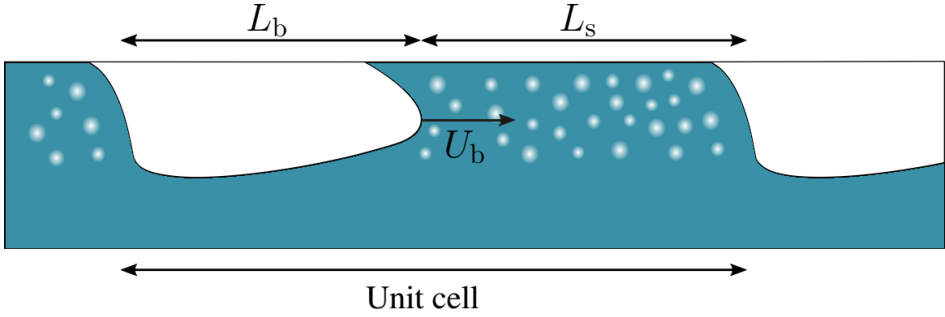


**Figure 2.3:** Diagram of slug flow. The large gas pockets are assumed to be of constant length  $L_b$  separated by slugs of length  $L_s$ .

where  $A$ ,  $H_g$ ,  $S_g$ ,  $S_l$  and  $S_i$  are computed directly from  $H_1$  and pipe diameter  $D$ . The unknown liquid holdup  $H_1$  is obtained from numerical solution of (2.2).

### 2.2.2 Slug flow

Conveniently, the modeling of stratified flow naturally extends to slug flow. Figure 2.3 illustrates the unit cell concept introduced by Dukler and Hubbard [32]. One unit cell comprises a bubble zone of length  $L_b$  followed by a slug zone of length  $L_s$ . In terms of fractions, the slug zone covers  $s = L_s/(L_b + L_s)$ . The slugs entrain gas bubbles, and the amount is significant. The average liquid holdup  $H$  in the pipe is the average liquid holdup in the unit cell, which is the weighted average of the bubble zone and slug zone,

$$H = (1 - s)H_1 + sH_s, \quad (2.3)$$

where  $H_1$  is the solution to (2.2) while  $H_s$  and  $s$  are obtained from empirical closure laws discussed below. The slug fraction  $s$  is restricted to  $[0, 1]$ . However, in the process of deciding flow regimes, we might temporarily operate with invalid values for  $s$ , where  $s \leq 0$  is stratified flow and  $s \geq 1$  is bubbly flow.

The gas velocity and the liquid velocity in a slug are not equal by default. The ratio of gas to liquid velocity is called the slip ratio and is modeled by empirical closure laws [33, 34]. Moreover, the case of equal velocities is called no-slip or homogeneous flow, and the slip ratio is then one [30]. Furthermore, the slug velocities equal the mixture velocity  $U_m = U_g + U_l$ . Inserting the mixture velocity for the slug velocities into mass continuity equations for the slugs, yields a slug fraction equal to

$$s = 1 + \frac{(1 - H_s)U_l - H_sU_g}{(H_s - H_1)U_b}, \quad (2.4)$$

where  $U_b$  is the velocity of the large gas bubbles as illustrated in Figure 2.3 [31].

### 2.2.3 Bubbly flow

Bubbly flow is characterized by the dispersion and shapes of the gas bubbles. Application of no-slip and the relations in Table 2.1 yields

$$\begin{aligned}\bar{u}_g &= \bar{u}_l \\ \Leftrightarrow \frac{U_g}{1-H} &= \frac{U_l}{H} \\ \Leftrightarrow H &= \frac{U_l}{U_m},\end{aligned}\tag{2.5}$$

where  $H$  again is the average liquid holdup in the pipe.

### 2.2.4 Pressure drop

The pressure gradient in the main flow direction is also called the pressure drop and is frequently the primary quantity of interest [15]. Analogous to (2.3), the pressure drop is the weighted average

$$\frac{\partial p}{\partial x} = s \frac{\partial p_s}{\partial x} + (1-s) \frac{\partial p_l}{\partial x}.\tag{2.6}$$

Rearranging (2.1) yields the bubble zone pressure gradient, and modified (2.1b) applies to the slug zone, such that

$$\frac{\partial p_s}{\partial x} = -\frac{4\tau_s}{D} - \rho_m^s g \sin \theta,\tag{2.7a}$$

$$\frac{\partial p_l}{\partial x} = -\frac{S_g \tau_g}{A} - \frac{S_l \tau_l}{A} - \rho_m^l g \sin \theta,\tag{2.7b}$$

where  $\tau_s$  is the wall shear stress in the slug zone and  $\rho_m^p = (1-H_p)\rho_g + H_p\rho_l$  is the mix density where  $p$  is l for the bubble zone and s for the slug zone.

## 2.3 Closure laws

The averaging procedures in Section 2.2 produce a solution of low resolution and some information about the flow is instead reintroduced from empirical modeling. For instance, it is rarely feasible to model friction locally on a microscopic scale. Instead we capture the macroscopic or average effect of friction by theoretical simplifications or deduction from experiments. The various models used to approximate effects are here referred to as closure laws because they are necessary to close the set of flow equations.

A vast collection of theoretical and empirical works forms the development of closure laws in steady-state flow. Shippen et al. list several works on each closure [15, 35]. The basic closure laws encountered in the thesis are presented below.

### 2.3.1 Wall shear

Fluids incur shear stress  $\tau$  when they move along the pipe wall, which is force per area. Consider a single fluid of viscosity  $\mu$  in a cylinder with radial coordinate  $r \in [0, R]$ . For Newtonian fluids, Newton's law of viscosity states

$$\tau(r) = \mu \frac{\partial u}{\partial r}, \quad (2.8)$$

where  $v$  is the flow velocity and  $\partial u/\partial r$  is called shear velocity or strain rate. In fully developed steady-state laminar flow the pressure is  $p = p(x)$  and the velocity is expressed as a profile  $u = u(r)$ . The velocity profile is obtainable by solving the horizontal force balance on a cylinder lamina of differential thickness  $\partial r$  and length  $\partial x$  given by

$$2\pi r \partial r (p(x) - p(x + \partial x)) = 2\pi r \partial r \tau(x) + 2\pi (r + \partial r) \partial x \tau(r + \partial r). \quad (2.9)$$

Integration, no-slip on the wall and radial flow symmetry yield the velocity flow profile  $u(r) = 2\bar{u}(1 - 4r^2/R^2)$ . Consequently, the wall shear stress is

$$\tau_w = \mu \left. \frac{\partial u}{\partial r} \right|_{r=R} = -\frac{8\mu\bar{u}}{D}. \quad (2.10)$$

The pressure drop over a length  $L$  of the pipe is  $\Delta p = \tau \cdot 4L/D$ , which combined with (2.10) is the Hagen-Poiseuille equation. This result was first experimental [36, 37], but later justified theoretically [38].

A modified version of (2.10) applies to two-phase stratified laminar flow [31]. In the example above, the fluid fills the entire cross-section  $A = \pi D^2/4$  and wall shear applies to the perimeter  $S = \pi D$ . When two fluids share cross-section, the ratios of area to perimeter within each phase are different. The change in geometry from one phase to two phases is captured by replacing  $D = A/S$  in (2.10) by the hydraulic diameters  $D_{\text{hg}} = 4A_g/(S_g + S_l)$  and  $D_{\text{hl}} = 4A_l/S_l$ . The interface is assumed to act as a wall for the gas, but not for the liquid [30, p. 211].

### 2.3.2 Friction factors

The fanning friction factor  $f_p$  is the ratio of local shear stress  $\tau$  to dynamic pressure  $\frac{1}{2}\rho_p \bar{u}_p^2$  [39], and is dimensionless. Inserting (2.10) for laminar flow of phase  $p$  yields

$$f_p^{\text{f}} = \frac{\tau_{\text{wp}}}{\frac{1}{2}\rho_p \bar{u}_p^2} = \frac{16\mu_p}{\rho_p \bar{u}_p^2 D_{\text{hp}}} = \frac{16}{\text{Re}_p}, \quad (2.11)$$

where  $\text{Re}_p$  is the phase Reynolds number. In this situation, the Reynolds number compactly represents the relative importance of friction to viscosity, and helps

determine whether turbulence will occur [40]. Generally, nonviscous fluids are more prone to turbulence. Experiments show that turbulent flow is characterized by larger friction factors than the model (2.11) [41]. Thus a separate model is required for turbulent flow, for instance the Haaland equation [42]

$$f_p^t = 0.07716 \cdot \log_{10}^{-2} \left( \frac{6.9}{\text{Re}_p} + 0.234 \left( \frac{\varepsilon}{D} \right)^{1.11} \right), \quad (2.12)$$

where  $\varepsilon$  is the roughness of the pipe wall [43, p. 294]. The friction factor is shown to increase monotonically with the roughness ratio  $\varepsilon/D$  for turbulent flow [44]. Moody diagrams [39], such as Figure 2.4, present the friction factor in terms of  $\text{Re}_p$  and  $\varepsilon/D$  on a log-log scale. The model is in this work divided into three regions at  $a = 1700$  and  $b = 4000$ . The laminar model (2.11) applies to  $\text{Re}_p < a$  and does not depend on  $\varepsilon/D$ . The turbulent model (2.12) applies to  $\text{Re}_p > b$  and is plotted for select values of  $\varepsilon/D$  listed on the right-hand side of Figure 2.4. The friction factor is interpolated in the transition region  $1700 < \text{Re}_p < 4000$  by

$$f_p = (1 - w')f_p^l + w'f_p^t, \quad (2.13a)$$

$$w' = \sin^2 \left( \frac{\pi}{2} \cdot \frac{\text{Re}_p - a}{b - a} \right), \quad (2.13b)$$

where  $w'$  are weights introduced in Chapter 6. The laminar value  $f_p^l$  is plotted as a dotted line in the transition region. Different treatment is given to the slug zone, where  $a$  is taken to be  $\text{Re}_s = D\rho_m^s U_m / \mu_1$  at the intersection between the laminar model and the turbulent model (dashed line). Fully turbulent flow is defined as  $b = 3000$  in the slug zone.

### 2.3.3 Slug zone holdup

In the unit-cell model, slug zone holdup  $H_s$  is determined empirically. Gregory et al. [45] fit a function of  $U_m$  from 157 low viscosity experiments with estimated mean squared prediction error of 0.034. Kora et al. [46] made closure laws for higher viscosities, which is applied to  $\mu_1 \geq 0.02$  in this work. The relative impact of gravity to viscosity is represented by the dimensionless number  $k = F_g F_v^{0.2}$ , where

$$F_g = \frac{U_m}{(gD)^{0.5}} \sqrt{\frac{\rho_l}{\rho_l - \rho_g}} \quad \text{and} \quad F_v = \frac{U_m \mu_1}{gD^2(\rho_l - \rho_g)}. \quad (2.14)$$

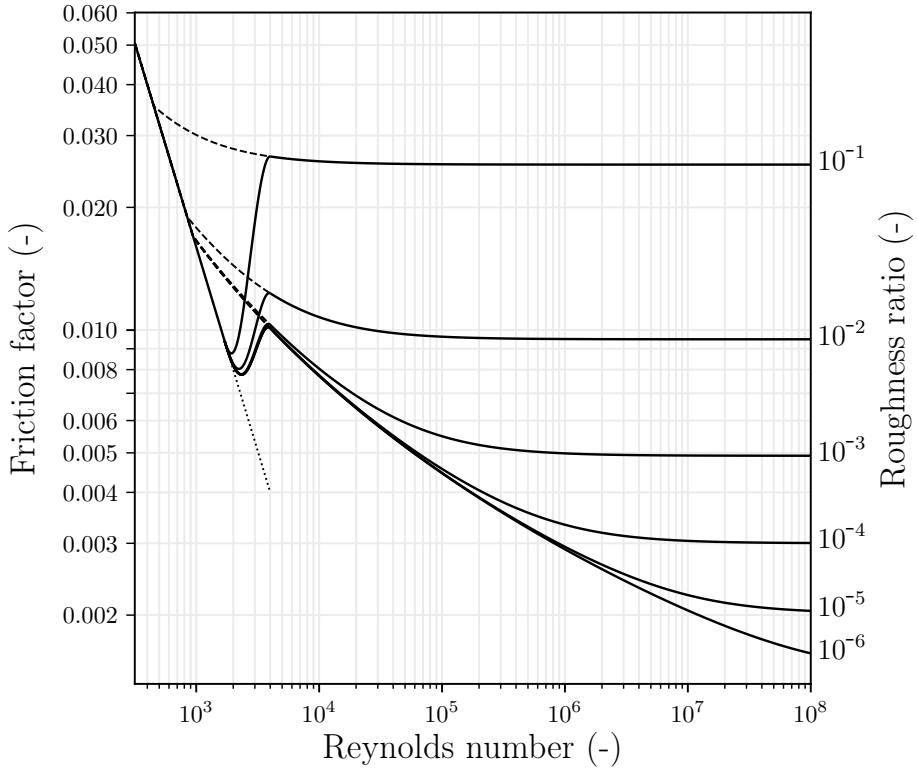


**Figure 2.4:** Moody diagram. The Fanning friction factor in terms of Reynolds number  $Re_p$  and roughness ratio  $\varepsilon/D$ . The friction factor depends on  $\varepsilon/D$  in the turbulent region  $Re_p > 4000$  but not in the laminar region  $Re_p < 1700$ . The friction factor is interpolated between laminar and turbulent values in the transition region  $1700 < Re_p < 4000$ .

The combined expression for the slug zone liquid holdup is

$$H_s = \begin{cases} \frac{1}{1+(U_m/\alpha)^{1.39}}, & \mu_l < 0.02 \\ 1, & \mu_l \geq 0.02, k \leq 0.15 \\ 1.012 \cdot e^{-0.085k}, & \mu_l \geq 0.02, 0.15 < k < 1.5 \\ 0.9473 \cdot e^{-0.041k}, & \mu_l \geq 0.02, k \geq 1.5 \end{cases} \quad (2.15)$$

where  $\alpha = 8.66$  m/s. Evidently, mixture velocity is the principal variable for predicting  $H_s$ .

### 2.3.4 Bubble nose velocity

The bubble nose velocity is illustrated in Figure 2.3. In similar fashion to Section 2.3.3, multiple experimental works together make a robust approximation [47–50]. Effectively,  $U_b$  is the sum of the bubble velocity in a stagnant fluid and a proportion  $C_0$  of the mixture velocity  $U_m$ . The factor  $C_0$  is interpolated between the laminar [48] and turbulent [51] values

$$C_0^l = 2, \quad (2.16a)$$

$$C_0^t = 1 + 2.5871\sqrt{f_s^t} + 1.4874f_s^t, \quad (2.16b)$$

with  $f_s^t$  from (2.12) and  $C_0$  interpolated like (2.13). The bubble nose velocity is modeled as

$$U_b = U_0(F + 0.351 \tan \theta) + U_m \cdot \max(C_0 + 0.15 \sin^2 \theta, 1.05 + 0.15 \sin^2 \theta, 1.2 - U_0 F / U_m), \quad (2.17)$$

where

$$U_0 = \cos \theta \sqrt{Dg(\rho_l - \rho_g) / \rho_l},$$

$$F = 0.53 \exp(-13.7 D^{-0.89} (g\rho_l)^{-0.33} (\rho_l - \rho_g)^{-0.23} \mu_l^{0.46} \sigma^{0.1}).$$

## 2.4 Simulators

A simulator here refers to an implementation of a model for multiphase flow. The origin and development of steady-state simulators is summarized in Shippen and Bailey [15], building on terminology from Brill and Arirachakaran [52], and is briefly discussed here. Naturally, the multiphase modelling was first an adaptation of the more mature single-phase field of research, around year 1950. The phases were treated as a mixture with no slip between them. The mixture was further represented by an average viscosity, density and Reynolds number weighted by the volume of each phase.

In the subsequent decades experiments were applied ad hoc. Increasingly more experiments tuned the effect of friction. Eventually slip was considered, which required a closure law for the liquid holdup. Soon after, new closure laws predicted flow regimes. It was around year 1975 when researchers returned to a more phenomenological representation of multiphase flow [15]. The limitations of the empirical approach became clear and computers were more relevant.

The core phenomenon is the joint momentum balance introduced in Section 2.2, supported by continuity equations and closure laws. The extent to which closure



**Table 2.2:** Experiments. Each paper, indicated in the first column, makes use of experiments. The project partners involved are listed in the second column followed by the year of execution and the facility. Columns five and six give the inner diameter of the test section and the pipe inclination. The number of experiments is given in the last column.

Paper	Partner	Year	Facility	$D$ [cm]	$\theta$ [deg]	#exp.
1	VOMS JIP	2012	SINTEF MFL	6.9	0.0	240
2	MultiFlow JIP	2018	IFE WFL	10.2	+2.5	46
			SINTEF MFL	19.4	+2.5	37
			SINTEF MFL	18.9	0.0	76
			SINTEF MFL	18.9	+0.5	76
3	LYTT Ltd.	2020	SINTEF MFL	12.7	+2.0	294

laws replace first principles depends on the information available [53]. Moreover, which closure laws to deploy depends on the input range.

In the 90s, models emerged that coupled the flow in reservoir, wellbore and export [54–56]. With increasingly ambitious and convoluted simulators, researcher were not able to develop the code unassisted, and commercial simulators commenced. The OLGAS simulator arrived on the market in 1989 and is in 2021 developed by Schlumberger. The Tulsa University Fluid Flow Project Unified simulator was published in 2003 [57, 58]. Shortly after Kongsberg released the LedaFlow Point Model [10].

OLGAS and LedaFlow are both trained primarily with data from Tiller Multiphase Flow Laboratory, while Tulsa University have separate facilities. All three simulators utilize more than ten thousand steady-state training points, of which only parts are published [59, 60].

## 2.5 Experiments

Along with first principles and observational studies, experiments is a major source for knowledge. Stable and repeatable conditions are required to avoid dilution of information from extraneous confounders [61]. Repeatability conditions for a series of experiments are defined by ISO as “same measurement procedure, same operators, same measuring system, same operating conditions and same location, and replicate measurements on the same or similar objects over a short period of time” [62].

The doctoral work benefits from the state of the art facilities SINTEF Multiphase Flow Laboratory and IFE Well Flow Loop. Data from several experimental cam-

paigns is studied. Chapter 6 includes published data from the Viscous Oil Multi Scale joint industry project [63], while the remaining data is not yet publicly available. Information about the employed data is listed in Table 2.2, with the associated paper index in the first column. Industrial partners request certain experiments and follow the experimental campaigns. Partner, year and facility are given in columns 2 to 4. The pipe diameter and inclination are listed in columns 5 and 6. Finally, the number of experiments are given in the last column.

# Uncertainty quantification

The absence of information about the state of a variable or model is also called uncertainty [64]. In engineering applications, measurements and prediction models are used to gauge quantities of interest. While the primary aim is to obtain the most accurate predictions and models, it is essential to also know the general level of accuracy. It is in 2021 commonplace to quantify uncertainty and the science of doing so is a central topic in several journals [65–70]. The field of multiphase flow follows suit [6].

## 3.1 Sources of uncertainty

There is perhaps no definitive way to categorize uncertainty about measurements and simulator predictions. In this thesis, uncertainty is divided into three categories suitable for multiphase flow applications. The appended papers focus on one category of uncertainty each, as will be explained in Chapter 4. The classification is based on Kennedy and O’Hagan [11] who operated with six categories of uncertainty, and their categories are recited in italics below.

### 3.1.1 Category I: Variable uncertainty (Chapter 6)

*Parameter uncertainty* and *observation error* [11]. With multiphase flow as example, features such as material properties and velocities are used to define the state of a process at any given time. Some of these variables change frequently, while other variables such as pipe diameter are almost constant for a particular process. The values of the variables are gauged by instruments such as densitometers and calipers, and the level of certainty depends on instrument. Other variables are read from tables of physical properties, supplemented by estimated standard deviations.

Variable uncertainty also includes error in direct measurements of quantities of interest.

The standard deviations of errors in instruments and table values are frequently reported, while the full error distributions are rarely seen. However, for a given standard deviation, the Gaussian distribution is the least informative according to the principle of maximum entropy [71, 72]. Thus, the Gaussian distribution is a suitable default.

### 3.1.2 Category II: Simulator uncertainty (Chapter 7)

*Model inadequacy* and *code uncertainty* [11]. A number of governing equations are required [73] to accurately describe multiphase flow and several mechanisms are minuscule. Despite great modeling efforts, considerable structural errors in simulators are recognized [19, 74]. Some errors could be avoided with further investigations or higher resolution in modeling.

In practice, computers are necessary to represent the simulator, which bring potential errors in implementation along with suboptimal representations of variables and operations. However, the thesis does not include detailed investigations of *code uncertainty* in particular.

### 3.1.3 Category III: Variability (Chapter 8)

*Residual variability* and *parametric variability* [11]. A simulator predicts values based on a set of variables. Even if the simulator and variables are correctly specified, some variations of process may be undescribed still. The process may be inherently stochastic on a fundamental level [11] or additional variables are required to describe more conditions of the process. Thus, the deviations may be partially reducible.

Repeatability is the closeness between multiple measurements of a variable under the same conditions [75]. Thus, repeatability measures both variability and variable uncertainty. In fact, it is not trivial to separate category I and category III uncertainty in a study of repeatability.

## 3.2 Framework

Probability theory is the preferred framework for uncertainty quantification considering the ability to structure partial information. Standard notation is to use  $x$  for the physical value of a variable and the random variable  $X$  as an uncertain counterpart, such as a measurement. In similar fashion, a quantity of interest is  $y$  or  $Y$ . The value of  $y$  may also be explained by a set of variables  $\mathbf{x} = (x_1, x_2, \dots, x_p)$

through a model  $f$ , where

$$y = f(\mathbf{x}). \quad (3.1)$$

Even though  $f$  is the true model and  $\mathbf{x}$  includes all the required variables, there may be inherent variability in the process such that  $f$  is stochastic. Commonly, neither  $f$  nor  $\mathbf{x}$  are fully known. In fact, some explanatory variables may be missing entirely. Moreover, the available variables are usually measured and are to some extent erroneous. A simulator  $\hat{f}$  is an approximation of  $f$ . Predictions for  $y$  are made by evaluating  $\hat{f}$  at a set of measured variables  $\mathbf{X}$ , which may be written

$$\hat{Y} = \hat{f}(\mathbf{X}). \quad (3.2)$$

Evaluating  $\hat{f}$  at a single realization of  $\mathbf{X}$  provides no certainty about the true value  $y$ . In fact, it is strictly necessary to estimate how different sources of uncertainty translate to the predictions. *Uncertainty propagation* is one strategy to estimate prediction uncertainty.

### 3.3 Uncertainty propagation

The aim of uncertainty propagation is a probability distribution for  $\hat{Y}$  that represents uncertainty. First, all sources of uncertainty in  $\hat{f}$  and  $\mathbf{X}$  must be identified and described by probability distributions. In trivial cases, the distribution  $\hat{f}(\mathbf{X})$  is tractable analytically, but this is the exception rather than the rule. Instead, the probability distributions are often approximated by samples. The simulator is then evaluated for each sample point.

#### 3.3.1 Monte Carlo methods

Monte Carlo (MC) methods refer to a wide range of algorithms that draw  $n$  samples  $\{\mathbf{x}^{(s)}\}_{s=1}^n$  from a prescribed joint probability distribution of  $\mathbf{X}$  and compute statistics directly from  $\{y^{(s)}\}_{s=1}^n$ . Some literature adopt a more exclusive definition of MC methods [76]. The approach is illustrated in Figure 3.1. Each input, here exemplified by gas or oil mass rates, is sampled according to the measured value and a prescribed measurement error distribution. For each sampled set of inputs, the simulator is evaluated, which yields outputs such as pressure drop or liquid holdup. Each output distribution can be represented by a histogram or more succinctly by the mean  $\mu$ , standard deviation  $\sigma$  or a 95% prediction interval for  $y$  from estimated quantiles  $y_{0.025}$  and  $y_{0.975}$ .

Uncertainty in closure laws (CL) may be sampled like inputs, but caution is required. First of all, closure laws are functions and not variables. Still, the error might take the form of a stochastic variable added or multiplied to the CL.

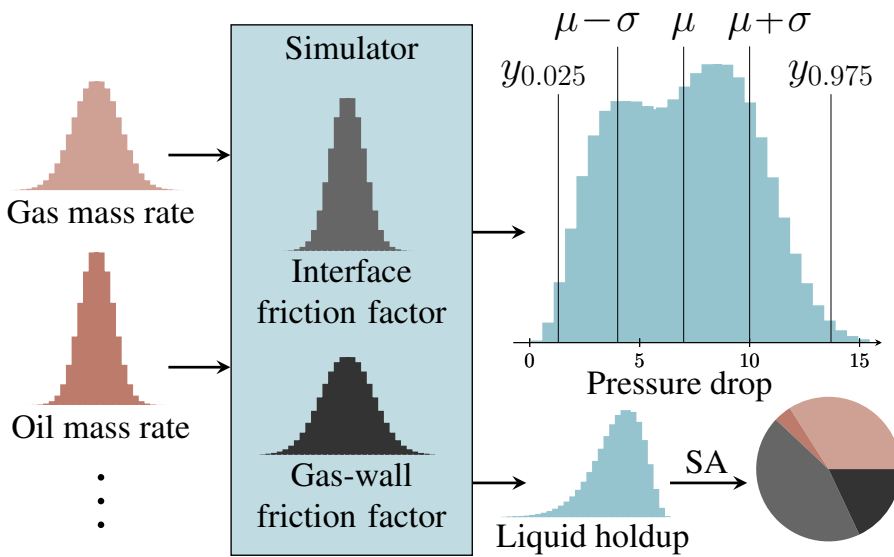


**Figure 3.1:** Propagation of uncertainty through a multiphase flow simulator. Measurement error is sampled from Gaussian distributions and used to perturb the input variables, such as the gas or oil mass rate. Each perturbation is evaluated by a simulator to produce many predictions of pressure drop and liquid holdup, which is here represented by histograms. The histogram of pressure drop predictions is annotated by the mean, one standard deviation from the mean, and quantiles. Errors in the interface and gas-wall friction factors are also sampled. The pie chart in the bottom right illustrates variance-based sensitivity indices for the uncertain variables.

However, while appropriate error distributions in input often derive directly from instrumentation, there are no prominent distributions for CLs. One angle is to parameterize the uncertainty in CLs in terms of unknowns to be optimized as an inverse problem [77, 78].

Sensitivity indices are defined as the proportion of the output variance subject to each uncertain input, or groups thereof, illustrated by the pie chart in Figure 3.1. By imposing a certain correlation structure in the sampling, it is possible to identify the impact of each input as demonstrated by Saltelli et al. [79]. In certain circumstances it is possible to define sensitivity indices for closure laws as well. Yet, it depends on the parametrization of CL uncertainty, and dependency on the stochastic inputs. Classic sensitivity analysis operate on independent input distributions, but dependency is manageable [80, 81].

### 3.3.2 Polynomial chaos expansions

The simplicity and generality of Monte Carlo methods come with computational cost if each evaluation of the simulator is considerable [82]. Parallel computing is suitable and provides some remedy [83]. However, other non-intrusive methods specializes on computationally expensive simulators. Surrogate models approximate the simulator, and have the benefit of cheap predictions. Even better, estimates for the output uncertainty sometimes derive directly from the surrogate model. A non-intrusive polynomial chaos (PC) expansion is a projection of the output onto polynomials in the stochastic inputs [13]. Output mean, variance and sensitivity indices directly derive from fit coordinates of the expansion. Evaluations of the actual simulator is still required to fit the expansion, but presumably fewer than for non-parametric methods [84]. It is challenging to set the complexity of the expansion, which is determined by the basis functions. The basis functions are polynomials, and a high order means flexibility, but also computational cost and risk of over-fitting [85, Ch. 2].

### 3.3.3 Other surrogate models

This section provides a brief discussion of surrogate models beyond the PC expansions presented in Chapter 6. The field of machine learning models deploys numerous surrogate models, such as neural networks, support vector machines and kriging [86]. If the uncertainty distributions for some variables and parameters are unknown a priori, it is necessary for the surrogate model to parametrize these distributions in terms of unknowns. Fitting the unknown uncertainty parameters is then an inverse problem to be solved with Bayesian inference. Exact inference may be replaced by Markov chain Monte Carlo when necessary [87].

An example of complex surrogate uncertainty modeling is given in Liu et al. [77],

regarding vertical bubbly flow in a rectangular channel. They apply two differential transport equations parametrized in terms of five uncertain coefficients relating to closure laws. Each parameter is assigned a conservative prior distribution based on software defaults [88] and expert elicitation. The simulator is evaluated at five hundred samples. However, because the outputs are given on a series of grid points, the dimension is 6720, but principal component analysis is used for dimension reduction. A feedforward neural network is fit to the simulator, which implies an implicit representation of the closure law uncertainty. Additional sources of uncertainty are included, but added separately afterwards to ensure a manageable complexity in the Bayesian inference. Specifically, a Gaussian process with radial kernel across the channel is added as an extra uncertainty to the output space, and is fit by MCMC. Moreover, input uncertainty is quantified by separate experiments and treated as known in the larger framework. Finally, uncertainty propagation through sampling gives probability intervals for the quantities of interest.

Bayesian networks are parametric in terms of likelihood kernels and prior distributions and also include several parameters related to discretization and fitting. The Bayesian approach is theoretically appealing because the likelihood functions for the model uncertainty parameters are computed directly. Still, it is worth considering other less parametric yet robust options. One option is to try out different values for the uncertainty parameters, and find the closest match between the predicted output distribution and measured output in terms of probability [89].

### 3.3.4 Sampling

The classic sampling on computers is called pseudorandom [90], and the general approach is to adaptively increase the sample size until the sample statistics converge. Sometimes using *quasirandom* sequences improves the rate of convergence [91]. Quasirandom sequences have low discrepancy, which means even distribution of points on the domain.

A case of multiple uncertain variables  $X_1, X_2, \dots$  with dependency, may be handled by first sampling  $X_1^{(s)}$  from  $P(X_1)$ , then sampling  $X_2^{(s)}$  from  $P(X_2|X_1)$ , and so on. A more complex case is a stochastic process  $(X_t, t \in T)$  where the index set  $T$  is of infinite dimensions in time or space. If the mean and covariance of the process is known, the Karhunen-Loève (KL) expansion provides a finite dimensional approximation. KL expansions have been applied to model porosity and permeability fields in petroleum reservoir simulations [92].

### 3.3.5 Intrusive methods

Intrusive methods replace uncertain parts of the simulator by stochastic variables and the result is a stochastic system. However, it is non-trivial to resolve stochastic



systems. For instance, a velocity  $u$  in a deterministic simulator is generally a stochastic variable  $U$  in the stochastic system and depends on uncertain variables  $\mathbf{X} = (X_1, X_2, \dots, X_k)$ . In cases where the exact distribution  $P(U)$  is unattainable, approximating  $U(\mathbf{X})$  by a polynomial chaos expansion is an alternative. For each input  $X_j$  the expansion applies basis functions that are orthogonal with respect to the probability density function  $\rho_j(X_j)$ . A standard normal  $X_j$  corresponds to Hermite polynomials [93] and a uniform distribution corresponds to Legendre polynomials [94]. The polynomial expansion for  $U(\mathbf{X})$  provides an estimate for  $P(U)$ , and may additionally enter into a more complex stochastic system.

The Navier-Stokes equations are traditionally deterministic. However, it is possible to allow for stochastic velocity, viscosity and more. The first step is to identify a set of independent stochastic variables  $\mathbf{X}$  [95, p. 44]. Velocity and other state variables can then be replaced by PC expansions in  $\mathbf{X}$  to produce a stochastic system. Stochastic Navier-Stokes equations are implemented in the Fortran package multiUQ [96, 97]. A single solution of the equations is required to predict quantities of interest and their uncertainty, and in this regard stochastic solvers have the potential for low computational cost. The primary disadvantage of stochastic solvers is the implementation effort. It is not possible to deploy an existing deterministic solver, but instead the stochastic solver is almost fully rebuilt [96].



# Chapter 4

## Summary of appended papers

All the appended papers were on the topic of multiphase pipe flow. The research aspired to a comprehensive study of sources for uncertainty in experiments and predictions. Thus, the papers follow the structure of Section 3.1. The emphasis of the first paper was variable uncertainty, while the focus shifted to simulator uncertainty in the second paper, and variability in the third.

### **Paper 1** (Chapter 6)

Uncertainty Propagation through a Point Model for Steady-State Two-Phase Pipe Flow, *A. Strand, I.E. Smith, T.E. Unander, I. Steinsland, L.R. Hellevik*  
Published in *Algorithms*, 2020.

This paper describes investigations of variable uncertainty in simulators for multiphase flow as described in Section 3.1.1. A simple model was implemented in Python in order to clearly see the behaviour of methods for propagation of uncertainty in input variables. The targets were prediction intervals for pressure drop and liquid holdup, along with sensitivity indices. It was clear that transitions in flow regimes caused issues for UP, partly within the closure laws. The non-smooth transitions impeded approximations by polynomial chaos expansions and to some degree MC methods.

The complexity of two-phase flow implies several input variables in terms of geometry and physical properties of each fluid. Propagation of ten uncertain inputs proved to be on the computational limit, even with highly parallel implementation on supercomputers. The UQ estimates were based on thousands of evaluations of the simulator. Increasingly more samples were evaluated until the prediction statis-

tics converged. While the PC expansions showed high potential for swift results, they failed to converge in some cases, and overall MC was preferred.

Estimates from MC and PC were in close agreement. The uncertainty about pipe diameter and liquid viscosity comprised most of the prediction uncertainty. Consequently, the estimates for liquid holdup and pressure drop would be much more certain by improving measurements of diameter and liquid viscosity.

The coverages were generally high. However, the liquid holdup in the slug flow experiments tended to be over-predicted while the stratified experiments tended to be under-predicted. Regardless of flow regime, the pressure drop was slightly under-predicted for low values and over-predicted for high values. After all, some deviations were expected, both from excluded entrainment and imperfect closure laws.

The uncertainty analysis also uncovered discontinuities in the formulation of the simulator, and corrections were suggested.

### **Paper 2** (Chapter 7)

Closure Law Model Uncertainty Quantification, *A. Strand, J. Kjølås, T.H. Bergstrøm, I. Steinsland, L.R. Hellevik*

Published in *International Journal for Uncertainty Quantification*, 2021.

This paper contributes to new methods for describing simulator uncertainty, a topic described in Section 3.1.2. This work built on the first paper by extending the uncertainty propagation framework to also include simulator uncertainty. However, while the input uncertainty was prescribed, the model uncertainty was estimated. Two methods for estimation were developed and demonstrated on the commercial simulator LedaFlow. Experiments were grouped by flow pattern and analyzed. The aim was to find uncertainty parameters that produce calibrated distributions with respect to output measurements.

The model uncertainty was attributed to five closure laws. It is accepted that closure laws deviate from the physical values they represent. While there are unlimited ways to represent closure law errors, a multiplicative Gaussian error was satisfactory in the presented applications in terms of prediction coverage. For each case study, only closure laws that significantly affected predictions were included in the parameter estimation, while the remaining were fixed.

**Paper 3** (Chapter 8)

Repeatability in a Multiphase Pipe Flow Case Study, *A. Strand, C. Brekken, P.R. Leinan, I. Steinsland, L.R. Hellevik*

Submitted to *International Journal of Multiphase Flow*, 2021.

This paper describes a study of variability as defined in Section 3.1.3. A large set of replicated experiments were conducted at the SINTEF Multiphase Flow Laboratory. The flow loop comprised a main flow of oil with multiple injections of oil, water and air along the main test section. The fluid mass flow rates were carefully set to certain values and regulated. Each setting for mass rates were replicated many times, in order to study the variability in quantities of interest.

Pressure was measured at several locations. The relative replicate deviations in pressure were less than one percent at most locations. The volume flow rates were generally even less variable. The volume flow rates were computed from mass flow rates, densities and in some cases pressures and temperatures.

## 4.1 Statement of authorship

In Chapter 6 Andreas Strand developed and implemented all methods, performed all simulations and drafted the manuscript.

In Chapter 7 Andreas Strand co-developed and co-implemented all methods, performed all simulations, and drafted the manuscript.

In Chapter 8 Andreas Strand co-developed and implemented all methods, performed all analyses and drafted the manuscript.



## Conclusions and directions for further work

### 5.1 Conclusions

The uncertainty propagation study (Chapter 6) demonstrated how Monte Carlo methods may require hundreds of thousands of model evaluations, even for a steady-state point model. The polynomial chaos expansions did not converge for some cases in the transitional flow regimes. Evidently, the non-smooth regions of the simulator demanded an expansion of high polynomial order.

The Monte Carlo method and polynomial chaos expansions provided similar estimates for prediction intervals and sensitivity indices despite their computational disparity. Pipe diameter and liquid viscosity were found to contribute most to the uncertainty in the steady-state point model predictions. The prediction coverage was apt for holdup but not for pressure drop.

Inclusion of model uncertainty improved the coverage of the prediction intervals in the second paper (Chapter 7) as presumed. Both methods yielded clear optima for the closure law uncertainty parameters. The commercial simulator LedaFlow was studied with use of two datasets. As expected, flow regime determined which closure laws were critical. The gas-wall friction factor was decisive for stratified/annular flow, while the liquid-wall friction factor and the slug-bubble velocity were decisive for slug flow.

The third paper (Chapter 8) covers an investigation of variability in experiments,

where eleven settings for mass flow rates were replicated between 23 and 28 times each. The quantities of interest such as pressure drop and volume flow rates were repeatable, with relative errors mostly much less than one percent. The geometries of the flow loops in the first two papers (Chapter 6 & 7) were less elaborate than in the third paper, which suggests low variability in all three studies. Low variability further supports the choice to run each input setting only once in the experimental campaigns of the first two papers.

The prediction uncertainty is most efficiently reduced with focus on the primary contributors. In Chapter 6, contributions from the input variables are readily given by the sensitivity indices. Evidently, liquid viscosity is a primary contributor to uncertainty, and may be regarded as a weak link. One solution is to monitor liquid viscosity throughout the experiments, rather than to prescribe a fixed value from reference data. Generally, it is also essential to target the weak links in the simulator itself. The results in Chapter 7 do in fact direct our attention to closure laws which comprise substantial prediction uncertainty. Evidently, refining wall friction factors is key. In contrast, it appears that variability in input variables is a minor contributor to prediction uncertainty (Chapter 8).

When the uncertainty in input variables and closure laws is aptly quantified, forward propagation of uncertainty (UP) through the simulator yields predictive distributions conforming to the available information. Throughout the thesis work, it has been apparent that flow conditions determine the total prediction uncertainty and the main contributors thereto. Thus, relevant data is required for representative UQ and calibrated predictions.

Considering the thesis as a whole, there are promising implications for the multiphase industry already in the short term. To assist computations for complex multiphase pipeline transport, operators may readily adopt the work flow presented in Chapter 7 and supported by Chapters 6 & 8. The benefit is more effective decisions through probabilistic predictions with all major sources of uncertainty rigidly quantified. Importantly, the method is compatible with any simulator, without changes to the simulator software.

## 5.2 Future work

The attempts to fit PC expansions in the first paper were not exhaustive, and it is perhaps worthwhile to consider sparser expansions [98].

While the state of the art multiphase software is ever more capable of prediction, UQ tools therein are in an earlier stage of development. At the same time, general software for optimization and UQ are highly sophisticated [99–102]. The UQ software is capable of calling a deterministic simulator and perform a non-intrusive



analysis. With some insight into the software, the workflow is manageable to set up. Yet, it would be an improvement to have more UQ tools built into the multiphase software, such that uncertainty is considered by default.

Also intrusive UQ methods are suitable for integration in commercial simulators. Intrusive simulators were not implemented in the thesis work despite their rigor and potential to outperform more brute methods [103, 104]. The software multiUQ demonstrates the potential for intrusive stochastic implementations of multiphase processes. The creators stated a need for further development of three dimensional solutions, interface capturing and general computational efficiency [96].

In Chapter 7, the model for closure law uncertainty was promising, but not necessarily optimal. Optimization with comparisons of multiple uncertainty models is possible. Still, a more sophisticated approach is to attain specific prior information about the sources and distributions of modeling errors as demonstrated in Oliver et al. [105]. They simulated a mass-spring-damper system where the damping coefficient is estimated. The coefficient was known to depend on temperature, but the model form was unknown. They were able to extrapolate uncertainty estimates to other systems by qualitative arguments related to temperature. In multiphase flow, such arguments could be effective to extrapolate uncertainty estimates in closure laws to new operations.

Bayesian approaches are intuitive and rigorous, yet not frequently applied to multiphase pipe flow. One example for bubbly flow is demonstrated by Liu et al. [77], where a neural network and a Gaussian process formed the basis for Bayesian inference of uncertainty parameters. Complexity, both in the sense of over-fitting and computational cost, is a recurrent challenge for maximum likelihood estimation in Bayesian networks, but Liu et al. used principal component analysis for regularization. In summary, Liu et al. combined three machine learning tools, and the sophistication is daunting. However, there are helpful software available, such as PyTorch [106] and TensorFlow [107]. Bayesian modeling of multiphase flow in porous media is a mature field [92, 108–110], and knowledge therein may translate to pipe flow.



# Bibliography

- [1] Research Council of Norway, Programplan - PETROMAKS2 2013-2022, Tech. rep., Research Council of Norway, Oslo (2013).
- [2] OG21, TTA4 – future technologies for production, processing, and transportation, [Online; accessed 8-March-2018] (2018).  
URL <http://og21.no>
- [3] Petromaks2 – stort program petroleum, [Online; accessed 15-August-2021] (2021).  
URL <https://prosjektbanken.forskningsradet.no/en>
- [4] G. Strømsheim, G. M. Haugnes, Rørene gjorde oljeeventyret mulig, Aftenposten.  
URL <https://www.aftenposten.no/okonomi/i/Xgle7>
- [5] A. S. Martin, Deeper and colder, Tech. rep., Sustainalytics, [https://www.longfinance.net/media/documents/sa\\_arcticdrilling\\_2011.pdf](https://www.longfinance.net/media/documents/sa_arcticdrilling_2011.pdf) (2012).
- [6] S. Cremaschi, G. E. Kouba, H. J. Subramani, Characterization of confidence in multiphase flow predictions, *Energy & fuels* 26 (7) (2012) 4034–4045.
- [7] S.-Y. Lee, K. Hnottavange-Telleen, W. Jia, et al., Risk assessment and management workflow – an example of the southwest regional partnership, *Energies* 14 (7) (2021) 1908.
- [8] S. M. Elgsaeter, O. Slupphaug, T. A. Johansen, Oil and gas production optimization; lost potential due to uncertainty, *IFAC Proceedings Volumes* 41 (2) (2008) 4540–4547.

- [9] Y. Yan, L. Wang, T. Wang, et al., Application of soft computing techniques to multiphase flow measurement: A review, *Flow Measurement and Instrumentation* 60 (2018) 30–43.
- [10] T. J. Danielson, K. M. Bansal, R. Hansen, E. Leporcher, LEDA: the next multiphase flow performance simulator, in: 12th International Conference on Multiphase Production Technology, no. H4 in BHR, OnePetro, Barcelona, Spain, 2005, pp. 477–492.
- [11] M. C. Kennedy, A. O’Hagan, Bayesian calibration of computer models, *Journal of the Royal Statistical Society: Series B (Statistical Methodology)* 63 (3) (2001) 425–464.
- [12] S. H. Lee, W. Chen, A comparative study of uncertainty propagation methods for black-box-type problems, *Structural and multidisciplinary optimization* 37 (3) (2009) 239.
- [13] H. N. Najm, Uncertainty quantification and polynomial chaos techniques in computational fluid dynamics, *Annual review of fluid mechanics* 41 (2009) 35–52.
- [14] D. Picchi, P. Poesio, Uncertainty quantification and global sensitivity analysis of mechanistic one-dimensional models and flow pattern transition boundaries predictions for two-phase pipe flows, *International Journal of Multiphase Flow* 90 (2017) 64–78.
- [15] M. Shippen, W. J. Bailey, Steady-state multiphase flow – past, present, and future, with a perspective on flow assurance, *Energy & fuels* 26 (7) (2012) 4145–4157.
- [16] B. Boyack, I. Catton (UCLA), R. Duffey (INEL), et al., Quantifying reactor safety margins part 1: An overview of the code scaling, applicability, and uncertainty evaluation methodology, *Nuclear Engineering and Design* 119 (1) (1990) 1–15. doi:[https://doi.org/10.1016/0029-5493\(90\)90071-5](https://doi.org/10.1016/0029-5493(90)90071-5).
- [17] H. Holm, P. Saha, V. Suleymanov, et al., Shtokman flow assurance challenges—a systematic approach to analyze uncertainties—part 1, in: 15th International Conference on Multiphase Production Technology, BHR Group, 2011, pp. 173–189.
- [18] H. Holm, P. Saha, V. Suleymanov, et al., Shtokman flow assurance challenges—a systematic approach to analyze uncertainties—part 2, in: 15th

- International Conference on Multiphase Production Technology, BHR Group, 2011, pp. 191–206.
- [19] N. Hoyer, M. Kirkedelen, D. Biberg, et al., A structured approach for the evaluation of uncertainties in flow assurance systems, in: 16th International Conference on Multiphase Production Technology, BHR Group, 2013, pp. 77–91.
- [20] T. Babadagli, X. Ren, K. Develi, Effects of fractal surface roughness and lithology on single and multiphase flow in a single fracture: an experimental investigation, *International Journal of Multiphase Flow* 68 (2015) 40–58.
- [21] M. Leporini, B. Marchetti, F. Corvaro, et al., Sand transport in multiphase flow mixtures in a horizontal pipeline: An experimental investigation, *Petroleum* 5 (2) (2019) 161–170.
- [22] H. Vuthaluru, V. Pareek, R. Vuthaluru, Multiphase flow simulation of a simplified coal pulveriser, *Fuel Processing Technology* 86 (11) (2005) 1195–1205.  
URL <https://doi.org/10.1016/j.fuproc.2004.12.003>
- [23] R. T. Lahey, E. Baglietto, I. A. Bolotnov, Progress in multiphase computational fluid dynamics, *Nuclear Engineering and Design* 374 (2021) 111018.  
URL <https://doi.org/10.1016/j.nucengdes.2020.111018>
- [24] S. Balachandar, S. Zaleski, A. Soldati, G. Ahmadi, L. Bourouiba, Host-to-host airborne transmission as a multiphase flow problem for science-based social distance guidelines, *International Journal of Multiphase Flow* 132 (2020) 103439.  
URL <https://doi.org/10.1016/j.ijmultiphaseflow.2020.103439>
- [25] Y. Taitel, A. E. Dukler, A model for predicting flow regime transitions in horizontal and near horizontal gas-liquid flow, *AIChE journal* 22 (1) (1976) 47–55.
- [26] O. Baker, Speed-up flow calculations for design of gas gathering systems, *Oil and Gas J.* 53 (12) (1954) 185–190.
- [27] J. Weisman, S. Kang, Flow pattern transitions in vertical and upwardly inclined lines, *International Journal of Multiphase Flow* 7 (3) (1981) 271–291.
- [28] S. Ban, W. Pao, M. S. Nasif, Numerical simulation of two-phase flow regime in horizontal pipeline and its validation, *International Journal of Numerical Methods for Heat & Fluid Flow*.

- [29] R. Farokhpoor, L. Liu, M. Langsholt, et al., Dimensional analysis and scaling in two-phase gas–liquid stratified pipe flow–methodology evaluation, *International Journal of Multiphase Flow* 122 (2020) 103139.
- [30] C. E. Brennen, C. E. Brennen, *Fundamentals of multiphase flow*, Cambridge university press, 2005.
- [31] I. E. Smith, J. Nossen, J. Kjølås, B. Lund, Development of a steady-state point model for prediction of gas/oil and water/oil pipe flow, *Journal of Dispersion Science and Technology* 36 (10) (2015) 1394–1406.
- [32] A. E. Dukler, M. G. Hubbard, A model for gas-liquid slug flow in horizontal and near horizontal tubes, *Industrial & Engineering Chemistry Fundamentals* 14 (4) (1975) 337–347.
- [33] D. Chisholm, *Two-phase flow in pipelines and heat exchangers*, G. Godwin in association with Institution of Chemical Engineers, London, 1983.
- [34] P. Feenstra, D. Weaver, R. Judd, An improved void fraction model for two-phase cross-flow in horizontal tube bundles, *International Journal of Multiphase Flow* 26 (11) (2000) 1851–1873.
- [35] OnePetro, The modeling of multiphase systems under steady-state and transient conditions – a tutorial, no. 0403 in PSIG Annual Meeting.
- [36] S. P. Suter, R. Skalak, The history of poiseuille’s law, *Annual review of fluid mechanics* 25 (1) (1993) 1–20.
- [37] I. Szabó, *Geschichte der mechanischen Prinzipien und ihrer wichtigsten Anwendungen*, Birkhäuser Verlag, Basel, 1979.
- [38] G. G. Stokes, On the theories of the internal friction of fluids in motion, and of the equilibrium and motion of elastic solids, *Transactions of the Cambridge Philosophical Society* 8 (1845) 287–341.
- [39] L. F. Moody, Friction factors for pipe flow, *Trans. Asme* 66 (1944) 671–684.
- [40] G. Falkovich, *Fluid mechanics: A short course for physicists*, Cambridge University Press, 2011.
- [41] C. F. Colebrook, T. Blench, H. Chatley, et al., Turbulent flow in pipes, with particular reference to the transition region between the smooth and rough pipe laws., *Journal of the Institution of Civil engineers* 12 (8) (1939) 393–422.

- 
- [42] S. E. Håland, Simple and explicit formulas for the friction factor in turbulent pipe flow, *J. Fluids Eng.* 105.
- [43] F. M. White, *Fluid mechanics*, 3rd Edition, McGraw-Hill, New York, 2011.
- [44] J. Nikuradse, et al., *Laws of flow in rough pipes*, National Advisory Committee for Aeronautics Washington, 1950.
- [45] G. Gregory, M. Nicholson, K. Aziz, Correlation of the liquid volume fraction in the slug for horizontal gas-liquid slug flow, *International Journal of Multiphase Flow* 4 (1) (1978) 33–39.
- [46] C. Kora, C. Sarica, H.-Q. Zhang, A. Al-Sarkhi, E. Alsafran, Effects of high oil viscosity on slug liquid holdup in horizontal pipes, in: *Canadian Unconventional Resources Conference*, no. 146954 in CSUG/SPE, OnePetro, 2011, pp. 338–352.
- [47] T. B. Benjamin, Gravity currents and related phenomena, *Journal of Fluid Mechanics* 31 (2) (1968) 209–248.
- [48] K. H. Bendiksen, An experimental investigation of the motion of long bubbles in inclined tubes, *International journal of multiphase flow* 10 (4) (1984) 467–483.
- [49] Bubble front velocity in horizontal slug flow with viscous Newtonian, shear thinning and Bingham fluids.
- [50] B. C. Jeyachandra, B. Gokcal, A. Al-Sarkhi, C. Sarica, A. K. Sharma, Drift-velocity closure relationships for slug two-phase high-viscosity oil flow in pipes, *SPE Journal* 17 (02) (2012) 593–601.
- [51] J. Hinze, *Turbulence*, McGraw-Hill, New York, 1975.
- [52] J. Brill, S. Arirachakaran, et al., State of the art in multiphase flow, *Journal of Petroleum Technology* 44 (05) (1992) 538–541.
- [53] OnePetro, *Advancements in two-phase slug flow modeling*.
- [54] K. Brekke, T. Johansen, R. Olufsen, A new modular approach to comprehensive simulation of horizontal wells, in: *Production Operations and Engineering*, no. 26518 in SPE Annual Technical Conference and Exhibition, OnePetro, 1993, pp. 109–124.
- [55] G. Hepguler, S. Barua, W. Bard, Integration of a field surface and production network with a reservoir simulator, *SPE Computer Applications* 9 (03) (1997) 88–92.

- [56] V. Penmatcha, K. Aziz, Comprehensive reservoir/wellbore model for horizontal wells, *Spe Journal* 4 (03) (1999) 224–234.
- [57] H.-Q. Zhang, Q. Wang, C. Sarica, J. P. Brill, Unified Model for Gas-Liquid Pipe Flow via Slug Dynamics—Part 1: Model Development , *Journal of Energy Resources Technology* 125 (4) (2003) 266–273.  
URL [https://asmedigitalcollection.asme.org/energyresources/article-pdf/125/4/266/5851565/266\\_1.pdf](https://asmedigitalcollection.asme.org/energyresources/article-pdf/125/4/266/5851565/266_1.pdf)
- [58] H.-Q. Zhang, Q. Wang, C. Sarica, J. P. Brill, Unified Model for Gas-Liquid Pipe Flow via Slug Dynamics—Part 2: Model Validation , *Journal of Energy Resources Technology* 125 (4) (2003) 274–283.  
URL [https://asmedigitalcollection.asme.org/energyresources/article-pdf/125/4/274/5851922/274\\_1.pdf](https://asmedigitalcollection.asme.org/energyresources/article-pdf/125/4/274/5851922/274_1.pdf)
- [59] Kongsberg Digital, LedaFlow software, accessed on 20.07.2021 (2021).  
URL <https://www.kongsberg.com/no/digital/products/flow-assurance/ledaflow-software/>
- [60] C. Sarica, Eightieth semi-annual advisory board meeting brochure and presentation slide copy, Tech. rep., McDougall School of Petroleum Engineering, University of Tulsa, Oklahoma (2013).  
URL <https://www.bsee.gov/sites/bsee.gov/files/tap-technical-assessment-program//302al.pdf>
- [61] J. M. Bland, D. Altman, Statistical methods for assessing agreement between two methods of clinical measurement, *The lancet* 327 (8476) (1986) 307–310.
- [62] I. BIPM, I. IFCC, I. IUPAC, O. ISO, International vocabulary of metrology—basic and general concepts and associated terms (VIM), 3rd edn, JCGM 200: 2012, accessed on April 3, 2021 (2012).  
URL [https://www.bipm.org/utis/common/documents/jcgm/JCGM\\_200\\_2012.pdf](https://www.bipm.org/utis/common/documents/jcgm/JCGM_200_2012.pdf)
- [63] A. Strand, Replication Data for: Uncertainty propagation through a point model for steady-state two-phase pipe flow (January 2020).  
URL <https://doi.org/10.18710/OWKABR>
- [64] H. Nowotny, P. B. Scott, M. T. Gibbons, Re-thinking science: Knowledge and the public in an age of uncertainty, John Wiley & Sons, 2013.
- [65] *Journal of the american statistical association* (1922).



- 
- [66] Annual review of statistics and its application (2014).
- [67] Reliability engineering and system safety (1983).
- [68] Journal of risk and uncertainty (1988).
- [69] Siam/ asa journal on uncertainty quantification (2013).
- [70] International journal for uncertainty quantification (2014).
- [71] E. T. Jaynes, Information theory and statistical mechanics, Physical review 106 (4) (1957) 620.
- [72] E. T. Jaynes, The relation of bayesian and maximum entropy methods, in: Maximum-entropy and Bayesian methods in science and engineering, Springer, 1988, pp. 25–29.
- [73] R. Fernandes, R. Semiat, A. E. Dukler, Hydrodynamic model for gas-liquid slug flow in vertical tubes, AIChE Journal 29 (6) (1983) 981–989.
- [74] D. Posluszny, K. Klavetter, S. Cremaschi, C. Sarica, H. Subramani, Uncertainty analysis of multiphase flow modelling: A case study for vertical flows, in: 7th North American Conference on Multiphase Technology, OnePetro, 2010, pp. 397–407.
- [75] I. BIPM, I. IFCC, I. IUPAC, O. ISO, International vocabulary of metrology–basic and general concepts and associated terms (VIM), 3rd edn, JCGM 200: 2012, accessed on April 3, 2021 (2012).  
URL [https://www.bipm.org/utis/common/documents/jcgm/JCGM\\_200\\_2012.pdf](https://www.bipm.org/utis/common/documents/jcgm/JCGM_200_2012.pdf)
- [76] M. H. Kalos, P. A. Whitlock, Monte carlo methods, John Wiley & Sons, 2009.
- [77] Y. Liu, D. Wang, X. Sun, N. Dinh, R. Hu, Uncertainty quantification for multiphase-CFD simulations of bubbly flows: a machine learning-based Bayesian approach supported by high-resolution experiments, Reliability Engineering & System Safety 212 (2021) 107636.
- [78] Y. A. Goncharova, I. M. Indrupskiy, Replacement of numerical simulations with machine learning in the inverse problem of two-phase flow in porous medium, Journal of Physics: Conference Series 1391 (2019) 012146.  
URL <https://www.doi.org/10.1088/1742-6596/1391/1/012146>

- [79] A. Saltelli, P. Annoni, I. Azzini, et al., Variance based sensitivity analysis of model output. design and estimator for the total sensitivity index, *Computer physics communications* 181 (2) (2010) 259–270.
- [80] S. Kucherenko, S. Tarantola, P. Annoni, Estimation of global sensitivity indices for models with dependent variables, *Computer physics communications* 183 (4) (2012) 937–946.
- [81] T. A. Mara, S. Tarantola, Variance-based sensitivity indices for models with dependent inputs, *Reliability Engineering & System Safety* 107 (2012) 115–121.
- [82] R. W. Shonkwiler, F. Mendivil, *Explorations in Monte Carlo Methods*, Springer Science & Business Media, 2009.
- [83] A. Cunha, R. Nasser, R. Sampaio, H. Lopes, K. Breitman, Uncertainty quantification through the monte carlo method in a cloud computing setting, *Computer Physics Communications* 185 (5) (2014) 1355–1363.  
URL <https://doi.org/10.1016/j.cpc.2014.01.006>
- [84] M. Hadigol, A. Doostan, Least squares polynomial chaos expansion: A review of sampling strategies, *Computer Methods in Applied Mechanics and Engineering* 332.  
URL <https://www.doi.org/10.1016/j.cma.2017.12.019>
- [85] G. James, D. Witten, T. Hastie, R. Tibshirani, *An introduction to statistical learning*, Vol. 112, Springer, 2013.
- [86] J. Friedman, T. Hastie, R. Tibshirani, et al., *The elements of statistical learning*, Springer series in statistics New York, 2001.  
URL <https://doi.org/10.1007/978-0-387-84858-7>
- [87] S. Brooks, A. Gelman, G. Jones, X.-L. Meng, *Handbook of Markov chain Monte Carlo*, CRC press, 2011.
- [88] P. Siemens, *Simcenter star-ccm+ user guide v13. 04*, Plano: Siemens PLM.
- [89] T. Gneiting, A. E. Raftery, Strictly proper scoring rules, prediction, and estimation, *Journal of the American statistical Association* 102 (477) (2007) 359–378.
- [90] H. Niederreiter, Quasi-monte carlo methods and pseudo-random numbers, *Bulletin of the American mathematical society* 84 (6) (1978) 957–1041.

- 
- [91] P. Bratley, B. L. Fox, H. Niederreiter, Implementation and tests of low-discrepancy sequences, *ACM Transactions on Modeling and Computer Simulation (TOMACS)* 2 (3) (1992) 195–213.
- [92] H. Li, D. Zhang, Efficient and accurate quantification of uncertainty for multiphase flow with the probabilistic collocation method, *Spe Journal* 14 (04) (2009) 665–679.
- [93] R. G. Ghanem, P. D. Spanos, *Stochastic finite elements: a spectral approach*, Courier Corporation, 2003.
- [94] D. Xiu, *Numerical methods for stochastic computations*, Princeton university press, 2010.
- [95] D. Xiu, G. E. Karniadakis, The Wiener–Askey polynomial chaos for stochastic differential equations, *SIAM journal on scientific computing* 24 (2) (2002) 619–644.
- [96] B. Turnquist, M. Owkes, multiuq: A software package for uncertainty quantification of multiphase flows, *Computer Physics Communications* (2021) 108088.
- [97] D. Xiu, G. E. Karniadakis, Modeling uncertainty in flow simulations via generalized polynomial chaos, *Journal of Computational Physics* 187 (1) (2003) 137–167.  
URL [https://doi.org/10.1016/S0021-9991\(03\)00092-5](https://doi.org/10.1016/S0021-9991(03)00092-5)
- [98] N. Lüthen, S. Marelli, B. Sudret, Sparse polynomial chaos expansions: Literature survey and benchmark, *SIAM/ASA Journal on Uncertainty Quantification* 9 (2) (2021) 593–649.
- [99] S. Marelli, B. Sudret, UQLab: A framework for uncertainty quantification in matlab, in: *Vulnerability, uncertainty, and risk: quantification, mitigation, and management*, American Society of Civil Engineers, 2014, pp. 2554–2563.
- [100] J. Feinberg, H. P. Langtangen, Chaospy: An open source tool for designing methods of uncertainty quantification, *Journal of Computational Science* 11 (2015) 46–57.
- [101] B. M. Adams, P. D. Hough, J. A. Stephens, *Dakota software training: Uncertainty quantification.*, Tech. rep., Sandia National Lab. Albuquerque, NM (United States); Sandia National Lab. Livermore, CA (2016).

- [102] J.-B. Blanchard, G. Damblin, J.-M. Martinez, G. Arnaud, F. Gaudier, The uranie platform: an open-source software for optimisation, meta-modelling and uncertainty analysis, arXiv preprint arXiv:1803.10656.
- [103] O. P. Le Maître, O. M. Knio, A stochastic particle-mesh scheme for uncertainty propagation in vortical flows, *Journal of Computational Physics* 226 (1) (2007) 645–671.
- [104] K.-D. Kantarakias, M. E. Chatzimanolakis, V. G. Asouti, K. C. Giannakoglou, On the development of the 3d euler equations using intrusive pce for uncertainty quantification, in: 2nd ECCOMAS Thematic Conference on Uncertainty Quantification in Computational Sciences and Engineering, UNCECOMP 2017, *Eccomas Procedia*, 2017, pp. 588–597.
- [105] T. A. Oliver, G. Terejanu, C. S. Simmons, R. D. Moser, Validating predictions of unobserved quantities, *Computer Methods in Applied Mechanics and Engineering* 283 (2015) 1310–1335.
- [106] A. Paszke, S. Gross, F. Massa, et al., PyTorch: An imperative style, high-performance deep learning library, *Advances in neural information processing systems* 32 (2019) 8026–8037.
- [107] M. Abadi, P. Barham, J. Chen, et al., Tensorflow: A system for large-scale machine learning, in: 12th {USENIX} symposium on operating systems design and implementation ({OSDI} 16), 2016, pp. 265–283.
- [108] G. Ren, J. Rafiee, S. A. Aryana, R. M. Younis, A bayesian model selection analysis of equilibrium and nonequilibrium models for multiphase flow in porous media, *International Journal of Multiphase Flow* 89 (2017) 313–320. URL <https://doi.org/10.1016/j.ijmultiphaseflow.2016.11.006>
- [109] N. Z. Govinda Anantha Padmanabha, A bayesian multiscale deep learning framework for flows in random media, *Foundations of Data Science* 3 (2) (2021) 251–303.
- [110] S. Scheurer, A. Schäfer Rodrigues Silva, F. Mohammadi, et al., Surrogate-based bayesian comparison of computationally expensive models: application to microbially induced calcite precipitation, *Computational Geosciences* (2021) 1–19.

**Part II**

**Research Papers**



# Chapter 6

## Uncertainty Propagation through a Point Model for Steady-State Two-Phase Pipe Flow


The content of this chapter was published in *Algorithms*, 2020.

**Paper 1: Uncertainty Propagation through a Point Model for Steady-State Two-Phase Pipe Flow**

*A. Strand, I.E. Smith, T.E. Unander, I. Steinsland, L.R. Hellevik*

Article

# Uncertainty propagation through a point model for steady-state two-phase pipe flow

Andreas Strand <sup>1,\*</sup> , Ivar Eskerud Smith <sup>2</sup>, Tor Erling Unander <sup>2</sup>, Ingelin Steinsland <sup>3</sup> and Leif Rune Hellevik <sup>1</sup>

<sup>1</sup> Department of Structural Engineering, Faculty of Engineering, Norwegian University of Science and Technology, 7491 Trondheim, Norway; leif.r.hellevik@ntnu.no (L.R.H.)

<sup>2</sup> SINTEF Multiphase Flow Laboratory, 7491 Trondheim, Norway; ivareskerud.smith@sintef.no (I.E.S.); torerling.unander@sintef.no (T.E.U.)

<sup>3</sup> Department of Mathematical Sciences, Faculty of Information Technology and Electrical Engineering, Norwegian University of Science and Technology, 7491 Trondheim, Norway; ingelin.steinsland@ntnu.no (I.S.)

\* Correspondence: andreas.strand@ntnu.no; Tel.: +47 90681168

Received: 31 January 2020; Accepted: 25 February 2020; Published: 28 February 2020

**Abstract:** Uncertainty propagation is used to quantify the uncertainty in model predictions in the presence of uncertain input variables. In this study, we analyze a steady-state point-model for two-phase gas-liquid flow. We present prediction intervals for holdup and pressure drop that are obtained from knowledge of the measurement error in the variables provided to the model. The analysis also uncovers which variables the predictions are most sensitive to. Sensitivity indices and prediction intervals are calculated by two different methods, Monte Carlo and polynomial chaos. The methods give similar prediction intervals, and they agree that the predictions are most sensitive to the pipe diameter and the liquid viscosity. However, the Monte Carlo simulations require fewer model evaluations and less computational time. The model predictions are also compared to experiments while accounting for uncertainty, and the holdup predictions are accurate, but there is bias in the pressure drop estimates.

**Keywords:** two-phase flow; unit cell; uncertainty quantification; sensitivity analysis; Monte Carlo; polynomial chaos

## 1. Introduction

Multiphase flow models are used in a range of applications, such as petroleum transport, nuclear energy and biomechanics. Accuracy in the model output is required to ensure the models to be useful decision support tools. Consequently, there is a rapid development in methods for quantifying the uncertainty in these models.

Lee and Chen [1] compared several types of uncertainty propagation methods, including Monte Carlo methods (MC), polynomial chaos expansions (PC), full-factorial numerical integration (FFNI) and univariate dimension reduction (UDR). They explain the relative strengths of each method, and one conclusion is that PC is most viable in comparison to FFNI and UDR when input distributions are normal but output distributions are not. This is the situation in our analysis. Later, Cremaschi *et al.* [2] discussed applications of the methods discussed in Lee and Chen [1] to multiphase flows. Furthermore, they asked in the short-term that vendors of multiphase simulators implement tools for propagating uncertainty and yield sensitivities and prediction intervals. It was also requested that the simulators incorporate uncertainty in closure laws and that researchers accompany experimental data with uncertainty estimates. In the long term, Cremaschi *et al.* [2] recommended producing scale-up data to improve extrapolation in multiphase models. A case study is presented



in Holm *et al.* [3,4], where they demonstrated how uncertainty propagation may be used for flow assurance on the Shtokman gas and condensate field. Their analysis included pressure drop and liquid holdup predictions using a one-dimensional model in the software OLGA. They determined probability distributions for a selection of input variables and closure laws and they propagated these uncertainties through the multiflow model using a Monte Carlo method. The result is the 10th, 50th, and 90th output percentiles for pressure drop and liquid holdup predictions and measures of sensitivity to the input variables. Hoyer *et al.* [5] used Monte Carlo simulations with OLGA in order to identify influential variables and closure laws in several groups of data with different flow conditions. They are only able to construct satisfactory probability distributions for each closure law when using a group of data where the closure law is significant.

Klavetter *et al.* [6] modeled liquid holdup and pressure drop in two-phase pipe flow using the TUFFP Unified Model for two-phase flow. They assumed an uncertainty range for each input variable and compared perturbation, Taylor series approximations and Monte Carlo methods for uncertainty propagation. They concluded that Taylor series approximations overestimate the output uncertainty while the other methods perform well. Keinath *et al.* [7] also demonstrated the importance of selecting an appropriate framework when handling uncertainty in multiphase modeling and highlighted the value of quantitative information about the input uncertainty distributions for decision making.

Just recently, in Liu *et al.* [8], a Gaussian process and principal component analysis were applied to a complex two-phase flow model in order to explore the uncertainty and reduce the complexity of the model. Picchi and Poesio [9] considered a one-dimensional model for two-phase pipe flow. Known distributions for input variables are propagated through the model using Monte Carlo methods to obtain first-order and total sensitivity indices as well as output distributions. In the thesis of Klinkert [10], a similar method was applied to the point model Shell Flow Correlations and the one-dimensional model PIPESIM by Schlumberger. Polynomial chaos expansions were also applied, and both analyses were implemented in the open-source software UQLab [11].

In this work, we compare uncertainty estimates obtained by Monte Carlo simulations with those of polynomial chaos for the two-phase point model presented in Smith *et al.* [12]. The analyses include quantifying the uncertainty in the model output and estimating the sensitivity to each input variable. Furthermore, we explicitly compare the computational cost of MC to that of PC. These comparisons are important for practical use but uncommon in the literature.

The flow model predicts average holdup and pressure drop based on mass rates, viscosities, densities, pipe diameter, hydraulic roughness, surface tension and pipe inclination. The uncertainty framework provides prediction intervals and the sensitivity to each input variable. We use 240 experiments of stratified flow or slug flow from the SINTEF Multiphase Flow Laboratory as reference. These experiments were also studied in Smith *et al.* [12]. The comparison of prediction intervals to measurement intervals provides high-quality information about any bias in the physical model because the uncertainty is handled in a careful manner.

Section 2 contains details on the flow model and the uncertainty quantification framework. The results are presented in Section 3 and discussed in Section 4.

## 2. Materials and Methods

### 2.1. Flow model

We analyzed the model developed in Smith *et al.* [12], only with a small change to turbulent interpolation. This section briefly outlines their model, which considers two-phase flow in a circular pipe and predicts liquid holdup  $H$  and pressure drop  $-p' = -\partial p / \partial x$  in the longitudinal direction  $x$ . The model predictions are based on ten measured input variables listed in Table 1. In contrast to the presented approach, *system identification* with a backward elimination method [13,14], forward selection [15] or stepwise regression [16] can be used for the same purpose. This would raise the model

quality, but also increase the experiment cost and computational time significantly, and is not applied in this paper.

**Table 1.** Input to the flow model. The index  $p$  refers to phase, where g is gas and l is liquid.

Symbol	Description	unit
$\dot{m}_p$	Mass rate	kg/s
$\mu_p$	Viscosity	Pa s
$\rho_p$	Density	Pa s
$D$	Pipe diameter	m
$\varepsilon$	Hydraulic roughness	m
$\sigma$	Surface tension	N/m
$\theta$	Pipe inclination	rad

The flow is categorized as either stratified, bubbly or slug flow. All cases are covered by a unit-cell model, as introduced in Dukler and Hubbard [17]. The holdup is the weighted average

$$H = sH_s + (1 - s)H_l, \tag{1}$$

where  $s$  is slug fraction,  $H_s$  is the slug zone holdup and  $H_l$  is the bubble zone holdup. Slug flow is illustrated in Figure 1. The model allows for gas bubbles in the slug. Note that  $s \leq 0$  is stratified flow and  $s \geq 1$  is bubbly flow, and  $s$  is then limited to 0 and 1, respectively, in the weighting.

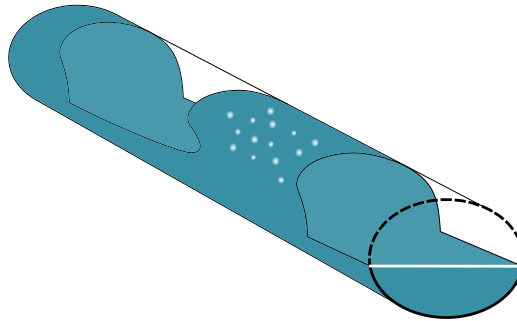


**Figure 1.** Slug flow. Gas bubbles are separated by liquid slugs. At the near end of the pipe, we have illustrated the gas–wall perimeter  $S_g$  (black dashed line), liquid–wall perimeter  $S_l$  (black line) and the interface perimeter  $S_i$  (white line).

The estimation procedure consists of two main steps, deciding the flow regime and computing the holdup conditional on that regime. In general, we need the conditional holdups in order to decide on the regime.

### 2.1.1. Slug zone

The slug zone holdup is computed first. We apply Gregory *et al.* [18] for low liquid viscosities and Kora *et al.* [19] for higher ones. It is convenient to introduce average superficial velocities, defined as

$$U_p = \frac{4\dot{m}_p}{\pi D^2 \rho_p}, \tag{2}$$

where the index  $p$  refers to phase, with  $g$  for gas and  $l$  for liquid. The slug zone holdup is

$$H_s = \begin{cases} \frac{1}{1+0.05\{U_m\}^{1.39}}, & \mu_1 < 0.02 \\ 1, & \mu_1 \geq 0.02, k \leq 0.15 \\ 1.012 \cdot e^{-0.085k}, & \mu_1 \geq 0.02, 0.15 < k < 1.5 \\ 0.9473 \cdot e^{-0.041k}, & \mu_1 \geq 0.02, k \geq 1.5 \end{cases} \quad (3)$$

where  $k = U_m^{1.2} D^{-0.9} g^{-0.7} \mu_1^{0.2} \rho_1^{0.5} (\rho_1 - \rho_g)^{-0.7}$  and  $U_m = U_g + U_l$  is the mix velocity with the numerical value denoted as  $\{U_m\}$ . Using the slug zone holdup, we can easily check for bubbly flow. The holdup for bubbly flow is

$$H = \frac{U_l}{U_m} \quad \text{if } U_l > U_m H_s. \quad (4)$$

The requirement corresponds to a slug fraction greater than 1. In order to find the average holdup in slug flow, we need the bubble nose velocity, which is also empirical. Smith *et al.* [12] used a modified version of the function proposed in Bendiksen [20]. The bubble nose velocity is assumed linear in the mix velocity with an intercept determined by the experiments conveyed in Jeyachandra *et al.* [21]. The slope  $C_0$  is interpolated from a laminar value and a turbulent value, as proposed in Nuland [22], with some additional restrictions. Details are given in section 2.1.5. The laminar and turbulent values are

$$C_0^l = 2 \quad (5a)$$

$$C_0^t = 1 + 2.5871 \sqrt{f_s^t} + 1.4874 f_s^t, \quad (5b)$$

where  $f_s^t$  is the slug friction factor defined later. The turbulent value is as reported in Hinze [23]. Using this approach, the bubble nose velocity is

$$u_b = U_0 (F + 0.351 \tan \theta) + U_m \cdot \max \left( C_0 + 0.15 \sin^2 \theta, 1.05 + 0.15 \sin^2 \theta, 1.2 - \frac{U_0 F}{U_m} \right), \quad (6)$$

where  $U_0 = \cos \theta \sqrt{Dg(\rho_1 - \rho_g) / \rho_1}$  and  $F = 0.53 \exp(-13.7 D^{-0.89} (g\rho_1)^{-0.33} (\rho_1 - \rho_g)^{-0.23} \mu_1^{0.46} \sigma^{0.1})$ .

### 2.1.2. Bubble zone

Let  $H_g = 1 - H_l$  be the gas fraction in the bubble zone. The liquid holdup in the bubble zone is the solution to the momentum balance for both phases, that is  $H_l$  such that

$$\rho_g f_g S_g u_g^2 H_g^3 - \rho_l f_l S_l u_l^2 H_l^3 + \rho_g f_l S_l (u_l H_l - u_g H_g) |u_l H_l - u_g H_g| + (\rho_1 - \rho_g) \frac{\pi}{4} D^2 H_g^3 H_l^3 g \sin \theta = 0, \quad (7)$$

where the perimeters  $S_p$  and  $S_i$  are defined in Figure 1, and the friction factors  $f_p$  and  $f_i$  are defined below. The superficial velocities  $u_p$  must be chosen according to the flow regime. The superficial velocities equal the average superficial velocities in Equation (2) for stratified flow, while they are functions of the bubble zone holdup for slug flow, namely

$$\text{Stratified flow: } u_p = U_p \quad (8a)$$

$$\text{Slug flow: } \begin{cases} u_g = U_g + \Delta \\ u_l = U_l - \Delta. \end{cases} \quad (8b)$$

where  $\Delta = (H_s - H_l)u_b + (1 - H_s)U_l - H_s U_g$ . Furthermore, the interface friction factor is a modified version of the expression proposed in Andreussi and Persen [24] and is given by

$$f_i = f_{i0} \left( 1 + 10h \left( \frac{2u_g}{H_g D} \sqrt{\frac{S_i \rho_g}{\pi H_g g (\rho_l - \rho_g) \cos \theta}} - 0.36 \right)^{0.67} \right), \tag{9}$$

where  $h$  is the line fraction approximated by

$$h = 1 - \cos \left( \frac{1}{3} + \left( \frac{3\pi}{2} \right)^{\frac{1}{3}} + \left( \pi - \frac{2}{3} \right) H_l + H_l^{\frac{1}{3}} + H_g^{\frac{1}{3}} \right) \tag{10}$$

and we impose a minimum of  $f_{i0} = f_g(\epsilon = 0)$ . The friction factors  $f_{i0}$ ,  $f_g$ ,  $f_l$  and  $f_s$  are interpolated from laminar and turbulent values, as described in section 2.1.5. We use the Hagen-Poiseuille and Haaland formulas found in White [25] given as

$$f_p^l = 16 \text{Re}_p^{-1} \tag{11a}$$

$$f_p^t = 0.07716 \cdot \log_{10}^{-2} \left( 6.9 \text{Re}_p^{-1} + 0.234 \left( \frac{\epsilon}{D} \right)^{1.11} \right), \tag{11b}$$

where

$$\text{Re}_p^{-1} = \begin{cases} \frac{\mu_g (S_g + S_l)}{\pi D^2 \rho_g |u_g|}, & p = g \\ \frac{\mu_l S_l}{\pi D^2 \rho_l |u_l|}, & p = l \\ \frac{\mu_l}{D \rho_s^m U_m}, & p = s \end{cases} \tag{12}$$

and  $\rho_m^p = (1 - H_p)\rho_g + H_p\rho_l$  is the mix density where  $p$  is  $l$  or  $s$  for bubble zone or slug zone, respectively. The comparative study in Brkić and Praks [26] suggests a more accurate and computationally efficient approximation than Equation (11b) for the Colebrook turbulent friction factor. However, model tuning is not the main objective for this work. Instead, we use the Haaland approximation to allow for comparison to Smith *et al.* [12]. The friction factor is a small contributor to the computational cost of the point model. Thus, it is not essential to find the most efficient approximation.

### 2.1.3. Slug fraction

The fraction of the unit-cell covered by the slug is called the slug fraction, and it may be computed as

$$s = 1 + \frac{(1 - H_s)U_l - H_s U_g}{(H_s - H_l)u_b}. \tag{13}$$

Figure 2 shows a flowchart of the steady-state point model solution procedure. The first step is to compute the slug zone holdup from (3). Next, we determine the correct flow regime and average liquid holdup. Finally, the pressure drop is computed.

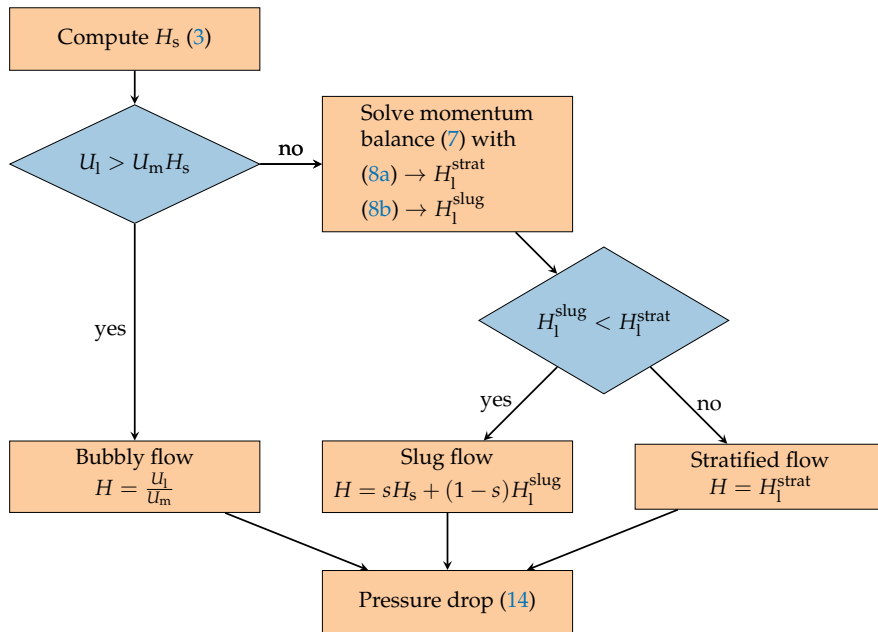


Figure 2. Flowchart of the point model. First holdup is computed, then pressure drop.

2.1.4. Pressure gradient

The pressure gradient is the weighted average

$$p' = s p'_s + (1 - s) p'_l, \tag{14}$$

where the slug zone and bubble zone pressure gradients are

$$p'_s = -\frac{2}{D} \rho_m^s f_s U_m^2 - \rho_m^s g \sin \theta \tag{15a}$$

$$p'_l = -\frac{2}{\pi D^2} \left( \frac{\rho_g f_g S_g u_g^2}{H_g^2} + \frac{\rho_l f_l S_l u_l^2}{H_l^2} \right) - \rho_m^l g \sin \theta, \tag{15b}$$

where  $H_g$  and  $H_l$  is the solution to Equation (7).

2.1.5. Interpolation by Reynolds number

Several dimensionless numbers  $g$  in the model are computed as  $g_l$  for laminar cases and as  $g_t$  for turbulent cases. By interpolation, we ensure continuity in  $g(Re_p)$ , also in the transition from laminar to turbulent. Let the laminar region be  $Re_p < a$ , the transitional region be  $a < Re_p < b$  and the turbulent region be  $b < Re_p$ . A natural interpolation is

$$g(Re_p) = w g_l + (1 - w) g_t \tag{16a}$$

$$w = \frac{b - Re_p}{b - a}. \tag{16b}$$

We chose  $a = 1700$  and  $b = 4000$  for the friction factors in Equation (11) except for  $f_s$ . For  $f_s$  and the slopes in Equation (5), we use  $b = 3000$  and  $a$  such that  $f_l(Re = a) = f_t(Re = a)$ .

However, using weights  $w$  will not produce a smooth function  $g$ . In fact, the derivative of  $g$  with respect to  $Re$  is discontinuous at  $a$  and  $b$ . This far, we have outlined the model given by Smith *et al.* [12],

but we suggest replacing the weights by  $w' = \sin^2(\pi w/2)$ . These weights provide continuity in the derivative of  $g$ . The change is demonstrated in Figure 3. The histograms in the left panel show the distribution of holdup estimates obtained by perturbation of a certain set of inputs with a Reynolds number close to 3000. Blue gives the holdup estimates using the original model with weights  $w$ , while orange gives the estimates obtained using the new weights  $w'$ . The right panel shows  $C_0(\text{Re})$  in the transition from laminar to turbulent Reynolds numbers. We prefer the modified model because the distribution with small changes in input is more straightened out. However, the distribution of pressure drop is nearly unchanged.

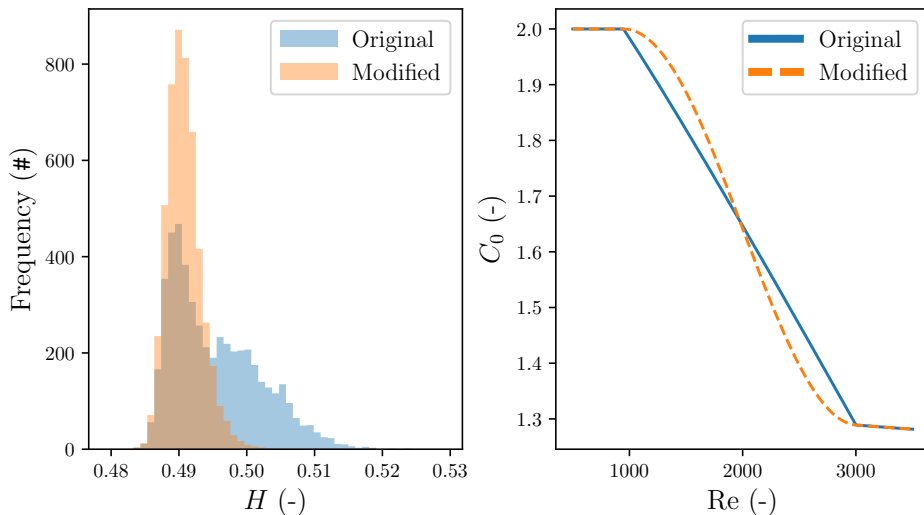


**Figure 3.** Comparison of two methods of interpolation by Reynolds number. *Left:* Histograms of holdup for small perturbation of input around  $\text{Re} \approx 3000$  for the original model (blue) and the modified model (orange). *Right:* The bubble nose variable  $C_0(\text{Re})$  in the transition from laminar to turbulent for the original model (blue line) and the modified model (orange dashed line).

## 2.2. Uncertainty quantification

Section 2.1 describes how we can predict holdup or pressure drop from measured inputs. In this section, we explain how to compute the effect of measurement error in input variables on the predictions. First, we will discuss the measurement error in each input and output. The uncertainties are attained from Table 2 in Smith *et al.* [12] and follow-up discussion with the laboratory staff. Additional details regarding the uncertainty estimates can be found in Khaledi *et al.* [27]. The uncertainties should be understood as defined by the *Guide to the Expression of Uncertainty in Measurement* [28], and the uncertainties are quantified as one standard deviation. Next, we have summarized the discussion on measurement error in each input variable. We refer to Section 2.3 in Smith *et al.* [12] for details on the uncertainty in output measurements.

**Table 2.** Uncertainty in the model variables given as one standard deviation.

(a) Input.			(b) Output.		
Variable	Unit	Uncertainty	Variable	Unit	Uncertainty
$\dot{m}_g$	kg/s	$\dot{m}_g \cdot 0.4\%$	$H$	–	0.03
$\dot{m}_l$	kg/s	$\dot{m}_l \cdot 0.05\%$	$-\partial p/\partial x$	Pa/m	$\max(3 \text{ Pa/m}, -\partial p/\partial x \cdot 0.5\%)$
$\mu_g$	Pa s	$\mu_g \cdot 2\%$			
$\mu_l$	Pa s	$\mu_l \cdot 3\%$			
$\rho_g$	kg/m <sup>3</sup>	0.2 kg/m <sup>3</sup>			
$\rho_l$	kg/m <sup>3</sup>	1 kg/m <sup>3</sup>			
$D$	m	$D \cdot 1\%$			
$\varepsilon$	m	$1 \cdot 10^{-6}$ m			
$\sigma$	N/m	$\sigma \cdot 30\%$			
$\theta$	rad	$2 \cdot 10^{-4}$ rad			

### 2.2.1. Measurement error

**Mass rate.** The devices used to measure the mass rates have uncertainties relative to the measured value. The uncertainties are reported as 0.05% of the measured value for liquid and 0.4% of the measured value for gas.

**Viscosity.** The gas viscosity is found from reference data, and the value for various gases are in the range  $1 \cdot 10^{-5}$  Pa s to  $2 \cdot 10^{-5}$  Pa s, and the viscosity has only a slight dependence on pressure and temperature. The uncertainty in the reference data is quoted as 2%, and it is reasonable to use this value for the uncertainty in gas viscosity. Liquid viscosity is difficult to measure under relevant conditions and is significantly affected by temperature. If the viscosity of a hydrocarbon fluid is measured, a typical uncertainty will be 3% of the reading. The viscosity of a single-compound fluid such as water can be obtained from reference data. The uncertainty in water reference data in the relevant range is 0.5%.

**Density.** For well-known gas compositions, the gas density can be calculated accurately from reference data. Alternatively, the density can be measured by weighing. In both cases, the uncertainty will typically be 0.2 kg/m<sup>3</sup>. This value also includes the effect of various degrees of saturation of vapors from the liquid present in the loop. Liquid density can be measured using Coriolis meters and a reasonable uncertainty in such measurements is 1 kg/m<sup>3</sup>.

**Pipe diameter.** If the pipe diameter is obtained from the nominal diameter, the production tolerance must be used to infer the uncertainty. Typically, such an analysis will yield an uncertainty in diameter of 1%. If the diameter is measured by filling experiments, an uncertainty in diameter of 0.2% can be obtained. Note that the pipe diameter enters into many calculated quantities, and usually to a high degree. This includes the superficial velocities and hydraulic roughness. In the evaluation of the uncertainty in these quantities, the contribution from the uncertainty in pipe diameter is not included. The contribution from error in pipe diameter is unique because it will be the same for all experiments carried out in one particular test section.

**Hydraulic roughness.** The hydraulic roughness is inferred from single phase liquid flow experiments, and the uncertainty in roughness in the current case is 1  $\mu$ m.

**Surface tension.** Surface tension is a parameter that can only be measured off-line. The actual value of the surface tension in situ is hardly known due to contamination and dynamic effects. The uncertainty in surface tension is set to 30%.

**Pipe inclination.** The uncertainty in pipe inclination is estimated based on how the pipes are mounted. By inspection of the setup, we believe that the pipe can deviate 6 mm in the vertical direction over a section of 30 m. This corresponds to an uncertainty in the pipe inclination of  $2 \cdot 10^{-4}$  rad.

### 2.2.2. Uncertainty propagation

Uncertainty propagation is a term for how the measurement error in each input is propagated through the model; for instance, whether the measurement error in the mass rates results in uncertainty in the estimated holdup. We can write the model as

$$Y = y(\dot{m}_g, \dot{m}_l, \rho_g, \rho_l, \mu_g, \mu_l, D, \varepsilon, \sigma, \theta) = y(\mathbf{Z}), \quad (17)$$

where  $Y$  is either holdup or pressure drop. Our model is represented as a function  $y$ , which takes the vector  $\mathbf{Z}$  of random variables as input. The uncertainties of  $\mathbf{Z}$  are propagated through the model  $y$  to produce a new random variable  $Y$ .

We can simulate the effect of measurement error by changing the inputs slightly and observe the change in the output. If we do this many times, we will get a distribution for the output. The change in input represents the measurement error. We sample the measurement errors based on the uncertainties presented in the previous section and Table 2a. We assume independent measurement errors from normal distributions with standard deviations given in the table. All the variables except pipe inclination are truncated at zero.

### 2.2.3. Input sampling

The measurement error is sufficiently simulated without true randomness. Instead, we use a classical pseudo-random sequence denoted  $\{\mathbf{z}^{(j)}\}_{j=1}^n$ , where  $n$  is the sample size. The error in the estimated statistics decays by  $1/n$ , while the rate is only  $1/\sqrt{n}$  for truly random sampling. Furthermore, the pseudo-random sequence cover the input space almost uniformly, while a random sequence may have clusters and holes.

Pseudo-random normal samples of input are generated by applying a copula to the sequence, which is a transformation function for uniform sequences. A dependency between the measurement errors in the inputs could easily be simulated by the use of a different copula.

### 2.2.4. Statistics

The uncertainty analysis can be summarized by some key figures. We have a good overview of the propagated uncertainty if we know the mean  $E[Y]$ , variance  $\text{Var}[Y]$  and the quantiles  $y_{0.025}$ ,  $y_{0.05}$ ,  $y_{0.95}$  and  $y_{0.975}$ . Furthermore, we can list the contribution to  $\text{Var}[Y]$  from each input. If the input  $Z_i$  contributes much to  $\text{Var}[Y]$ , we have much to gain from reducing the measurement error in  $Z_i$ . The reduction in  $\text{Var}[Y]$ , if we could eliminate the measurement error in  $Z_i$ , is equal to  $\text{Var}_{Z_i} [E_{Z_{\sim i}} [Y|Z_i]]$ , where  $Z_{\sim i}$  are all inputs except  $Z_i$ . The relative reduction in output uncertainty is

$$S_i = \frac{\text{Var}_{Z_i} [E_{Z_{\sim i}} [Y|Z_i]]}{\text{Var}[Y]}, \quad (18)$$

which is known as the first-order sensitivity index proposed in Sobol [29]. The same article defines the total sensitivity index  $S_{Ti}$  which also includes the interaction effect with other variables. The total index is the remaining output variance when we fix all inputs but  $Z_i$ . That is

$$S_{Ti} = 1 - \frac{\text{Var}_{Z_{\sim i}} [E_{Z_i} [Y|Z_{\sim i}]]}{\text{Var}[Y]}. \quad (19)$$

Sections 2.3 and 2.4 each provide a simulation method. When we talk about sensitivity indices for multiple cases,  $AS_i$  is the average index weighted by  $\text{Var}[Y]$  for each case. That is

$$AS_i = \frac{\sum_c S_i^c \text{Var}[Y_c]}{\sum_c \text{Var}[Y_c]}, \quad (20)$$



where  $S_i^c$  is the first-order sensitivity index of input  $Z_i$  for case  $c$ , and  $\text{Var} [Y_c]$  is the output variance for case  $c$ .

### 2.3. Monte Carlo methods

Monte Carlo methods treat the model as a black box. We get estimates for sensitivities by computing changes in the output for systematic changes to the input. This is done by dividing the samples into two parts. Let the first half of the sample be the matrix  $A$  and the second half  $B$ . Denote  $A_B^{(i)}$  a matrix equal to  $A$  but with column  $i$  from  $B$ . The preferred estimators for the mean output and output variance are the sample average and the unbiased sample variance. We will use estimators for the sensitivity indices based on the best practices discussed in Saltelli *et al.* [30]. Since the work in Sobol [29], improvements have been proposed in Saltelli [31] and Sobol *et al.* [32]. Further improvements for the first-order indices are suggested in Saltelli *et al.* [30]. The total indices are estimated as proposed in Jansen [33]. The estimators are

$$\bar{Y} = \frac{1}{n} \sum_{j=1}^n y(\mathbf{z}^{(j)}), \tag{21a}$$

$$\bar{\sigma}_Y^2 = \frac{1}{n-1} \sum_{j=1}^n \left( y(\mathbf{z}^{(j)}) - \bar{Y} \right)^2, \tag{21b}$$

$$\bar{S}_i = \frac{2}{\bar{\sigma}_Y^2 n} \sum_{j=1}^{n/2} y(B)_j \left( y(A_B^{(i)})_j - y(A)_j \right), \tag{21c}$$

$$\bar{S}_{Ti} = \frac{1}{\bar{\sigma}_Y^2 n} \sum_{j=1}^{n/2} \left( y(A_B^{(i)})_j - y(A)_j \right)^2, \tag{21d}$$

$$\bar{y}_{\alpha/2} = F_n^{-1}(\alpha/2), \tag{21e}$$

$$\bar{y}_{1-\alpha/2} = F_n^{-1}(1 - \alpha/2), \tag{21f}$$

where  $F_n$  is the empirical distribution of  $y(\mathbf{z}^{(j)})$  and  $1 - \alpha$  is the confidence level. The number of model evaluations with ten inputs is  $5n$  for  $A_B^{(i)}$  and  $n/2$  each for  $A$  and  $B$ . Thus, a total number of  $6n$  evaluations is required.

### 2.4. Polynomial chaos

When the model  $y$  is not on a simple explicit form, directly computing the distribution of  $y(\mathbf{Z})$  is not feasible. However, we can first approximate the model by a simplified version, namely a polynomial expansion. This is known as the general polynomial chaos (gPC) expansion. An introduction of gPC is found in the book of Xiu [34]. Let the polynomial expansion be

$$Y_p = \sum_{j=1}^p a_j \Phi_j(\mathbf{Z}), \tag{22}$$

where  $a_j$  are coefficients found by regression and  $\Phi_j(\mathbf{Z})$  are orthonormal polynomials constructed from three terms recursion. Orthonormality is not required but simplifies estimators. We terminate the recursion when it reaches the desired polynomial order. A high polynomial order corresponds to a close approximation, but note that the number of polynomials  $p = (10 + \text{order})! / (10! \text{order}!)$  grows

fast with the order. Next, we draw an input sample of size  $n$  as described in Section 2.2.3. Let  $\epsilon$  be the differences in output between the model and the expansion, that is

$$\begin{pmatrix} y(\mathbf{z}^{(1)}) \\ \vdots \\ y(\mathbf{z}^{(n)}) \end{pmatrix} = \begin{pmatrix} \Phi_1(\mathbf{z}^{(1)}) & \cdots & \Phi_p(\mathbf{z}^{(1)}) \\ \vdots & \ddots & \vdots \\ \Phi_1(\mathbf{z}^{(n)}) & \cdots & \Phi_p(\mathbf{z}^{(n)}) \end{pmatrix} \begin{pmatrix} a_1 \\ \vdots \\ a_p \end{pmatrix} + \begin{pmatrix} \epsilon_1 \\ \vdots \\ \epsilon_n \end{pmatrix}. \tag{23}$$

Ordinary least squares provides estimates  $\hat{a}_1, \dots, \hat{a}_p$ . These inserted in Equation (22) gives an explicit representation of the flow model. Furthermore, estimates for the statistics in Section 2.2.4 are

$$\tilde{Y} = \hat{a}_1, \tag{24a}$$

$$\tilde{\sigma}_Y^2 = \sum_{j=2}^p \hat{a}_j^2, \tag{24b}$$

$$\tilde{s}_i = \frac{1}{\tilde{\sigma}_Y^2} \sum_{j \in \mathcal{A}_i} \hat{a}_j^2, \tag{24c}$$

$$\tilde{s}_i = 1 - \frac{1}{\tilde{\sigma}_Y^2} \sum_{j \notin \mathcal{A}_i} \hat{a}_j^2, \tag{24d}$$

$$\tilde{y}_{\alpha/2} = F_p^{-1}(\alpha/2), \tag{24e}$$

$$\tilde{y}_{1-\alpha/2} = F_p^{-1}(1 - \alpha/2), \tag{24f}$$

where  $\mathcal{A}_i = \{j | \Phi_j(\mathbf{z}) = \Phi_j(z_i)\}$  is the set of polynomials depending solely on  $z_i$ , and  $F_p$  is the empirical distribution of  $Y_p$  for ten thousand Monte Carlo samples and  $1 - \alpha$  is the confidence level.

### 2.5. Simulations

The Monte Carlo simulations are initialized at 6000 samples and expanded by 30% for each iteration until estimates of Equation (21) converge. For both MC and PC, we define convergence as a change from previous iteration less than 0.01 for sensitivity indices and a relative change less than 0.01 for the mean, the variance and the quantiles.

For polynomial chaos, we first use order two and increase the order until estimates of Equation (24) converge. For each order, we increase the sample size repeatedly by  $p + 1$  until the fit on a test set does not longer improve. The test set consists of 6006 combinations of input, and we deem the fit satisfactory when the mean absolute deviation in the fitted output for consecutive iterations changes less than 20%. This indicates that we have enough evaluations of the model for an accurate polynomial approximation.

The pseudo-random sampling is most efficient if we first construct a large sample matrix and evaluate the point model for an incrementally larger subset when required. For PC, we construct a sample of size ten times the number of polynomials in the three terms recursion of order five. A sample size of 300,000 seems to suffice for the MC method.

## 3. Results

The input variables to the pipe flow model are listed in Table 1. From these variables, the point model predicts the liquid *holdup* (volume fraction) in the pipe and the *pressure drop* per meter. The input variables are taken from 240 gas-liquid experiments in a horizontal pipe from the SINTEF Multiphase Flow Laboratory. We compare the measured holdup and pressure drop with the results from the fluid model. The presented approach is implemented in Python 3.6, and the uncertainty analysis is based on the Python module *Chaospy* presented in Feinberg and Langtangen [35]. The uncertainty in each experiment is computed with Monte Carlo (MC) simulations and polynomial chaos (PC) expansions. The details on the uncertainty methods are given in Section 2.2.

### 3.1. Holdup

Figure 4 shows the estimated average sensitivity for the holdup predictions. The sensitivities quantify how sensitive the holdup predictions are to each input variable. In other words, it is the contribution of the uncertainty in each input to the uncertainty in holdup predictions. The estimated total sensitivity index and the estimated first-order index never differ more than 0.02. Thus, we use first-order indices in plots and refer to them simply as sensitivities. In the left panel, we see the averages weighted by the variance in each experiment. The right panel gives the plain averages with standard errors. The combined effect of liquid viscosity, pipe diameter and gas density account for ninety percent of the uncertainty in the holdup predictions. We have removed 7 out of the 240 cases from the results because the polynomial chaos expansions for pressure drop do not converge with polynomial order. The criteria for convergence is a change in estimates for the sensitivities, the output mean and the output variance from one order to the next less than 0.01. For the output mean and variance, we use the relative change. The criteria must be reached the latest at order 5. Table 3 contains information about the pressure drop statistics for the seven cases that do not converge. The holdup statistics actually change less than the threshold of 0.01, but we still exclude these results because we treat the pressure drop and the holdup as a joint variable in the simulations. For each case, we show the variable with the largest change from order 4 to 5 and the values of that variable for order 3, 4 and 5. All seven cases are on the border between two regimes, meaning that the model changes regime based on the sampled measurement error. The regimes assigned by the flow model are listed in the last column of the table.

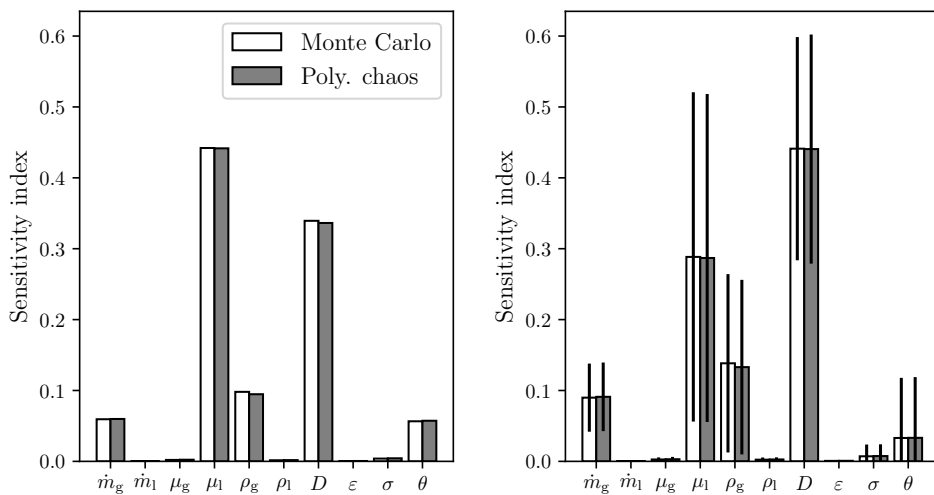


**Figure 4.** Holdup sensitivity estimates averaged over 233 experiments. *Left:* Weighted by the variance in each experiment. *Right:* Plain averages with standard error bars.

**Table 3.** Seven cases where the polynomial chaos expansions for pressure drop do not converge with polynomial order. The first column denotes the variable with the maximal change in the last iteration (absolute change for the sensitivities and relative change for the mean and the variance). The values of that variable for polynomial orders 3-5 are given in the next columns, and the last column gives the regime assigned by the flow model.

Variable	Polynomial order			Unit	Flow Regime
	3	4	5		
$S_D$	0.9961	0.9518	0.9882	—	Bubbly/slug
$S_{T,\mu}$	0.4814	0.5044	0.5215	—	Slug/stratified
Var $[\partial p/\partial x]$	24.214	24.906	25.196	Pa <sup>2</sup> /m <sup>2</sup>	Slug/stratified
Var $[\partial p/\partial x]$	28.301	29.042	31.399	Pa <sup>2</sup> /m <sup>2</sup>	Slug/stratified
Var $[\partial p/\partial x]$	217.10	291.76	269.55	Pa <sup>2</sup> /m <sup>2</sup>	Slug/stratified
Var $[\partial p/\partial x]$	514.15	528.26	521.32	Pa <sup>2</sup> /m <sup>2</sup>	Slug/stratified
Var $[\partial p/\partial x]$	5833.6	6555.0	6980.1	Pa <sup>2</sup> /m <sup>2</sup>	Bubbly/slug

Figure 5 provides a more refined view of the holdup sensitivities. Each panel gives the histogram of sensitivity to one input based on the 233 cases. We plot separate histograms for slug flow (blue) and stratified flow (red). Furthermore, we compare MC (solid lines) to PC (dotted). There are only small deviations between the two methods. Half of the input variables have sensitivities consistently under 2%. The gas mass rate and density are moderately sensitive, while the diameter and liquid viscosity are in some cases highly sensitive, but not for all cases.

We compare predicted holdup to measured holdup in Figure 6. Only cases with converging prediction intervals from both MC and PC are included. In the left panel, each experiment is drawn as a cross. The horizontal part represents measurement error, and the vertical part (much smaller) represents prediction uncertainty. To be more precise, the crosses are the measured holdup with two standard deviations either way and the predicted mean and interval from MC simulations. The standard deviation in holdup measurements is set to 0.03. Furthermore, the diagonal line is where measurements and predictions are equal, and cases where the uncertainty box does not cover this line are highlighted. All cases with over-predicted holdup are observed slug flow. Conversely, under-predicted cases are stratified. The 90% intervals do not cover the observations in 20 (10.3%) out of 194 cases, while the 95% intervals are off in 12 (11.4%) out of 105 cases.

The right panels of Figure 6 show the relative difference in the PC predictions and MC predictions. The mean holdup (solid line) is very similar, the upper quantile (dashed) is slightly larger, and the lower quantile (dash-dotted) is slightly smaller with PC. Thus, the PC predictions are overall similar to those of MC, but the intervals are wider.

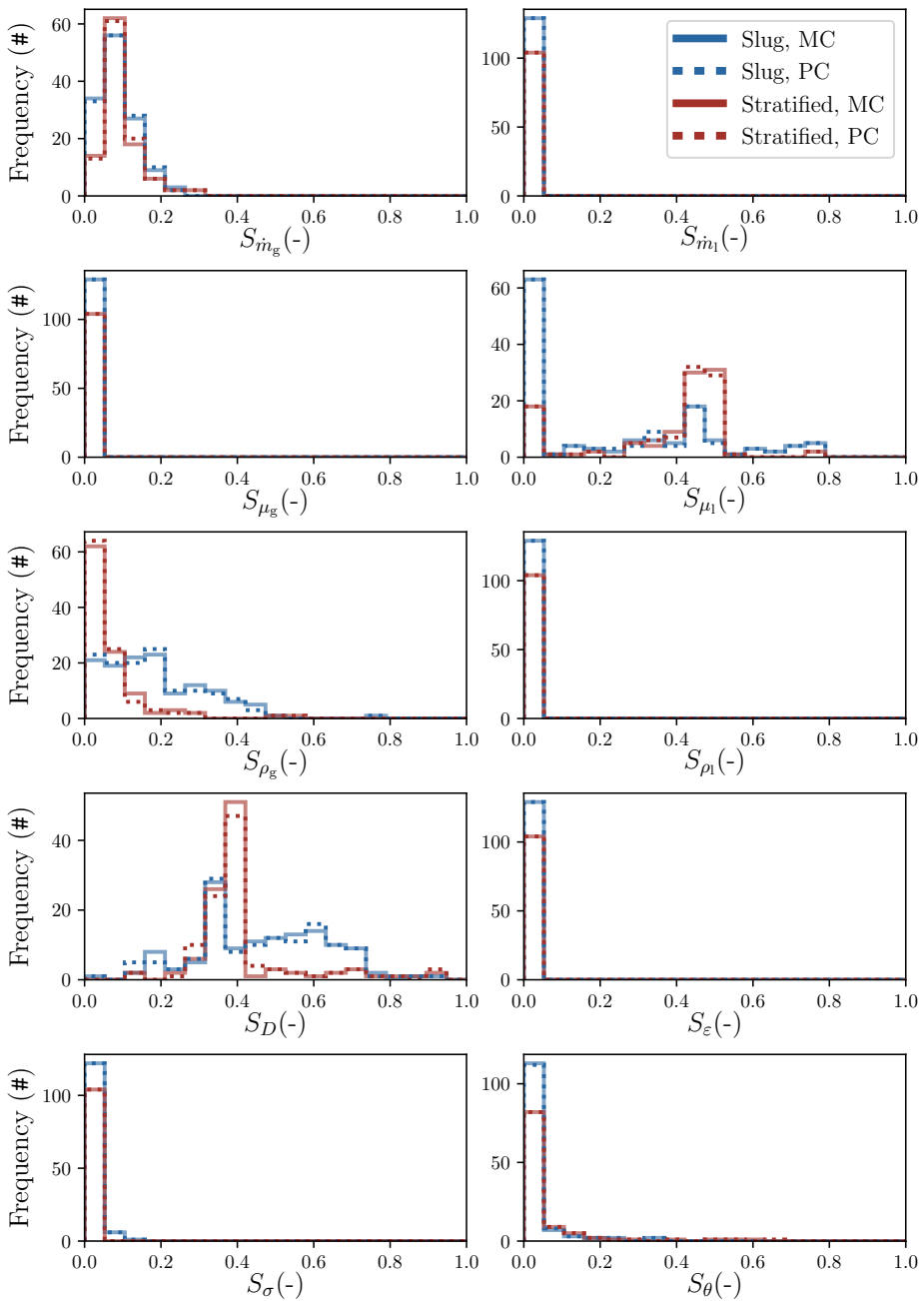
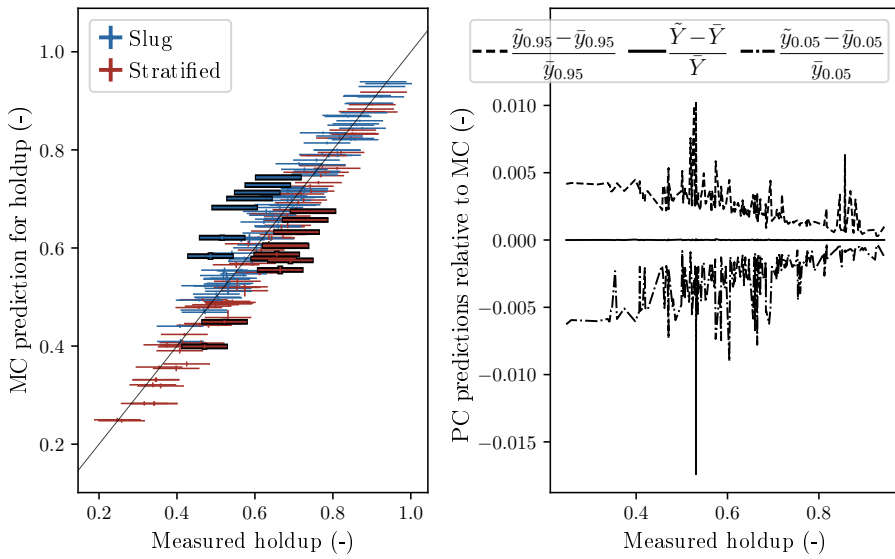
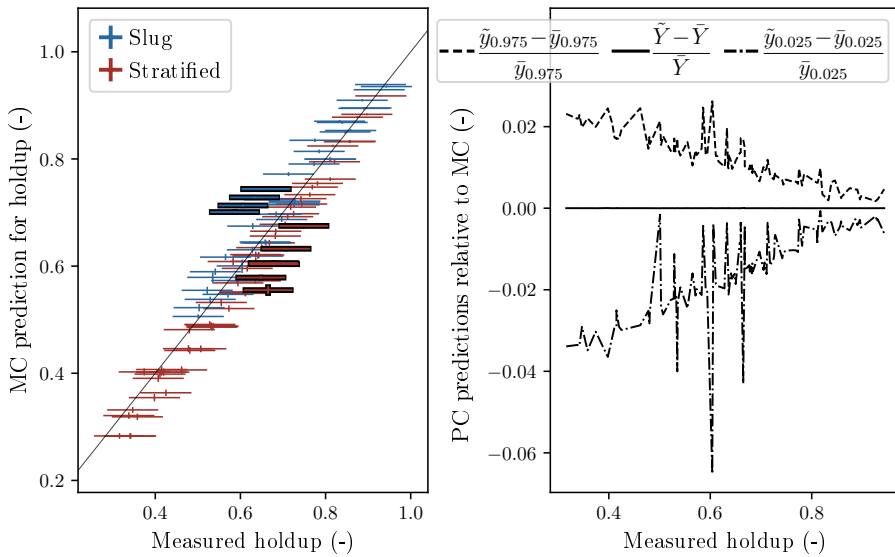


**Figure 5.** Frequency histograms of the holdup sensitivity estimates across 233 experiments. The sensitivity distribution for one input variable is given in each panel. The experiments are categorized as slug (blue) or stratified (red) and we compare estimates from Monte Carlo (solid lines) and PC (dotted).



(a) 90% prediction intervals.



(b) 95% prediction intervals.

**Figure 6.** *Left:* Predicted versus measured holdup for 194 experiments. The diagonal line is where the coordinates are equal, and cases with a discrepancy between prediction and observation are highlighted. The first axis gives measured value with two standard errors either way. The second axis is predicted mean, lower quantile and upper quantile. Slug experiments are blue and stratified ones are red. *Right:* The relative difference in PC predictions compared to MC predictions with respect to measured holdup. Upper quantiles (dashed), means (solid) and lower quantiles (dash-dotted).

### 3.2. Pressure drop

As for holdup, we summarize the pressure drop results in terms of sensitivity and prediction. The averaged sensitivities are given in Figure 7. The weighted average is similar to the plain average. The uncertainty in the diameter measurement is responsible for 90 percent of the uncertainty in pressure drop predictions. The liquid viscosity also contributes, and in some low-variance cases, the pipe inclination. Figure 8 shows the sensitivities by regime. The distributions of sensitivities are similar for stratified flow and slug flow.

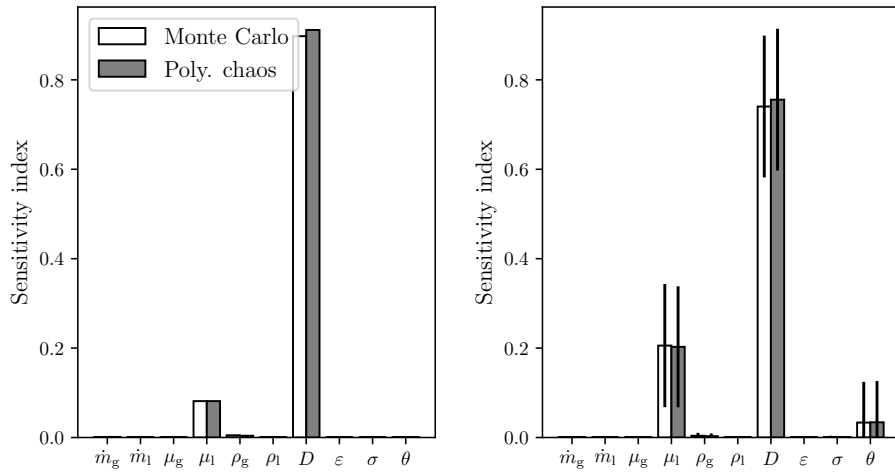


**Figure 7.** Pressure drop sensitivity estimates averaged over 233 experiments. *Left:* Weighted by the variance in each experiment. *Right:* Plain averages with standard error bars.

Pressure drop predictions are compared to measurements in Figure 9. Only converged cases are included. The prediction uncertainty is much larger than the measurement uncertainty and increases with the pressure drop. The model under-predicts the pressure drop for small values and over-predicts for large values. The pressure drop predictions are much less accurate than the holdup predictions. The 90% intervals are off in 126 (64.9%) out of 194 cases, while the 95% intervals are off in 62 (59.0%) out of 105 cases.

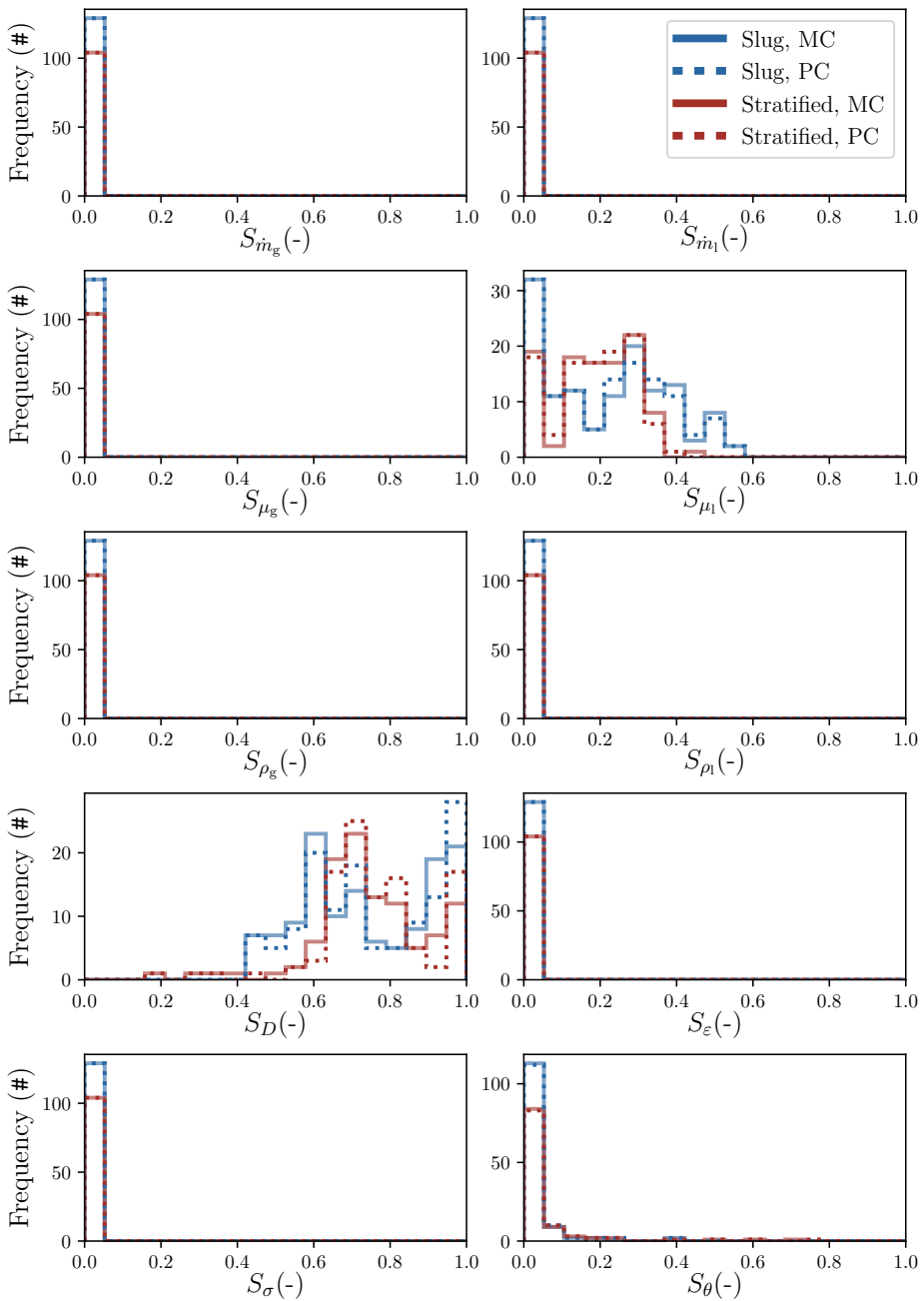
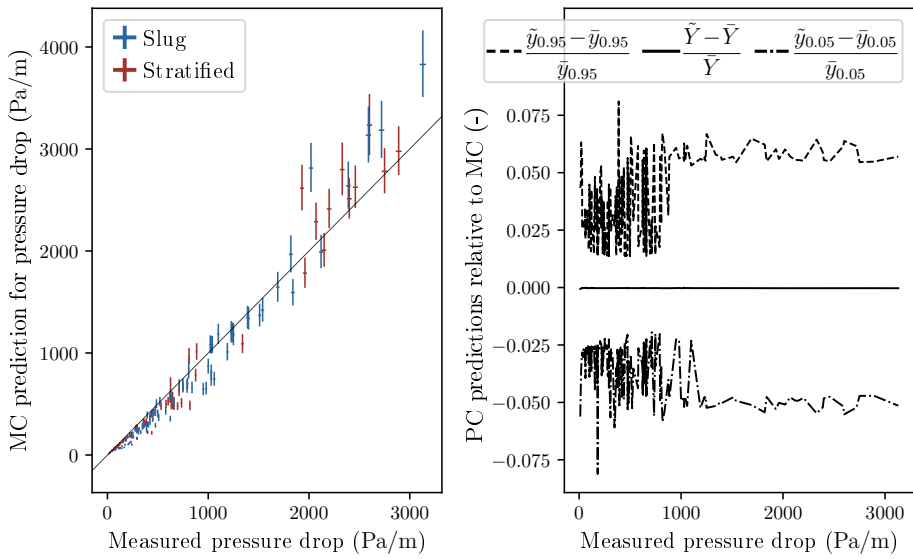
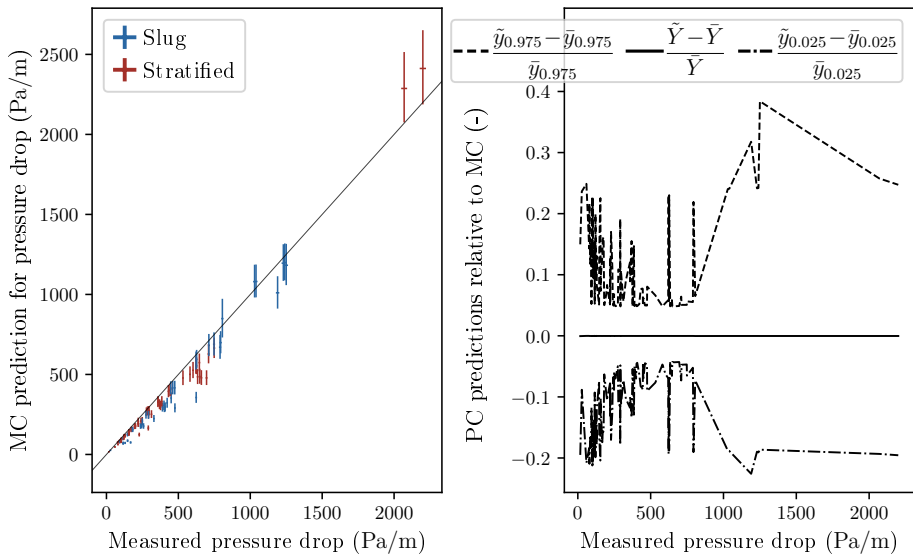


**Figure 8.** Frequency histograms of the pressure drop sensitivity estimates across 233 experiments. The sensitivity distribution for one input variable is given in each panel. The experiments are categorized as slug (blue) or stratified (red), and we compare estimates from Monte Carlo (solid lines) and PC (dotted).





(a) 90% prediction intervals.



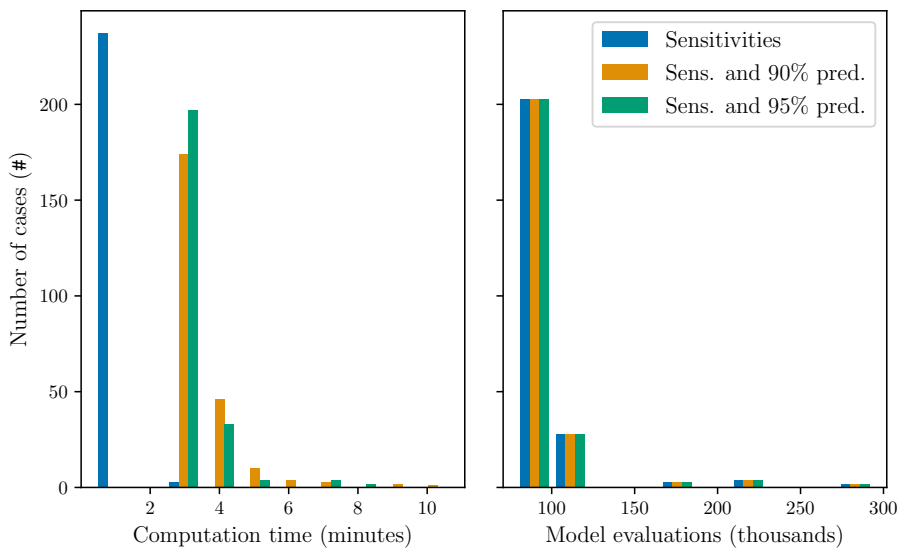
(b) 95% prediction intervals.

**Figure 9.** *Left:* Predicted versus measured pressure drop for 194 experiments. The diagonal line is where the coordinates are equal. The first axis gives measured value with two standard errors either way. The second axis is predicted mean, lower quantile and upper quantile. Slug experiments are blue, and stratified ones are red. *Right:* The relative difference in PC predictions compared to MC predictions with respect to measured pressure drop. Upper quantiles (dashed), means (solid) and lower quantiles (dash-dotted).

### 3.3. Computational cost

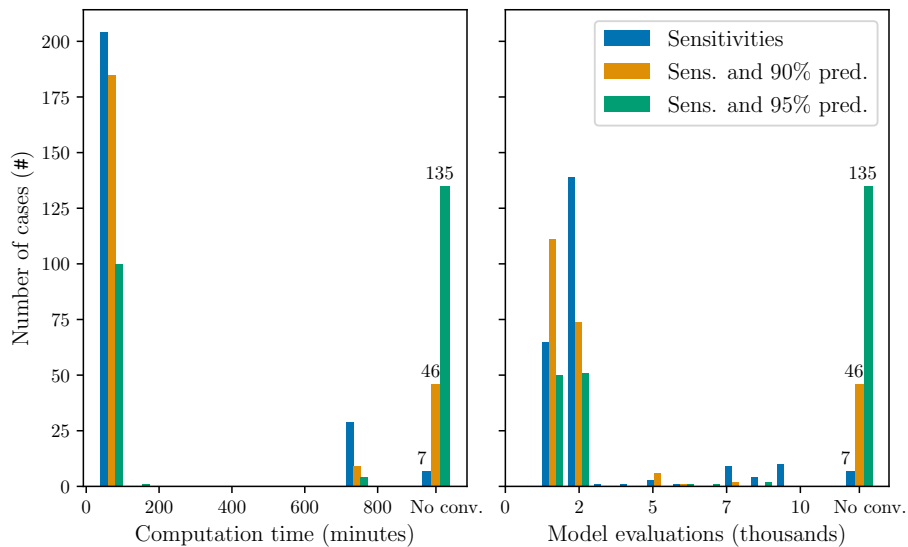
The computational cost of the Monte Carlo simulations is mainly from evaluating the model many times. The polynomial chaos expansion requires fewer model evaluations but also involves large regressions to obtain expansion coefficients. In Figure 10, the computation time (left) and number of model evaluations (right) required for convergence are compared between MC and PC. The colors represent the criteria used for convergence. Blue is only convergence in sensitivities while orange and green is the cost if we also want convergence in prediction intervals on confidence level 90% and 95%, respectively. All cases converge for MC while some do not for PC. The number of cases without convergence is given as an entry on the right hand side. Notice the different scales on the axes for MC and PC.

The computation time is obtained from timing python scripts on the Norwegian HPC infrastructure. We run one MC script and one PC script for each of the 240 cases for each of the three convergence criteria. We terminate each uncertainty analysis at convergence or after 15 hours. Thus, the maximum total computation time is  $2 \cdot 240 \cdot 3 \cdot 15 \text{ h} = 900 \text{ days}$ . However, because we can run hundreds of scripts in parallel and many cases finish soon, the results are available after one day. We have also implemented the option of parallel evaluations of the model within each script, but chose serial evaluation for this comparison.



(a) Monte Carlo.

Figure 10. Cont.



(b) Polynomial chaos.

**Figure 10.** Frequency histogram of computational cost across 240 experiments. Each color is one type of simulation criterion, namely only convergence in sensitivities (blue) or also 90% prediction intervals (orange) or 95% (green). The number of cases that did not converge is given as an entry on the right. *Left:* Computation time. *Right:* Number of model evaluations.

#### 4. Discussion

The sensitivity estimates are similar using Monte Carlo or polynomial chaos. The averages  $AS_i$  gives the clearest picture as they measure how much uncertainty each input brings to the output estimates across all cases. From the first panels of Figures 4 and 7, we see that the pipe diameter and liquid viscosity are important for both pressure drop and holdup, while the gas mass rate, gas density and pipe inclination only matters for the holdup estimates. We can utilize the sensitivity indices for efficiently reducing the uncertainty in the output estimates. The focus should be on reducing the measurement error of the most sensitive variables; in this case, the pipe diameter and the liquid viscosity. Reducing uncertainty in measurements of these variables will efficiently improve predictions. Keep in mind that sensitivity indices are not general but depend on the flow conditions. See Smith *et al.* [12] for a description of the experiments. The results can not directly be extrapolated to different experiments. A new analysis is required, but the methods described in Section 2 may be applied.

Also note that because first-order and total indices are similar, there are no decisive uncertainty interactions. Furthermore, we cannot conclude that the flow regime is important for sensitivity estimates.

The sensitivities are similar across each regime. However, the moments of the polynomial chaos expansions do not converge with order for some cases on the boundary between regimes. Two cases are on the boundary bubbly/slug and neither converge with PC. Among 24 cases on the boundary slug/stratified, five cases do not converge with PC. Thus, the current implementation of PC expansions is unreliable on the regime boundaries. The expansions do not capture the behavior of the flow model well on the boundaries because the model is not smooth there. Adding higher-order terms to the expansion would make the expansion better resemble non-smooth behavior, but this is not immediately possible due to computational expense. It is possible to construct high-order approximations with low complexity by applying variable selection, but this approach is less applicable.

We have also explored the technical details in the uncertainty computations, specifically the performance of Monte Carlo simulations compared to that of polynomial chaos methods. For the fluid model in question, we clearly prefer MC because this method provides uncertainty estimates for all cases, and it does so in the least amount of time. In contrast, PC fails in many cases and has a larger computation cost. The strength of PC lies in the low number of required model evaluations. Compared to MC, polynomial chaos is likely to perform better if the fluid model required more time for each evaluation.

We have compared measured holdup with predicted holdup accounting for uncertainty in both. The equivalent comparison was applied to the pressure drop. The holdup prediction matches the measured values well. We can observe that over-predicted cases are slug flow and under-predicted cases are stratified. The predictions of pressure drops are less accurate, with under-prediction for small values and over-prediction for large pressure drops. There is a clear bias in the estimates, which suggests there are physics that are not captured by the model. The authors of Smith *et al.* [36] pointed to the over-prediction of the slug velocity variable  $C_0$ . The claim is supported by follow-up experiments, which they discuss in their Section 3.4.

In summary, estimates for sensitivities and output predictions using MC are similar to those of PC, and the pipe diameter and the liquid viscosity have the largest sensitivity indices. The Monte Carlo method is preferred because it is more robust and requires less time. This conclusion applies to the flow model used and the implementation of each uncertainty method. The uncertainty analysis also provides evidence that holdup predictions are accurate, while pressure drop predictions are biased.

#### 4.1. Future research

We have seen that half of the input variables contribute less than 2% to the output uncertainty in all cases. For polynomial chaos, it is possible to construct the polynomial approximation by attempting to prioritize the important variables. One idea is to iteratively introduce higher order polynomials in significant variables. This way, we can reach a sufficiently high polynomial order without introducing too many regressors.

Applying the methods of Hoyer *et al.* [5] to create probability distributions for closure laws will make the analysis of the uncertainty in the flow model more complete. Currently, the closure laws are treated as known. We think it is possible to tune the closure law distributions by comparing the output predictions with measurements. An applicable tuning method is the minimum continuous ranked probability score (CRPS) estimation, as demonstrated in Gneiting *et al.* [37].

**Author Contributions:** Conceptualization, A.S., I.S. and L.R.H.; methodology, A.S., I.E.S., T.E.U., I.S. and L.R.H.; software, A.S. and I.E.S.; validation, A.S.; formal analysis, A.S.; investigation, I.E.S. and T.E.U.; resources, A.S., I.E.S. and T.E.U.; data curation, A.S.; writing—original draft preparation, A.S.; writing—review and editing, A.S., I.E.S., T.E.U. I.S. and L.R.H.; visualization, A.S.; supervision, A.S., I.S. and L.R.H.; project administration, A.S.; funding acquisition, I.S. and L.R.H. All authors have read and agreed to the published version of the manuscript.

**Funding:** This work is part of the project SUM (Scaling and Uncertainties in Multiphase Flow), which is supported by the Norwegian Research Council grant number 267620 and industrial partners from SINTEF, IFE and MULTIFLOW JIP (Schlumberger Information Solution, Equinor, Lundin Norway, LedaFlow Technologies DA, Gassco, ENI Norge and TechnipFMC).

**Acknowledgments:** Computational resources in Norwegian HPC infrastructure were granted by the Research Council of Norway project nr. NN9545K. Dept. of Process Technology at SINTEF Industry and Dept. of Flow Technology at Institute for Energy Technology have supported the discussion on multiphase flow. SINTEF Industry and Equinor made the data available. The colleagues at the Division of Biomechanics have been important in the scientific discussion, and Fredrik E. Fossan contributed in preparing the manuscript for publication.

**Conflicts of Interest:** The authors declare no conflict of interest.

#### References

1. Lee, S.H.; Chen, W. A comparative study of uncertainty propagation methods for black-box-type problems. *Struct. Multidiscip. Optim.* **2009**, *37*, 239.

2. Cremaschi, S.; Kouba, G.E.; Subramani, H.J. Characterization of confidence in multiphase flow predictions. *Energ. Fuel.* **2012**, *26*, 4034–4045.
3. Holm, H.; Saha, P.; Suleymanov, V.; Vanvik, T.; Hoyer, N. Shtokman flow assurance challenges—a systematic approach to analyze uncertainties—Part 1. In Proceedings of the 15th International Conference on Multiphase Production Technology, Cannes, France, 15–17 June, 2011.
4. Holm, H.; Saha, P.; Suleymanov, V.; Vanvik, T.; Hoyer, N. Shtokman flow assurance challenges—a systematic approach to analyze uncertainties—Part 2. In Proceedings of the 15th International Conference on Multiphase Production Technology, Cannes, France, 15–17 June, 2011.
5. Hoyer, N.; Kirkedelen, M.; Biberg, D.; Johnson, G.; Valle, A.; Johansson, P.; Nossen, J. A structured approach for the evaluation of uncertainties in flow assurance systems. In Proceedings of the 16th International Conference on Multiphase Production Technology, Cannes, France, 12–14 June, 2013.
6. Klavetter, K.; Posluszny, D.; Warr, J.; Cremaschi, S.; Sarica, C.; Subramani, H. Uncertainty analysis of multiphase flow models: a comparison of three propagation approaches. In Proceedings of the 8th North American Conference on Multiphase Technology, Banff, Canada, 20–22 June, 2012.
7. Keinath, B. Decision analysis in multiphase flow: uncertainty, risk and application. In Proceedings of the 18th International Conference on Multiphase Production Technology, Cannes, France, 7–9 June, 2017.
8. Liu, Y.; Dinh, N.T.; Smith, R.C.; Sun, X. Uncertainty quantification of two-phase flow and boiling heat transfer simulations through a data-driven modular Bayesian approach. *Int. J. Heat. Mass. Tran.* **2019**, *138*, 1096–1116.
9. Picchi, D.; Poesio, P. Uncertainty quantification and global sensitivity analysis of mechanistic one-dimensional models and flow pattern transition boundaries predictions for two-phase pipe flows. *Int. J. Multiphas. Flow* **2017**, *90*, 64–78.
10. Klinkert, J. The characterization of Uncertainty for Steady State Multiphase Flow Models in Pipelines. Master’s Thesis, Delft University of Technology, Delft, The Netherlands, 19 January 2018.
11. Lataniotis, C.; Marelli, S.; Sudret, B. Uqlab User Manual—The Input Module. 2015. Available online: [https://www.researchgate.net/profile/Bruno\\_Sudret/publication/281232688\\_UQLab\\_user\\_manual\\_-\\_the\\_INPUT\\_module/links/55dc1df708ae9d6594937608.pdf](https://www.researchgate.net/profile/Bruno_Sudret/publication/281232688_UQLab_user_manual_-_the_INPUT_module/links/55dc1df708ae9d6594937608.pdf) (accessed on 26 February 2020).
12. Smith, I.E.; Nossen, J.; Unander, T.E. Improved holdup and pressure drop predictions for multiphase flow with gas and high viscosity oil. In Proceedings of the 16th International Conference on Multiphase Production Technology, Cannes, France, 12–14 June, 2013.
13. Lichota, P.; Szulczyk, J.; Tischler, M.B.; Berger, T. Frequency Responses Identification from Multi-Axis Maneuver with Simultaneous Multisine Inputs. *J. Guid. Contr. Dynam.* **2019**, *42*, 2550–2556.
14. Lichota, P.; Noreña, D.A. A priori model inclusion in the multisine maneuver design. In Proceedings of the 17th International Carpathian Control Conference (ICCC), Tatranska Lomnica, Slovakia, 29 May–1 June 2016; pp. 440–445.
15. Chen, S.; Wang, X.; Harris, C.J. NARX-based nonlinear system identification using orthogonal least squares basis hunting. *IEEE Trans. Contr. Syst. Tech.* **2007**, *16*, 78–84.
16. Efremov, A. *System Identification Based on Stepwise Regression for Dynamic Market Representation*. International Conference on Data Mining and Knowledge Engineering: Rome, Italy, 29 April 2010; Volume 4, 28–30.
17. Dukler, A.E.; Hubbard, M.G. A model for gas-liquid slug flow in horizontal and near horizontal tubes. *Ind. Eng. Chem. Fund.* **1975**, *14*, 337–347.
18. Gregory, G.; Nicholson, M.; Aziz, K. Correlation of the liquid volume fraction in the slug for horizontal gas-liquid slug flow. *Int. J. Multiphas. Flow* **1978**, *4*, 33–39.
19. Kora, C.; Sarica, C.; Zhang, H.q.; Al-Sarkhi, A.; Al-Safran, E. Effects of high oil viscosity on slug liquid holdup in horizontal pipes. In Proceedings of the Canadian Unconventional Resources Conference, Calgary, Canada, 15–17 November 2011.
20. Bendiksen, K.H. An experimental investigation of the motion of long bubbles in inclined tubes. *Int. J. Multiphas. Flow* **1984**, *10*, 467–483.
21. Jeyachandra, B.; Gokcal, B.; Al-Sarkhi, A.; Sarica, C.; Sharma, A. Drift-velocity closure relationships for slug two-phase high-viscosity oil flow in pipes. *SPE J.* **2012**, *17*, 593–601.
22. Nuland, S. Bubble front velocity in horizontal slug flow with viscous Newtonian, shear thinning and Bingham fluids. In Proceedings of the 3rd International Conference on Multiphase Flow (ICMF’98), Lyon, France, 8–12 June 1998.

23. Hinze, J.O. *Turbulence*; McGraw-Hill: New York, NY, USA, 1975; Volume 2.
24. Andreussi, P.; Persen, L. Stratified gas-liquid flow in downwardly inclined pipes. *Int. J. Multiphas. Flow* **1987**, *13*, 565–575.
25. White, F.M. *Fluid mechanics*; McGraw-Hill: New York, NY, USA, 2011.
26. Brkić, D.; Praks, P. Accurate and efficient explicit approximations of the Colebrook flow friction equation based on the Wright  $\omega$ -function. *Mathematics* **2019**, *7*, 34.
27. Khaledi, H.A.; Smith, I.E.; Unander, T.E.; Nossen, J. Investigation of two-phase flow pattern, liquid holdup and pressure drop in viscous oil–gas flow. *Int. J. Multiphas. Flow* **2014**, *67*, 37–51.
28. ISO, I.; OIML, B. Guide to the Expression of Uncertainty in Measurement. 1995. Available online: [https://www.bipm.org/utis/common/documents/jcgm/JCGM\\_100\\_2008\\_E.pdf](https://www.bipm.org/utis/common/documents/jcgm/JCGM_100_2008_E.pdf) (accessed on 26 February 2020).
29. Sobol, I.M. Sensitivity estimates for nonlinear mathematical models. *Math. Model. Comput. Exp.* **1993**, *1*, 407–414.
30. Saltelli, A.; Annoni, P.; Azzini, I.; Campolongo, F.; Ratto, M.; Tarantola, S. Variance based sensitivity analysis of model output. Design and estimator for the total sensitivity index. *Comput. Phys. Comm.* **2010**, *181*, 259–270.
31. Saltelli, A. Making best use of model evaluations to compute sensitivity indices. *Comput. Phys. Comm.* **2002**, *145*, 280–297.
32. Sobol, I.M.; Tarantola, S.; Gatelli, D.; Kucherenko, S.; Mauntz, W.; others. Estimating the approximation error when fixing unessential factors in global sensitivity analysis. *Reliab. Eng. Syst. Saf.* **2007**, *92*, 957–960.
33. Jansen, M.J. Analysis of variance designs for model output. *Comput. Phys. Comm.* **1999**, *117*, 35–43.
34. Xiu, D. *Numerical methods for stochastic computations: a spectral method approach*; Princeton university press: Princeton, NJ, USA, 2010.
35. Feinberg, J.; Langtangen, H.P. Chaospy: An open source tool for designing methods of uncertainty quantification. *J. Comput. Sci.* **2015**, *11*, 46–57.
36. Smith, I.E.; Nossen, J.; Kjølås, J.; Lund, B. Development of a Steady-State Point Model for Prediction of Gas/Oil and Water/Oil Pipe Flow. *J. Dispers. Sci. Technol.* **2015**, *36*, 1394–1406.
37. Gneiting, T.; Raftery, A.E.; Westveld III, A.H.; Goldman, T. Calibrated probabilistic forecasting using ensemble model output statistics and minimum CRPS estimation. *Mon. Weather Rev.* **2005**, *133*, 1098–1118.

**Sample Availability:** Code and data are available online: <https://dataverse.no/dataset.xhtml?persistentId=doi:10.18710/OWKABR>.



© 2020 by the authors. Licensee MDPI, Basel, Switzerland. This article is an open access article distributed under the terms and conditions of the Creative Commons Attribution (CC BY) license (<http://creativecommons.org/licenses/by/4.0/>).

Chapter **7**

# Closure Law Model Uncertainty Quantification

The content of this chapter was published in  
*International Journal for Uncertainty Quantification*, 2021.

**Paper 2: Closure Law Model Uncertainty Quantification**

*A. Strand, J. Kjølaas, T.H. Bergstrøm, I. Steinsland, L.R. Hellevik*

Chapter **8**

# Repeatability in a Multiphase Pipe Flow Case Study

The content of this chapter was accepted for publication in  
*International Journal of Multiphase Flow*, 2021.

**Paper 3: Repeatability in a Multiphase Pipe Flow Case Study**

*A. Strand, C. Brekken, P.R. Leinan, I. Steinsland, L.R. Hellevik*



# Repeatability in a multiphase pipe flow case study

Andreas Strand<sup>a</sup>, Christian Brekken<sup>b</sup>, Paul Roger Leinan<sup>b</sup>, Ingelin Steinsland<sup>c</sup>, Leif Rune Hellevik<sup>a</sup>

<sup>a</sup>*Biomechanics Division, Department of Structural Engineering, Faculty of Engineering, NTNU*

<sup>b</sup>*Multiphase Flow, Department of Process Technology, SINTEF AS*

<sup>c</sup>*Statistics Group, Department of Mathematical Sciences, Faculty of Information Technology and Electrical Engineering, NTNU*

---

## Abstract

A high degree of repeatability is most often an underlying assumption for research and development based on multiphase flow experiments. In this paper repeatability in multiphase flow experiments are studied through an experimental campaign with 28 replicates for 11 unique settings.

The experiments were conducted in a flow loop with multiple injections of oil, water and air. A high degree of repeatability was found, with relative replicate deviations in volume flow rates and pressure drops of 0.1 % in magnitude. Further, several potential causes of replicate deviations were studied, and firmer control of temperature of the inflow fluids is proposed as a means to improve repeatability in volume flow rates and pressure.

We conclude that for practical use, the presented category of multiphase experiments sufficiently meets underlying repeatability assumptions.

*Keywords:* multiphase flow, repeatability, uncertainty, pipe flow

---

## 1. Introduction

Multiphase flow in pipelines occur in many industrial applications and is especially important in the oil and gas industry [1, 2, 3, 4]. Challenges of multiphase flow in pipes or channels include how the distribution of the phases in the cross section depends on the inflow rates, operational conditions, and thermodynamic state, leading to different multiphase flow regimes. With that in mind, models and simulators for multiphase flow in pipelines play important roles in hydrocarbon production, both during the field development and planning stage, and to ensure favorable flow conditions in the short- and long-term operation of pipelines. [5, 6]. Laboratory experiments support design and operation of field pipelines, either through tuning of simulator, calibration of experiments or otherwise representing the full-scale flow. Consequently, firm control and precision in the laboratory setting is essential for valid transfer to industry applications.

The development of models and simulators for multiphase flow in pipelines requires extensive high quality experimental data to cover a large span of the

possible flow conditions may occur in field in practice [7]. In multiphase experiments it is common not to repeat an experiment for a given setting, or to have only a few repeated experiments for some settings in an experimental campaign [8, 9, 10, 11]. This practice relies on an implicit assumption that performing the same experiment will give the same, or very similar, outcomes for the quantities of interest.

Repeatability is defined as measurement precision under conditions that include the same measurement procedure, same operators, same measuring system, same operating conditions and same location, and replicate measurements on the same or similar objects over a short period of time [12]. In this paper the aim is to study repeatability in a multiphase flow loop. To our knowledge there are no previous large studies of the implicit assumption of high degree of repeatability in multiphase pipe flow experiments.

We present highly unique experiments in a fixed multiphase pipe flow loop. A test matrix of 11 unique settings was replicated up to 28 times over the course of seventeen days. The experiments originally formed the foundation of a performance study of independent non-intrusive sensors where it was essential to provide identical volume flow rates of oil, water and air for each distinct setting repeatedly. The resulting data offered a rare opportunity to study repeatability of multiphase pipe flow experiments given instrumentation uncertainty, operational conditions and inflow conditions. In the described setup the mass flow rates were under automated regulation whereas pressure and temperature was not, apart from control of ambient temperature in the laboratory hall. Changes in fluid properties over time was also a factor to consider, especially for air and tap water.

The pipe inlet and outlet pressures along with volume flow rates were the primary quantities of interest. The main tasks were to (1) quantify repeatability of pressure measurements, (2) quantify repeatability of volume flow rates and (3) study possible causes of variation in pressure and volume flow rates through statistical modeling, using measurements of temperature, density, flow and pressure at multiple locations.

## 2. Experiments

The experiments were conducted at the SINTEF Multiphase Flow Laboratory. See Figure 1 for a simplified drawing of the flow loop setup. The  $+2^\circ$  inclined flow loop steel pipe test section consisted of

- a 49 m long fully welded inner pipe of inner/outer diameter 127.1/141.3 mm, with a 4.5 m long specially designed central inner pipe of inner/outer diameter 87.3/114.3 mm fitted to the main inner pipe by 127 mm long reducers; the central inner pipe had a perforated section consisting of 22 axial slits of dimensions  $6.5 \times 82.5$  mm covering the pipe circumference to allow fluid flow into the base pipe from an external annular space;

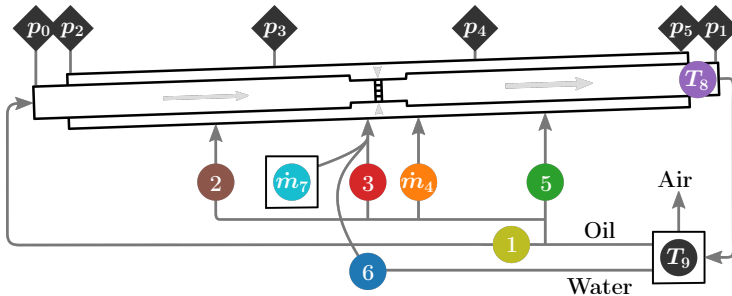


Figure 1: The laboratory setup. A pipe of length 49 m encases another pipe. The pipes are coaxial with inclination of  $2^\circ$  upward. The diameters are amplified 20 times in the drawing compared to length. The main flow runs through the inner pipe. Secondary flow is injected into the annulus and enters the inner pipe through a perforation in the center. The flow components are oil (1, 2, 3, 4, 5), water (6) and air (7). During each cycle, the fluids mix and separate (9). The circles are meters for mass rate, density and/or temperature. The black diamonds are pressure meters, where  $p_2$ ,  $p_3$ ,  $p_4$  and  $p_5$  are annulus pressures.

Table 1: Fluid system. Physical properties at  $20^\circ\text{C}$ .

Fluid	Viscosity [Pa s]	Density [ $\text{kg}/\text{m}^3$ ]
Exxsol D60	$1.39 \cdot 10^{-3}$	786
Tap water	$1.00 \cdot 10^{-3}$	1000
Air	$1.83 \cdot 10^{-5}$	1.204

- a 49 m long flanged outer pipe of inner/outer diameter 215.1/219.1 mm covering the inner pipe and defining an annular space between the coaxial inner and outer pipes; and
- 4 injection points at different axial locations along the test section for injection of fluids into the annular space. Upstream each injection point, a skid with regulation valves and flow meters controlled the mass inflow rates.

The box in Figure 1 labeled  $T_9$  represents a separation process, where fluids entered on the right-hand side. The upwards arrow represents air release, the line to 1 is oil and the line to 6 is water. The oil flow branched into the main flow 1 and the injection points 2, 3, 4 and 5. Air from 7 and water from 6 also entered at injection point 3. Exxsol D60 was used for the oil. The fluid properties at  $20^\circ\text{C}$  are listed in Table 1.

### 2.1. Variables

The experiments were monitored by non-intrusive instruments, and their locations are shown Figure 1. The black diamonds correspond to pressure meters, where  $p_0$  is inlet,  $p_1$  is outlet, and  $p_2$ ,  $p_3$ ,  $p_4$  and  $p_5$  are on the annulus. The remaining instruments are drawn as circles, numbered 1–9. Instruments  $\dot{m}_4$  and

Table 2: Measured variables with symbols, units and std. deviations of measurement errors.

Variable	Symbol	Unit	Standard deviation ( $\sigma$ )
Pressure	$p$	Pa/m	$p \cdot 0.09\%$
Air mass rate	$\dot{m}_7$	kg/s	$\dot{m}_7 \cdot 1.5\%$
Liquid mass rate	$\dot{m}$	kg/s	$\dot{m} \cdot 0.3\%$
Liquid density	$\rho$	kg/m <sup>3</sup>	1 kg/m <sup>3</sup>
Temperature	$T$	°C	0.21 °C

$\dot{m}_7$  are mass rate meters. Locations 1, 2, 3, 5 and 6 each have meters for mass rate, density and temperature. Instrument  $T_8$  is the outlet thermometer and  $T_9$  is the separator thermometer.

All the measured variables with symbols and units are listed in Table 2. The measurements were associated with some error, with presumed standard deviations  $\sigma$  given in the last column of the table. In short, the standard deviations are quantified by the laboratory staff according to product specifications and experiments [13]. The errors represent deviation from the physical value [14]. In addition, the physical values fluctuated slightly over a logging time of 5–10 min despite verification of a virtually steady state. Additional details on instrumentation are given in Appendix A.

## 2.2. Experimental design

The mass rates at locations 1–7 were kept close to target levels by closed-loop control. Henceforth, one combination of target mass rates is called a setting. Eleven settings were used as shown in Table 3, each replicated up to 28 times. The column labeled ‘Oil 1’ gives the target main flow, which was alike for all settings. The remaining columns give the rates of injection into the annulus, where ‘–’ corresponds to no injection at the given location. Additionally, setting 4 included 0.014 kg/m<sup>3</sup> sand and settings 5–7 included 0.057 kg/m<sup>3</sup> sand from annulus, but any impact from sand was not studied in this work.

On February 11, 2020 setting 1 was initialized. Steady-state was achieved after a couple of minutes, and then one set of measurements were made. Next, setting 2 was initialized, steady-state achieved and measurements made. The process continued according to numbering, and eventually setting 11 was measured. Thus far, one replicate of each setting was obtained. Again setting 1 was initialized, followed by the same steps as above. The process lasted until 28 replicates of each setting was obtained, at February 28, 2020. Experiments disrupted by any process deviation were pruned. Certain process deviations were deliberate choices to study other mass rates, but details are not disclosed here.

In effect, the flow loop was reset between each run of the same setting. It is then correct to call each run a *replicate* rather than a repeat [15]. Yet, it is customary to use the term *repeatability* for the closeness of replicates, as explained in Section 3.

In terms of notation, let  $i = 1, 2, \dots, 11$  be the setting index and let  $j = 1, 2, \dots, n_i$  be the replicate index. Furthermore, index  $k$  refers to location as

Table 3: Target mass rates of the experimental design. Eleven settings indexed in the first column. The number of replicates for each setting is given in column two. Columns 3–8 gives the mass rates in kg/s at each location. The value ‘–’ corresponds to zero.

Setting	# replicates	Oil 1	Oil 2	Oil 3	Oil 4	Oil 5	Water (6)	Air (7)
1	28	4.318	–	–	–	–	–	–
2	28	4.318	0.720	0.720	–	0.720	–	–
3	26	4.318	0.720	2.159	–	0.720	–	–
4	26	4.318	0.720	0.720	–	0.720	–	–
5	27	4.318	0.720	0.720	–	0.720	–	–
6	26	4.318	0.720	0.720	–	0.720	–	–
7	28	4.318	0.720	0.720	0.720	0.720	–	–
8	26	4.318	–	–	–	–	2.746	–
9	23	4.318	–	1.079	–	–	1.373	–
10	28	4.318	–	–	–	–	1.373	–
11	28	4.318	0.720	0.720	0.720	0.720	–	0.02087

given in Figure 1. Observations are written as  $x_{ijk}$  where  $x$  is pressure ( $p$ ), mass rate ( $\dot{m}$ ), density ( $\rho$ ) or temperature ( $T$ ).

### 3. Methodology

The International vocabulary of metrology [12] defines several characteristics of replicated measurements, such as precision, accuracy and repeatability, which are quoted in Sections 3.1 to 3.3. In effect, these definitions agree with those of the International Organization for Standardization [16].

#### 3.1. Measurement precision

Measurement precision is defined as “closeness of agreement between indications or measured quantity values obtained by replicate measurements on the same or similar objects under specified conditions”. In our case, replicates refer to measurements  $j = 1, 2, \dots, n_i$  of a fixed setting  $i$  and location  $k$ . The average over replicates is

$$\bar{x}_{ik} = \frac{1}{n_i} \sum_{j=1}^{n_i} x_{ijk}. \quad (1)$$

The measurement precision is in this work quantified as the relative deviation in each replicate from the sample mean, which is

$$\delta x_{ijk} = \frac{x_{ijk} - \bar{x}_{ik}}{\bar{x}_{ik}}. \quad (2)$$

#### 3.2. Measurement accuracy

Measurement accuracy is defined as “closeness of agreement between a measured quantity value and a true quantity value of a measurand”. The target

mass rates  $\dot{m}_{ik}^0$  given in Table 3 are *conventional quantity values*, which are canonical estimates for true quantity values [12, Section 2.12]. Measurement accuracy of mass rates is here defined by replacing the sample mean in (2) by  $m_{ik}^0$ , which gives

$$\delta_0 \dot{m}_{ijk} = \frac{\dot{m}_{ijk} - \dot{m}_{ik}^0}{\dot{m}_{ik}^0}. \quad (3)$$

### 3.3. Repeatability

Repeatability is measurement precision, see (2), under conditions that include “the same measurement procedure, same operators, same measuring system, same operating conditions and same location, and replicate measurements on the same or similar objects over a short period of time”.

### 3.4. Liquid density model

Liquids expands with temperature. The rate of volume change due to temperature alone is

$$\frac{dV}{dT} = \alpha_k V, \quad (4)$$

where  $V$  is the volume of the fluid and  $\alpha_k$  is the thermal expansion coefficient [17]. For our purpose (4) was represented in terms of densities and linearized about a temperature  $T^*$ . It was then necessary to assume  $\alpha_k$  constant in temperature. The result was a linear regression model for density as a function of temperature,

$$d_k(T) = \hat{a}_k + \frac{\hat{b}_k}{1 + \alpha_k(T - T^*)}, \quad (5)$$

where  $\hat{a}_k$  and  $\hat{b}_k$  were coefficients obtained from ordinary least squares [18] on observations  $T_{ijk}$  and  $\rho_{ijk}$  at settings  $K$  defined in Appendix B.3. Predictions from (5) are denoted  $\hat{\rho}_{ijk} = d_k(T_{ijk})$ . The residuals  $\hat{\epsilon}_{ijk} = \rho_{ijk} - \hat{\rho}_{ijk}$  were the part of the density observations not modeled by temperature. Furthermore, the fraction of variance in density explained by temperature at location  $k$  was

$$r_k^2 = 1 - \frac{\sum_{i \in K} \sum_{j=1}^{n_i} \hat{\epsilon}_{ijk}^2}{\sum_{i \in K} \sum_{j=1}^{n_i} (\rho_{ijk} - \bar{\rho}_k)^2} = r^2(\rho_{ijk}, \hat{\rho}_{ijk}), \quad (6)$$

with  $r$  from (B.4) and  $\bar{\rho}_k$  from (B.2). Conversely,  $1 - r_k^2$  was the fraction of variance in density from other sources than temperature, according to the fitted regression model.

### 3.5. Air density model

The air was assumed dry with a specific gas constant of  $R_{\text{air}} = 287.058 \text{ J/kg}\cdot\text{K}$ . According to the ideal gas law, density is pressure  $p$  divided by temperature  $T$  and  $R_{\text{air}}$ ,

$$d_7(T, p) = \frac{p}{R_{\text{air}} T}. \quad (7)$$

The air density was not measured directly, only inferred from (7).

## 4. Results

### 4.1. Pressure measurements

Figure 1 shows the placement of pressure meters. Figure 2 gives all measurements for inlet pressure  $p_0$  (crosses) and outlet pressure  $p_1$  (circles) for all settings (frames)  $i = 1, 2, \dots, 11$ . The vertical axes is pressure in kilopascal and the horizontal axes is time in days, from February 11 to 28 of year 2020. The horizontal axes are all identical. All vertical axes are of the same scale in order to provide visual comparisons of absolute replicate deviations.

Relative deviations in inlet pressure, outlet pressure and the pressure drop  $p_1 - p_0$  was computed from (2) and is plotted in Figure 3. The vertical axis is the number of observations that falls in each bin. The black curves are the distributions for each setting estimated by (B.1). The axes for the density curves are not included because the sole message is shape. The vertical dashed lines are  $\pm 1$  relative standard deviation in measurements, given in Table 2. Because inlet and outlet pressure had  $\sigma = 0.09\%$ , pressure drop had  $\sigma = \sqrt{2} \cdot 0.09\% \approx 0.13\%$ . The errors in instruments were treated as independent of each other. Figure 4 gives the distributions of relative deviations in annulus pressures  $p_2, p_3, p_4$  and  $p_5$ . All replicates of all settings are used for Figures 3 and 4.

### 4.2. Deviations in volume flow rate

Volume flow rates dictates flow regime and is defined simply as  $Q = \dot{m}/\rho$ . Volume flow rate is proportional to mass flow rate, and inversely proportional to density. Note that Gaussian distributions for measurements of  $\dot{m}$  and  $\rho$  implicates a Cauchy distribution for the volume flow rate [19]. The Cauchy distribution has no defined mean or variance. Consequently, it is impossible to directly translate the measurement error of mass flow rate and density to the volume flow rate.

The density was not measured at location 4, and  $\rho_1$  was used as a proxy. The air density was not measured directly either, but inferred from (7). Air mixed with oil and was expected be at a temperature close to  $T_3$  on annulus entry. Furthermore, air pressure was not measured at injection but instead approximated as  $p_4$ . In summary the reported injected air density was  $d_7(T_{ij3}, p_{ij4})$ .

The outlet volume rate was the sum of oil, water and air volume rates. Densities were not measured directly at the outlet, but both temperature  $T_8$  and pressure  $p_1$  were available. With densities from (5) and (7), the outlet volume rate was  $Q_{ij8} = \sum_{k=1}^7 \dot{m}_{ijk}/d_k(T_{ij8}, p_{ij1})$ , where  $d_1$  was used for all oil density models  $d_1, d_2, \dots, d_5$ .

The relative deviations in replicate volume flow rates at locations 1–8 were computed from (2) and are presented in Figure 5. Additionally, the outlet volume rates of oil, water and air were computed separately and the deviations in each are given in the bottom row of Figure 5.

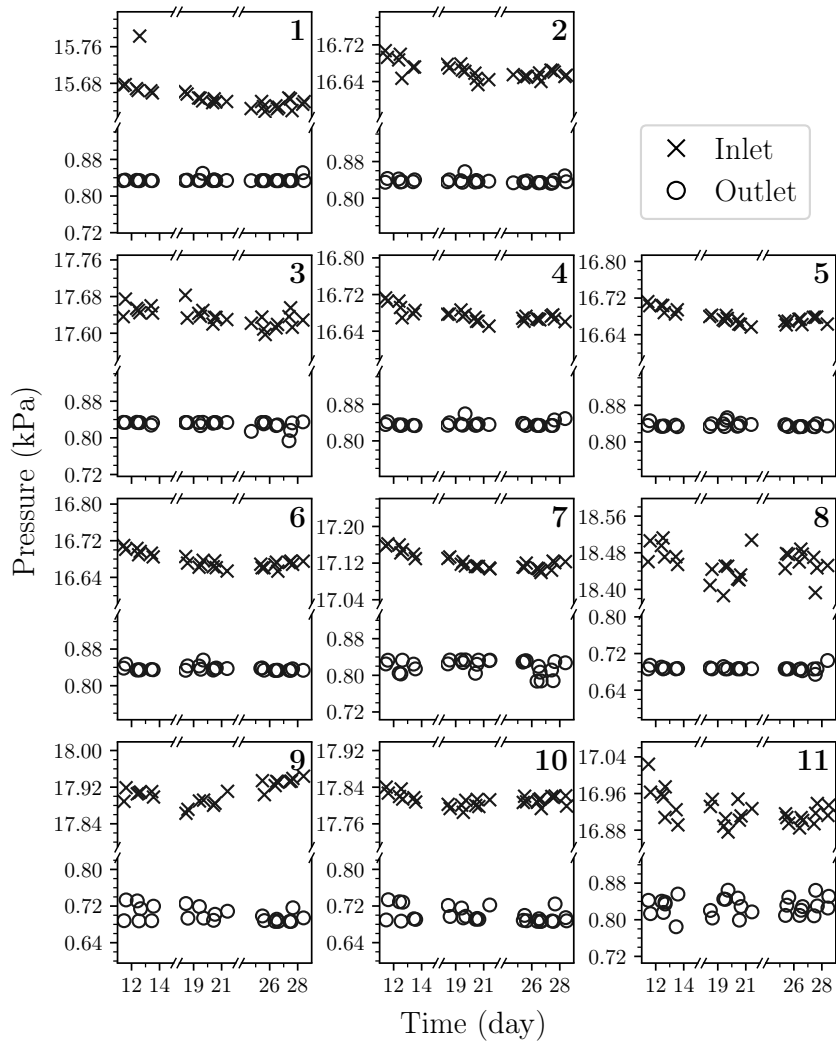


Figure 2: Pressure measurements at inlet (crosses) and outlet (circles) for all settings 1–11 (frames). The vertical axes are pressure in kPa and the same scale is used in all frames. The horizontal axes are all identical and give time in days with a resolution of one minute.



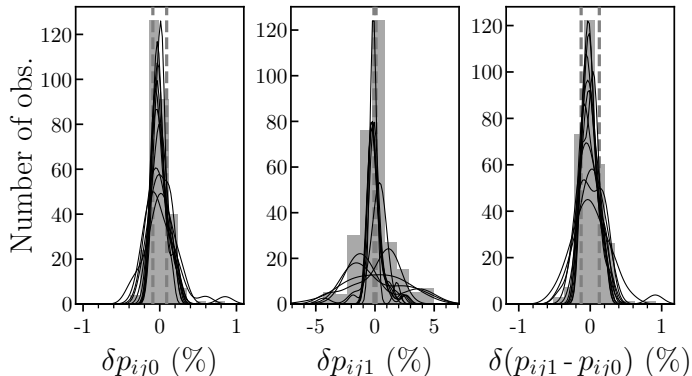


Figure 3: Relative deviations in pressure from the setting averages, for inlet (left), outlet (middle) and difference (right). The frequency histogram gives the distribution of relative deviations. The black curves are fitted distributions for each setting (scaled to frame size). The dashed vertical lines represent the measurement standard deviations of the pressure meters.

#### 4.3. Deviations in mass flow rate

Recall that each experiment was run with certain target mass rates, which was automatically regulated. Relative deviations in mass flow rates computed from (3) are plotted in Figure 6. For each location (frame), the histogram gives the distribution of relative errors over all settings and replicates. Naturally, only settings with flow at the given location were considered. An overview of the settings is given in Table 3.

#### 4.4. Temperature series

The fluid temperatures were 15–19 °C for all experiments. The fluids expanded with temperature, and consequently the volume flow rate increased. Strict control of temperature was *not* imposed on the experiments, and fluctuations over time were expected. Figure 7 gives all 294 measurements of temperatures  $T_1$  (yellow crosses) and  $T_8$  (purple circles). Location 1 and 8 are chosen as examples because they were relevant for all settings and relates to inlet and outlet. The horizontal axis represent time in days, with resolution of one minute. The trend each day was increasing temperature, on average 0.016 °C between subsequent measurements. However, 12 measurements (black) were clear exceptions to the trend, being at least 0.100 °C higher than the next measurement.

#### 4.5. Density

Temperature was expected to be the main contributor to variation in density. The change in density was aptly modeled as locally linear in temperature as

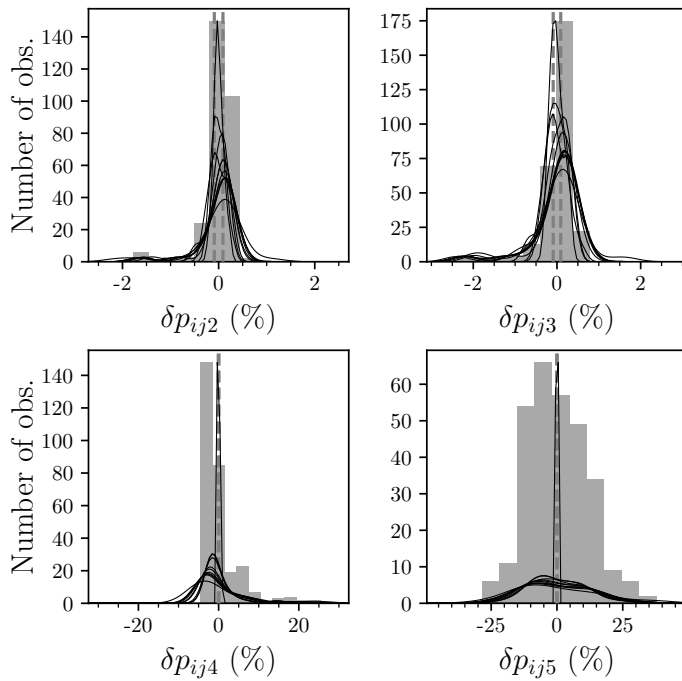


Figure 4: Relative deviations in annulus pressure from the setting averages. For each location (frame), the histogram gives the distribution of relative deviations. The black curves are fitted distributions for each setting (scaled to frame size). The dashed vertical lines represent the measurement standard deviations of the pressure meters.

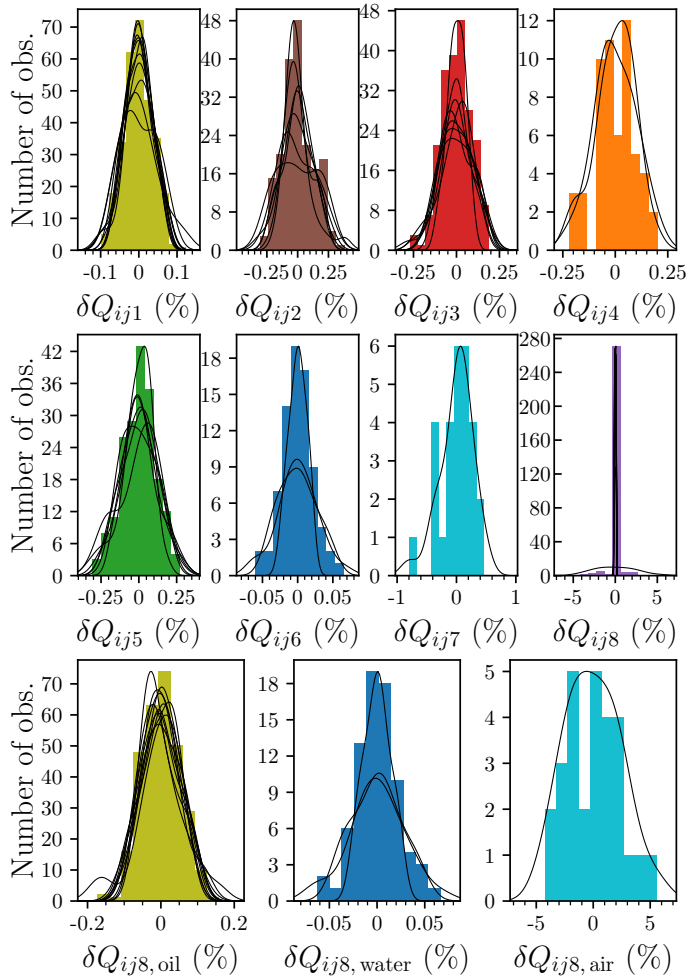


Figure 5: Relative deviations in volume flow rate from the setting averages. For each location (frame), the frequency histogram gives the distribution of relative deviations. The black curves are fitted distributions for each setting (scaled to frame size).

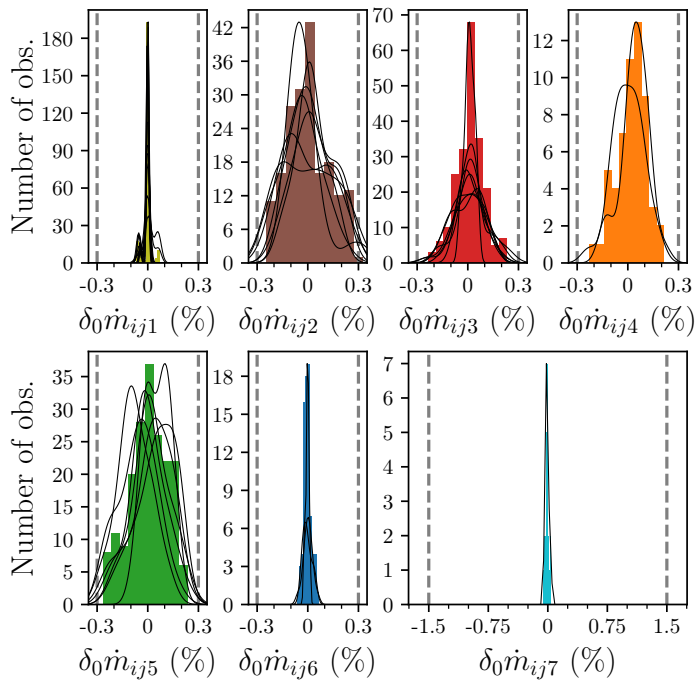


Figure 6: Relative deviations from target mass flow rates. For each location (frame), the histogram gives the distribution of relative deviations. The black curves are fitted distributions for each setting (scaled to frame size). The dashed vertical lines represent the measurement standard deviations of the mass flow rate meters.

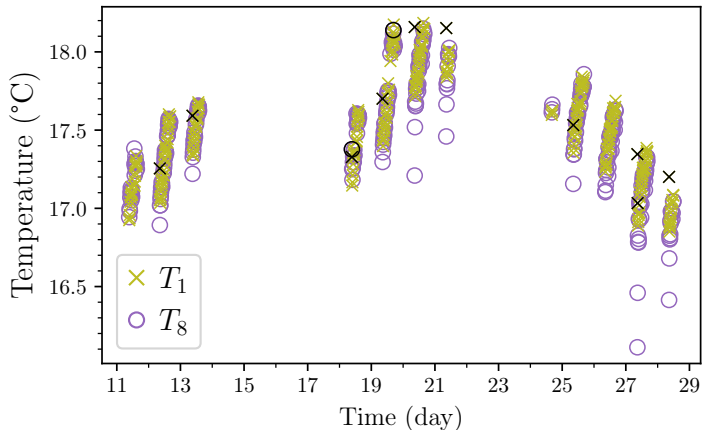


Figure 7: Temperature ( $^{\circ}\text{C}$ ) for all experiments at location 1 (yellow crosses) and location 8 (purple circles). The horizontal axis gives the time of each measurement. Subsequent measurements are in most cases about ten minutes apart. Temperatures were mostly increasing throughout each day, and clear exceptions are drawn in black.

explained in Section 3.4. Linear models were fitted to oil ( $k = 1$ ) and water ( $k = 6$ ), where all measurements of temperature were within  $1.5^{\circ}\text{C}$  of  $T^* = 17.5^{\circ}\text{C}$ . Thermal expansion coefficients were taken as  $\alpha_1 = 7.64 \cdot 10^{-4} \text{ }^{\circ}\text{C}^{-1}$  and  $\alpha_6 = 2.14 \cdot 10^{-4} \text{ }^{\circ}\text{C}^{-1}$ . For clarity units are left out in the fitted models given by

$$d_1(T) = -662.16 + \frac{1450.30}{1 + 7.64 \cdot 10^{-4}(T - 17.5)} \quad (8a)$$

and

$$d_6(T) = -99.56 + \frac{1095.88}{1 + 2.14 \cdot 10^{-4}(T - 17.5)}. \quad (8b)$$

The fractions of explained variance were  $r_1^2 = 99.3\%$  and  $r_6^2 = 57.7\%$ . The left panels of Figure 8 show observations (circles) and the fitted models (black lines). The vertical axes are densities, and the horizontal axes are the temperature regressor (left) and the residuals (right). The residuals of the regressions are plotted against the fitted values and the vertical gray lines marks the value of zero.

## 5. Discussion

We have analyzed experiments in a flow loop with coaxial pipes and multiple injection points with the purpose of quantifying repeatability. Repeatability entails the ability to control the state of the flow loop, which is a desirable quality.

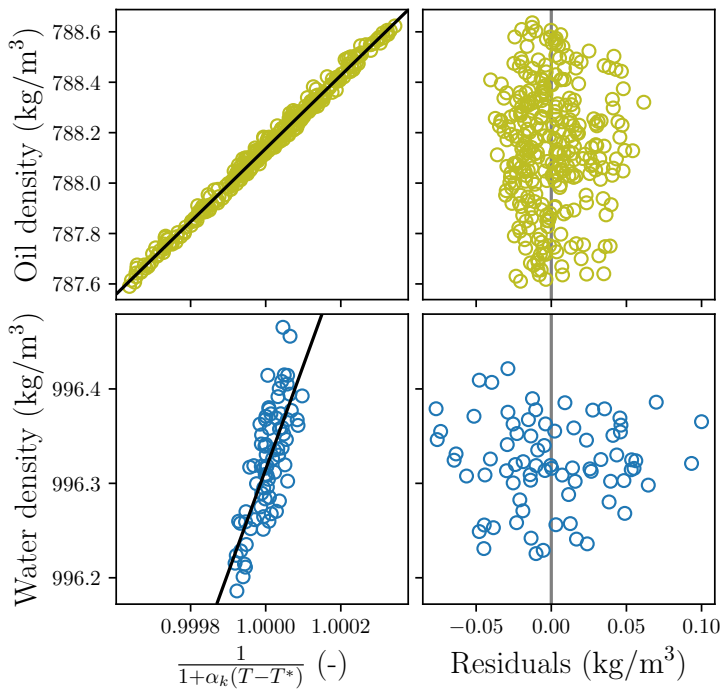


Figure 8: Model for thermal expansion of oil (top) and water (bottom). Location 1 is used for oil. The density is given on the vertical axis for observations (circles) and fitted model (black line). The horizontal axis gives the transformed temperature (left) and regression residuals (right). Residuals are plotted against fitted values and the vertical gray line is where residuals are zero.

The experiments were previously used to compare sensors, and the comparison benefitted from precision in volume rates and pressure across replicates. Precision in explanatory variables are also essential for tasks such as prediction.

The first results presented in Section 4 regarded repeatability of pressure measurements. As shown in Figure 3, inlet pressure deviated less than 1% relative to the sample mean, and mainly less than 0.1%. The outlet pressure deviated less than 5%, and mainly less than 1%. The pressure drop  $p_1 - p_0$  was of the same order of magnitude as the inlet pressure. All three distributions were bell-shaped and close to symmetric. The entropy of such distributions is large [20], which is appropriate for random errors.

The second panel of Figure 3 gives the distribution for each setting as a black curve. Setting 11 had the largest deviations  $\delta p_{ij1}$ , followed by settings 9, 10 and 7. These were also among the most complex settings, as seen in Table 3. The large deviations in setting 11 were likely due to the introduction of air into the flow loop. Air flow in this study was more unstable than liquids due to compressibility effects, and air also affected the multiphasic fluid system in a complex manner which may have lead to a higher degree of variance compared to liquid-only flows. Figure 4 gives the distributions of relative deviations in annulus pressures, which had higher variances than the inlet and outlet pressures. The positions of the annulus pressure meters are marked in Figure 1. Clearly, the pressures in the upper part of the annulus were more variable, up to about 30% relative deviations. Setting 11 was least variable and is represented by the narrowest probability density curves in distributions for  $\delta p_{ij4}$  and  $\delta p_{ij5}$ . There was possibly a fluctuating mixture of air and liquid in the upper annulus for all settings except setting 11 where air constantly occupied the upper annulus.

It is instructive to study the causes of variation in pressure, starting with volume flow rates. Relative deviations are given in Figure 5. The water rate was least variable, with most deviations smaller than 0.02% and the largest deviations at 0.06%. The deviations in oil inlet rates were about twice that. The deviations in injection rates  $Q_2$  through  $Q_5$  were less than 0.25% and mainly within 0.10%. The inlet air rates were more variable and deviated up to 0.80%. The behaviour of the different fluids was reflected at the outlet. Both oil and water have similar deviations at outlet and inlet, while water deviates more at the outlet, up to 5%. Volume flow rates impact pressure drop but the exact relation is complex for the flow loop considered. In the case of high flow rates, it is sometimes feasible to model pressure drop as a linear combination of the squared volume flow rates [21].

Volume flow rates were computed as mass flow rates divided by density. The mass rates deviations were well within one standard measurement errors of 0.3% and 1.5%. Of course, measurement errors also factored into the estimated relative deviations. In fact, the insight gained by comparing replicate deviations and measurement error is not clear. It is important to acknowledge that replicate deviations and measurement error are two distinct contributors to uncertainty about the physical values of the system variables. In our case, it seems that the prescribed measurement errors in the mass flow rates dominated the replicate deviations.

Figure 7 shows that temperature increased over the course of a day, and surely the density decreased accordingly. The fitted linear models in Figure 8 seemed appropriate and the residuals had no clear dependence on fitted densities. Moreover, temperature was estimated to explain 99.3% of the variance in oil density and 57.7% of the variation in water density. Most of the remaining variation in density is expected to be contamination of oil in water and vice versa. The separator did not perfectly separate oil and water, especially at high flow rates. Pressure would naturally also affect density to some extent.

Repeatability conditions is defined in 3.3 as a list of several requirements. Surely the replicates were conducted under the same measurement procedure, operators, measuring system and location, and describing similar objects. It is less obvious whether the operating conditions were sufficiently similar and whether the time span was short. It does not appear feasible to perform all experiments in significantly less time while also satisfying the remaining repeatability conditions. The temperature was not strictly controlled, yet no  $T_k$  spanned more than 2°C. Each time a new setting was imposed on the flow loop, only a single replicate was produced, before changing to a different setting. The procedure was meticulous but denied bias from confounders.

With similar conditions across replicates, repeatability translates to measurement precision, which for this purpose is quantified as relative deviations in replicates given by (2). Distributions of relative deviations are provided in Figures 3 to 6. Small deviations equal high repeatability which expresses the ability to impose specific conditions on the flow loop.

## 6. Conclusions

We have presented unique replicated experiments in a flow loop at the SINTEF Multiphase Flow Laboratory. Oil made up the main flow, but there were injections of oil, water and air through an annulus pipe surrounding the main test section. Eleven settings of the flow loop were run, ranging in complexity from only main flow to flow with several injections. Each setting was replicated up to 28 times. The conditions across replicates were compared and deemed sufficiently similar for a study of repeatability.

Inlet pressure, outlet pressure, pressure drop and volume flow rates were the quantities of interest. The relative deviations of all quantities of interest were mainly much less than 1%. Effectively, the experiments were highly repeatable. In other words, the system for controlling the flow loop was capable of closely replicating select conditions.

Temperature explained 99.3% of the variance in oil density and 57.7% of the variance in water density. The density fluctuations directly changed the volume flow rates which in turn influenced the pressure drop. Temperature control was not a requirement in the original industrial test campaign from which the data was shared. Significantly higher repeatability is expected with strict control of the flow loop temperature.

The replicate deviations were small both in comparison to deviation across settings and measurement error. The high degree of repeatability observed is



inevitably specific to the experimental setup. Still, it appears that satisfactory repeatability is achievable in multiphase experiments.

### Acknowledgments

LYTT Ltd. is acknowledged for sharing data for publication.

### References

- [1] H. Ladva, P. Tardy, P. Howard, E. Dussan V, et al., Multiphase flow and drilling fluid filtrate effects on the onset of production, in: SPE International Symposium on Formation Damage Control, Society of Petroleum Engineers, 2000.
- [2] O. Bratland, Pipe flow 2, multiphase flow assurance, electronic book (2010). URL <http://drbratland.com/PipeFlow2/>
- [3] A. A. Osiptsov, Fluid mechanics of hydraulic fracturing: a review, *Journal of petroleum science and engineering* 156 (2017) 513–535.
- [4] B. Sun, Y. Guo, W. Sun, Y. Gao, H. Li, Z. Wang, H. Zhang, Multiphase flow behavior for acid-gas mixture and drilling fluid flow in vertical wellbore, *Journal of Petroleum Science and Engineering* 165 (2018) 388–396.
- [5] E. Gharaiabah, A. Read, G. Scheuerer, et al., Overview of CFD multiphase flow simulation tools for subsea oil and gas system design, optimization and operation, in: OTC Brasil, Offshore Technology Conference, 2015.
- [6] Comparison of Commercial Multiphase Flow Simulators with Experimental and Field Databases, Vol. All Days of International Conference on Multiphase Production Technology, BHR-2011-I2. URL <https://onepetro.org/BHRICMPT/proceedings-pdf/BHR11/A11-BHR11/BHR-2011-I2/1663541/bhr-2011-i2.pdf>
- [7] M. Shippen, W. J. Bailey, Steady-state multiphase flow – past, present, and future, with a perspective on flow assurance, *Energy & fuels* 26 (7) (2012) 4145–4157.
- [8] S. Khor, M. Mendes-Tatsis, G. Hewitt, One-dimensional modelling of phase holdups in three-phase stratified flow, *International journal of multiphase flow* 23 (5) (1997) 885–897.
- [9] G. Oddie, H. Shi, L. Durlofsky, K. Aziz, B. Pfeffer, J. Holmes, Experimental study of two and three phase flows in large diameter inclined pipes, *International Journal of Multiphase Flow* 29 (4) (2003) 527–558.
- [10] T. Babadagli, X. Ren, K. Develi, Effects of fractal surface roughness and lithology on single and multiphase flow in a single fracture: an experimental investigation, *International Journal of Multiphase Flow* 68 (2015) 40–58.

- [11] M. Leporini, B. Marchetti, F. Corvaro, G. Di Giovine, F. Polonara, A. Terenzi, Sand transport in multiphase flow mixtures in a horizontal pipeline: An experimental investigation, *Petroleum* 5 (2) (2019) 161–170.
- [12] I. BIPM, I. IFCC, I. IUPAC, O. ISO, International vocabulary of metrology—basic and general concepts and associated terms (VIM), 3rd edn, JCGM 200: 2012, accessed on April 3, 2021 (2012).  
URL [https://www.bipm.org/utils/common/documents/jcgm/JCGM\\_200\\_2012.pdf](https://www.bipm.org/utils/common/documents/jcgm/JCGM_200_2012.pdf)
- [13] T. Unander, Uncertainty quantification in multiphase pipe flow experiments, Tech. Rep. 00102, SINTEF, ISBN 978-82-14-06488-9 (2021).
- [14] JCGM, Guide to the expression of uncertainty in measurement, accessed on March 17, 2021 (1995).  
URL [https://www.bipm.org/utils/common/documents/jcgm/JCGM\\_100\\_2008\\_E.pdf](https://www.bipm.org/utils/common/documents/jcgm/JCGM_100_2008_E.pdf)
- [15] M. S. Hamada, S. H. Steiner, R. J. MacKay, C. S. Reese, Planning and analyzing experiments with models that distinguish between replicates and repeats, *Quality and Reliability Engineering International* 33 (3) (2017) 657–668.
- [16] ISO, Accuracy (trueness and precision) of measurement methods and results – part 1: General principles and definitions, Standard, International Organization for Standardization, Geneva, CH (Mar. 1994).
- [17] D. L. Turcotte, G. Schubert, *Geodynamics*, Cambridge university press, 2002.
- [18] T. Hastie, R. Tibshirani, J. Friedman, *The elements of statistical learning: data mining, inference, and prediction*, Springer Science & Business Media, 2009.
- [19] N. S. Pillai, X.-L. Meng, An unexpected encounter with Cauchy and Lévy, *The Annals of Statistics* 44 (5) (2016) 2089 – 2097. doi:10.1214/15-AOS1407.  
URL <https://doi.org/10.1214/15-AOS1407>
- [20] E. T. Jaynes, Information theory and statistical mechanics, *Physical review* 106 (4) (1957) 620.
- [21] G. Brown, *The Darcy-Weisbach Equation*, Oklahoma State University–Stillwater (2000).

## Appendix A. Instrumentation

The instruments used for measurements are listed in Table A.4. The measured variables are given in the first column. Note that some instruments measure multiple variables. The position of the instruments along the test section are given in the second column followed by a description in the last column.

Table A.4: List of measuring instruments with variables measured in the first column, position along the test section in meters in the second column and product description in the last column.

Variables	Position [m]	Instrument description
$p_0$	00.00	Fuji differential pressure transmitter
$p_1$	52.00	Fuji differential pressure transmitter
$p_2$	00.20	FUJI FCX-A/C II DP Transmitter
$p_3$	16.30	Fuji differential pressure transmitter
$p_4$	32.40	Fuji pressure transmitter
$p_5$	48.40	Fuji pressure transmitter
$\dot{m}_1, \rho_1$	00.00	MicroMotion CMF200M elite series Coriolis meter
$T_1$	00.00	Inor Meso-HX temp transmitter with PT100 element, 3 mm edge and 1/2 inch tube clamp fitting
$\dot{m}_2, \rho_2, T_2$	11.60	Krohne Optimass 1400C S40
$\dot{m}_3, \rho_3, T_3$	23.60	Krohne Optimass 1400C S40
$\dot{m}_4$	27.60	Krohne Optimass 1400C S40
$\dot{m}_5, \rho_5, T_5$	37.60	Krohne Optimass 1400C S40
$\dot{m}_6, \rho_6, T_6$	23.60	Krohne Optimass 1400C S40
$\dot{m}_7$	23.60	Air flow meter EE771-CH1N025DKA1/RI6IMA P/N: S10757 S/N: 1702160000234C
$T_8$	52.00	PyroControl temperature transmitter rebuilt with PR5335D PT100
$T_9$	00.00	PyroControl temperature transmitter

Table B.5: Means and standard deviations of pressure measurements in kPa. Values are given separately for each setting (rows 1–11) and overall (last row).

Set.	$p_0$		$p_1$		$p_2$		$p_3$		$p_4$		$p_5$	
	Mean	$\hat{\sigma}$	Mean	$\hat{\sigma}$	Mean	$\hat{\sigma}$	Mean	$\hat{\sigma}$	Mean	$\hat{\sigma}$	Mean	$\hat{\sigma}$
1	15.650	0.0307	0.835	0.00436	16.542	0.0963	11.152	0.0736	6.813	0.535	6.150	0.978
2	16.663	0.0179	0.838	0.00532	17.607	0.0726	12.236	0.0700	7.808	0.439	7.138	0.912
3	17.637	0.0197	0.830	0.00897	18.590	0.0659	13.220	0.0663	8.758	0.422	8.082	0.923
4	16.675	0.0149	0.837	0.00590	17.611	0.0732	12.241	0.0709	7.815	0.428	7.153	0.920
5	16.679	0.0146	0.837	0.00494	17.612	0.0708	12.241	0.0688	7.842	0.446	7.199	0.936
6	16.676	0.0153	0.837	0.00519	17.609	0.0687	12.237	0.0669	7.802	0.416	7.133	0.906
7	17.123	0.0177	0.820	0.01510	18.102	0.0621	12.727	0.0735	8.232	0.394	7.552	0.868
8	18.457	0.0331	0.687	0.00484	19.574	0.0376	14.183	0.0402	9.437	0.335	8.701	0.844
9	17.909	0.0228	0.701	0.01600	19.037	0.0346	13.642	0.0343	8.958	0.349	8.244	0.857
10	17.811	0.0125	0.699	0.01570	18.899	0.0185	13.526	0.0213	8.853	0.328	8.114	0.820
11	16.923	0.0322	0.829	0.02000	17.912	0.0244	12.527	0.0299	9.950	0.027	9.879	0.025
All	17.090	0.7480	0.797	0.06160	17.565	0.8190	12.700	0.8170	8.378	0.948	7.752	1.280

## Appendix B. Sample statistics

### Appendix B.1. Kernel density estimation

The distribution of relative deviations in replicates  $\delta x_{ijk}$  for  $j = 1, 2, \dots, n_i$  was estimated as a Gaussian kernel with Scott's rule for bandwidth. Explicitly,

$$\hat{f}(z) = \frac{n_i^{5/4}}{\sqrt{2\pi}} \sum_{j=1}^{n_i} \exp\left(-\frac{1}{2}n_i^{2/5}(z - \delta x_{ijk})^2\right). \quad (\text{B.1})$$

### Appendix B.2. Mean and standard deviation

Let  $x_{ijk}$  be a measurement from an instrument, where  $x$  is a physical quantity,  $k$  is location,  $i$  is setting and  $j$  is replicate. Furthermore, let  $K = \{i : \hat{n}_{ik}^0 > 0\}$  be the settings with flow at location  $k$ . The sample mean and unbiased sample standard deviation are

$$\bar{x}_k = \frac{1}{\sum_{i \in K} n_i} \sum_{i \in K} \sum_{j=1}^{n_i} x_{ijk} \quad (\text{B.2})$$

and

$$\hat{\sigma}(x_k) = \sqrt{\frac{1}{\sum_{i \in K} n_i - 1} \sum_{i \in K} \sum_{j=1}^{n_i} (x_{ijk} - \bar{x}_k)^2}, \quad (\text{B.3})$$

taken over all replicates  $j$  and settings  $i \in K$ . Tables B.5 to B.7 lists the means and deviations of pressures, densities and temperatures for each setting separately and for all settings combined.

Table B.6: Means and standard deviations of density measurements in  $\text{kg/m}^3$  at locations 1, 2, 3, 5 and 6. Values are given separately for each setting (rows 1–11) and overall (last row).

Setting	$\rho_1$		$\rho_2$		$\rho_3$		$\rho_5$		$\rho_6$	
	Mean	$\hat{\sigma}$	Mean	$\hat{\sigma}$	Mean	$\hat{\sigma}$	Mean	$\hat{\sigma}$	Mean	$\hat{\sigma}$
1	788.119	0.254	—	—	—	—	—	—	—	—
2	788.181	0.249	782.763	0.310	783.238	0.273	781.888	0.609	—	—
3	788.173	0.257	782.611	0.277	783.156	0.267	781.706	0.604	—	—
4	788.166	0.252	782.657	0.265	783.197	0.261	781.920	0.598	—	—
5	788.142	0.255	782.612	0.271	783.164	0.264	781.851	0.595	—	—
6	788.137	0.252	782.600	0.259	783.155	0.257	781.848	0.567	—	—
7	788.105	0.252	782.539	0.257	783.088	0.255	781.725	0.542	—	—
8	788.087	0.254	—	—	—	—	—	—	996.356	0.0569
9	788.144	0.242	—	—	783.176	0.243	—	—	996.290	0.0528
10	788.141	0.242	—	—	—	—	—	—	996.317	0.0565
11	788.154	0.239	782.551	0.230	783.095	0.235	781.631	0.483	—	—
All	788.141	0.247	782.619	0.273	783.158	0.257	781.795	0.572	996.212	0.203

Table B.7: Means and standard deviations of temperature measurements in  $^{\circ}\text{C}$  at locations 1, 2, 3, 5, 6, 8 and 9. Values are given separately for each setting (rows 1–11) and overall (last row). Locations without flow are marked ‘—’. Air was only used at setting 11, with temperature  $T_7$  of mean  $18.96^{\circ}\text{C}$  and standard deviation  $0.400^{\circ}\text{C}$ .

Set.	$T_1$		$T_2$		$T_3$		$T_5$		$T_6$		$T_8$		$T_9$	
	Mean	$\hat{\sigma}$	Mean	$\hat{\sigma}$	Mean	$\hat{\sigma}$	Mean	$\hat{\sigma}$	Mean	$\hat{\sigma}$	Mean	$\hat{\sigma}$	Mean	$\hat{\sigma}$
1	17.52	0.327	—	—	—	—	—	—	—	—	17.32	0.422	18.16	0.362
2	17.44	0.324	17.45	0.346	17.50	0.334	17.12	0.530	—	—	17.38	0.363	18.15	0.363
3	17.44	0.334	17.51	0.347	17.56	0.341	17.16	0.529	—	—	17.45	0.343	18.17	0.359
4	17.45	0.326	17.50	0.337	17.53	0.335	17.11	0.524	—	—	17.41	0.337	18.15	0.364
5	17.48	0.332	17.54	0.343	17.56	0.342	17.17	0.532	—	—	17.46	0.345	18.17	0.371
6	17.49	0.325	17.55	0.335	17.57	0.334	17.16	0.507	—	—	17.46	0.335	18.16	0.370
7	17.53	0.330	17.60	0.337	17.62	0.336	17.20	0.489	—	—	17.53	0.335	18.19	0.370
8	17.55	0.327	—	—	—	—	—	—	17.42	0.285	17.47	0.322	18.18	0.367
9	17.49	0.315	—	—	17.58	0.320	—	—	17.45	0.277	17.49	0.295	18.14	0.360
10	17.52	0.313	—	—	—	—	—	—	17.49	0.290	17.51	0.314	18.17	0.385
11	17.53	0.307	17.60	0.314	17.62	0.314	17.26	0.464	—	—	17.49	0.313	18.19	0.386
All	17.50	0.320	17.53	0.335	17.57	0.329	17.17	0.505	17.46	0.282	17.45	0.340	18.16	0.363

*Appendix B.3. Correlation coefficient*

Let  $x_{ijk}$  and  $y_{ijl}$  be measurements from two instruments, where  $x$  and  $y$  are physical quantities,  $k$  and  $l$  are locations,  $i$  is setting and  $j$  is replicate. The joint linear variation in  $x_{ijk}$  and  $y_{ijl}$  can be estimated by the sample Pearson correlation coefficient. Let  $L = \{i : \dot{m}_{il}^0 > 0\}$  be the settings with flow at location  $l$ , and let  $M = K \cup L$ . The correlation coefficient across all settings is

$$r(x_k, y_l) = \frac{\sum_{i \in M} \sum_{j=1}^{n_i} (x_{ijk} - \bar{x}_k)(y_{ijl} - \bar{y}_l)}{\sqrt{\sum_{i \in M} \sum_{j=1}^{n_i} (x_{ijk} - \bar{x}_k)^2} \sqrt{\sum_{i \in M} \sum_{j=1}^{n_i} (y_{ijl} - \bar{y}_l)^2}}, \quad (\text{B.4})$$

with  $\bar{x}_k$  and  $\bar{y}_l$  from Section B.2. The correlation coefficient between instruments succinctly pointed out physics of the system. The correlations between densities, temperatures and mass flow rates were estimated from (B.4) and illustrated in Figure B.9. Each square in the grid, gives the correlation between the variables labeled on the axes. Values of larger magnitude than 0.6 is printed and the area of each square scales with magnitude.

The estimated correlation between the total mass flow rate  $\dot{m}_1 + \dot{m}_2 + \dots + \dot{m}_7$  and the pressure drop  $p_1 - p_0$  was 0.54.

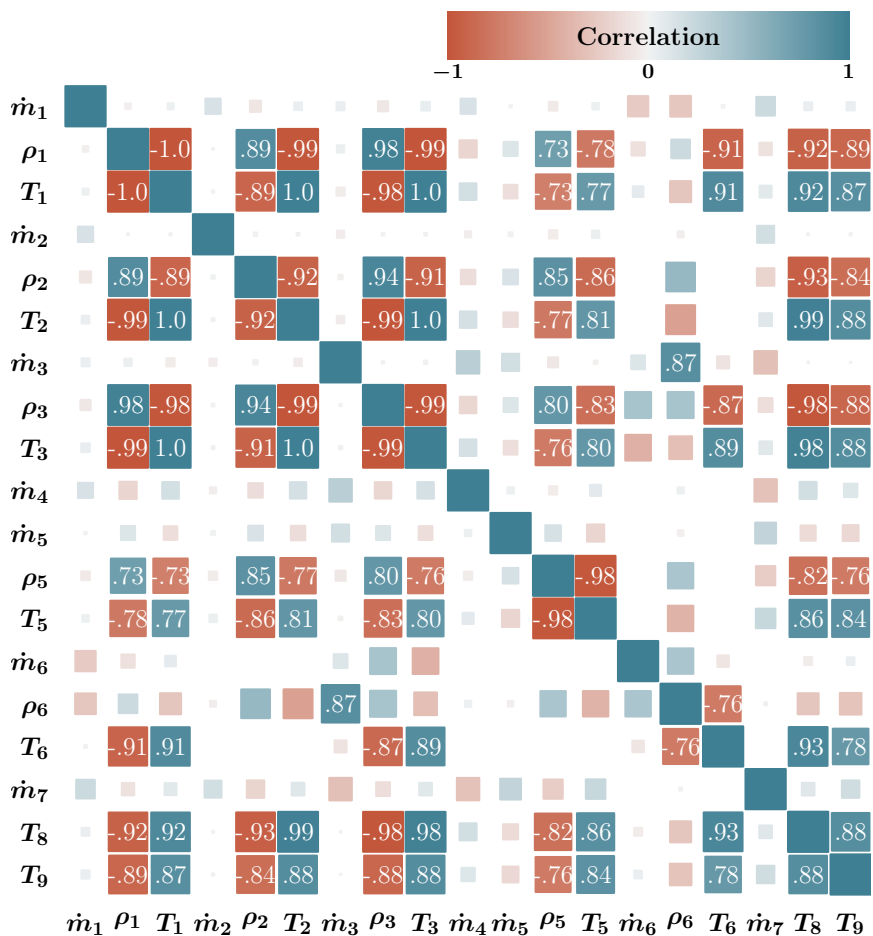


Figure B.9: Correlation between variables. Each square gives the correlation between the variables on the axes. Correlation larger than 0.6 in magnitude are printed. The areas of the squares also represent magnitude.







ISBN 978-82-326-6519-8 (printed ver.)  
ISBN 978-82-326-6928-8 (electronic ver.)  
ISSN 1503-8181 (printed ver.)  
ISSN 2703-8084 (online ver.)



**NTNU**

Norwegian University of  
Science and Technology